Future risk evaluation of the global COVID-19 pandemic

Zengyun Hu[1], Gang Yin[2], Daihai He[3], Qianqian Cui[4], Xiaomei Feng[5], Zhidong Teng[2], Qi Hu[6], Jiansen Li[7], and Xia Wang[8]

[1]Xinjiang Institute of Ecology and Geography, Chinese Academy of Sciences
[2]Xinjiang University
[3]Hong Kong Polytechnic University
[4]Ningxia University
[5]Yuncheng University
[6]University of Nebraska Lincoln
[7]Guangdong Provincial Center for Disease Control and Prevention
[8]Shaanxi Normal University

November 24, 2022

Abstract

The ongoing coronavirus disease 2019 (COVID-19) pandemic has caused more than 150 million cases of infection to date and poses a serious threat to global public health. In this work, global COVID-19 data were used to examine the dynamical variations from the perspectives of immunity and contact of 85 countries across the five climate regions: tropical, arid, temperate, cold, and polar. A new approach is proposed to obtain the transmission rates based on the COVID-19 data between the countries with the same climate region over the Northern Hemisphere (NH) and Southern Hemisphere (SH). Our results suggest that the COVID-19 pandemic will persist over a long period of time or enter into regular circulation in multiple periods of 1-2 years. Moreover, based on the simulated results by the COVID-19 data, it is found that the temperate and cold climate regions have higher infection rates than the tropical and arid climate regions, which indicates that climate may modulate the transmission of COVID-19. The role of the climate on the COVID-19 variations should be concluded with more data and more cautions. The non-pharmaceutical interventions still play the key role in controlling and prevention this global pandemic.

Future risk evaluation of the global COVID-19 pandemic

Xia Wang[1*], Gang Yin[2*], Zengyun Hu[3,4*†], Daihai He[5†], Qianqian Cui[6], Xiaomei Feng[7], Zhidong Teng[8†], Qi Hu[9], Jiansen Li[10]

[1]School of Mathematics and Information Science, Shaanxi Normal University, Xian 710119, China

[2]College of Resource and Environment Science, Xinjiang University, Urumqi, Xinjiang 830046, China

[3]State Key Laboratory of desert and Oasis Ecology, Xinjiang Institute of Ecology and Geography, Chinese Academy of Sciences, Urumqi, Xinjiang 830011, China

[4]Research Center for Ecology and Environment of Central Asia, Chinese Academy of Sciences, Urumqi, Xinjiang 830011, China

[5]Department of Applied Mathematics, Hong Kong Polytechnic University, Hong Kong SAR China

[6]School of Mathematics and Statistics, Ningxia University, Yinchuan, Ningxia 750021, China

[7]School of Mathematics and Informational Technology, Yuncheng University, Yuncheng 044000, China

[8]College of Mathematics and System Sciences, Xinjiang University, Urumqi, Xinjiang 830046, China

[9]School of Natural Resources and Department of Earth and Atmospheric Sciences, University of Nebraska Lincoln, Lincoln, Nebraska

[10]Guangdong Provincial Center for Disease Control and Prevention, Guangzhou 511430, China

---

Abstract: The ongoing coronavirus disease 2019 (COVID-19) pandemic has caused more than 150 million cases of infection to date and poses a serious threat to global public health. In this work, global COVID-19 data were used to examine the dynamical variations from the perspectives of immunity and contact of 85 countries across the five climate regions: tropical, arid, temperate, cold, and polar. A new approach is proposed to obtain the transmission rates based on the COVID-19 data between the countries with the same climate region over the Northern Hemisphere (NH) and Southern Hemisphere (SH). Our results suggest that the COVID-19 pandemic will persist over a long period of time or enter into regular circulation in multiple periods of 1-2 years. Moreover, based on the simulated results by the COVID-19 data, it is found that the temperate and cold climate regions have higher infection rates than the tropical and arid climate regions, which indicates that climate may modulate the transmission of COVID-19. The role of the climate on the COVID-19 variations should be concluded with more data and more cautions. The non-pharmaceutical interventions still play the key role in controlling and prevention this global pandemic.

*These authors contributed equally to this work.

†Corresponding author. Zengyun Hu, email: huzengyun@ms.xjb.ac.cn; Daihai He, email: daihai.he@polyu.edu.hk; Zhidong Teng, emial: zhidong@xju.edu.cn

Keywords: COVID-19 pandemic; Koppen-Geiger climate classification; periodic variation; scenario analysis.

1 Introduction

Rapidly spreading and ravaging the world, severe acute respiratory syndrome-coronavirus 2 (SARS-CoV-2) has caused the coronavirus disease 2019 (COVID-19) pandemic through human-to-human transmission (Armitage et al., 2020; Chinazzi et al., 2020; Wang et al., 2020), resulting in more than 158,000,000 total confirmed cases and more than 3,000,000 deaths in more than 200 countries/regions as of May 11, 2021 (WHO, https://covid19.who.int/). This global pandemic has serious impacts on public health and on social and economic development (Baker et al., 2020; Zerhouni et al., 2020). A great number of measures have been quickly adopted to reduce the transmission and to mitigate the impact of the pandemic (Cohen and Corey 2020; Hsiang et al., 2020; Thorp, 2020). The effective measures and strategies employed in China provided a useful example to other countries in preventing and curing COVID-19 (Guan et al., 2020; Kraemer et al., 2020; Wu and McGoogan, 2020; Xu et al., 2020; Zhou et al., 2020).

However, there is neither a specific drug nor vaccine treatment for COVID-19 because typically months to years are needed to develop and test such therapeutics (Ferretti et al., 2020; Tian et al., 2020). Therefore, non-pharmaceutical interventions have been widely used by all countries as the only immediate means of curbing SARS-CoV-2 transmission, e.g., physical (social) distancing, closing schools and workplaces, limiting the sizes of gatherings, wearing face masks and eye protection, and quarantine (Ali et al., 2020; Chu et al., 2020; Cui et al., 2020; Giordano et al., 2020; Hu et al., 2020; Matteo et al., 2020; Parmet and Sinha, 2020; Sjodin et al., 2020; Ruktanonchai et al., 2020). Physical distancing as implemented in China during the outbreak has been able to control COVID-19 (Zhang et al., 2020), and the national emergency response has delayed the growth and limited the size of the COVID-19 spread in China, averting hundreds of thousands of cases (Prem et al., 2020; Tian et al., 2020). Restrictive physical distancing measures combined with widespread testing and contact tracing could end the ongoing COVID-19 pandemic (Britton et al., 2020; Giordano et al., 2020; Hao et al., 2020; Lai et al., 2020).

To employ the correct measures at the right time in controlling the COVID-19 pandemic, it is of crucial importance to accurately understand the routes and timings of transmission, especially accurate prediction of COVID-19 variations in the future (Kissler et al., 2020). Mathematical models can not only probe the complexity of infectious disease dynamics (e.g. period, bifurcation and chaos), but can also elucidate the mechanisms of transmission and indicate new approaches for prevention and control strategies (Heesterbeek et al., 2015). Assuming that the COVID-19 pandemic adapts to similar climate scenarios based on known coronavirus biology, it will exhibit seasonal variations and become a seasonal epidemic according to the results of a climate-dependent epidemic model (Baker et al., 2020). Based on a SEIRS epidemic model, it was proposed in a recent work that COVID-19 can exist at any time of year, and it will likely enter into regular circulation if immunity to SARS-CoV-2 is not permanent (Kissler et al.2020).

However, they only used less than five years data of betacoronaviruses HCoV-OC43 and HCoV-HKU1 to predict COVID-19 variations which is a serious limitation based on the transmission characteristics of known coronavirus strains (Baker et al., 2020; Kissler et al., 2020).

It is well known that climate changes have significant impacts on large of human diseases which are concluded using numerous long term disease datasets and climate datasets, such as the impacts of temperature and specific humidity on the human influenza infections (Shaman et al., 2010; Tamerius et al., 2013; Liu et al., 2019), and the positive influence of low temperature and low relative humidity on the coronaviruses (Yang and Marr 2011; Sundell et al., 2016; Aboubakr, et al., 2020).

In terms of the COVID-19, the role of climate in COVID-19 mitigation strategies is still a dispute topic (OReilly et al., 2020). Although some literatures (Araujo et al., 2020; Liu et al., 2020; Sajadi et al., 2020; Wang et al., 2020) explore the impacts of climate factors (e.g., temperature and specific humidity) on the COVID-19 variations and suggest that SARS-CoV-2 is less transmissible in hot and humid climates, there is no sufficient evidence supporting that large numbers of COVID-19 cases are associated with cold and dry climates due to only not less than two years data (Baker et al., 2020; OReilly et al., 2020; Prata et al., 2020).

Environment changes (e.g., climate changes) affect the outbreak and transmission of many diseases directly or indirectly (Tamerius et al., 2013; Baker et al., 2021). Specific humidity has been shown to be important for influenza transmission in both laboratory settings and population-level studies. Therefore, it is important explore the disease transmission or outbreak characteristics in geospatial perspectives.

However, with limited data on the current epidemic, these early-stage results are inevitably inconclusive. Furthermore, the relative importance of climate drivers when compared with high population susceptibility during the pandemic stage of an emerging infection such as SARS-CoV-2 has not been fully characterized (Baker et al., 2020; Paraskevis et al., 2021). Therefore, any COVID-19 risk evaluations and predictions based on climate information alone should be interpreted with caution. The role of the climate changes on the COVID-19 variations will be not explored in this study because of the limited information from the no more than two years' COVID-19 transmission.

Projecting the transmission dynamics of the global COVID-19 pandemic is very important and urgent in order to employ the correct strategies and measures to control the outbreak of this disease. For the study of the global COVID-19 pandemic, the following questions must first be addressed (1) What are the differences in the present transmission of COVID-19 in the different climate regions of various countries? (2) Does a reasonable approach exist to explore the future changes of COVID-19 in the world, but not as previous studies based on known coronavirus strains? (3) What are the future risks of the global COVID-19 pandemic?

To address the above questions, this study aimed to (1) evaluate and predict the transmission dynamics of the COVID-19 pandemic over different climate regions, (2) to propose an innovated approach to investigate the future dynamical behaviors rather than relying on information on other coronaviruses, and (3) to explore the COVID-19 variations using different strategies in future. These analyses are only interpreted based on the COVID-19 data objectively.

2 Methods

2.1 SEICR model

Based on the transmission characteristics of the COVID-19 pandemic and previous literatures (Cui et al., 2020; Hu et al., 2020), the entire population at time t is divided into five components, i.e., susceptible individuals $S(t)$, exposed individuals $E(t)$, infectious individuals $I(t)$, confirmed individuals $C(t)$, and removed individuals $R(t)$. We assume that the confirmed individuals $C(t)$ cannot transmit among the population because they will be quarantined if they are confirmed. The COVID-19 disease is transmitted from $S(t)$ to $E(t)$ by the contact behaviours and the transmission characteristic of the SARS-CoV-2 composed a standard incidence rate. The exposed individuals $E(t)$ transitions to the infectious individuals $I(t)$ in a rate. Part of $I(t)$ becomes the confirmed individuals $C(t)$ by the COVID-19 detection, and the other $I(t)$ transitions to the removed individuals $R(t)$ in a recovery rate. The confirmed individuals $C(t)$ becomes death partly and the residual will be recovered as the removed individuals $R(t)$. The details of the disease transmission among the different individuals are well illustrated by the flowchart figure (Figure 1).

According to the above analysis, the corresponding SEICR disease model can be described by the following system of ordinary differential equations:

$$\begin{cases} S' = -\dfrac{c(t)pSI}{N}, \\ E' = \dfrac{c(t)pSI}{N} - \sigma E, \\ I' = \sigma E - (\delta(t) + \gamma_I)I, \\ C' = \delta(t)I - (\alpha_c + \gamma_c)C, \\ R' = \gamma_I I + \gamma_c C, \end{cases} \tag{2.1}$$

where the contact rate function is

$$c(t) = \begin{cases} c_0, & t \leq t_c \\ (c_0 - c_f)e^{-r_b(t-t_c)} + c_f, & t > t_c \end{cases} \tag{2.2}$$

and the detection rate function is

$$\frac{1}{\delta(t)} = \begin{cases} \dfrac{1}{\delta_0}, & t \leq t_c \\ (\dfrac{1}{\delta_0} - \dfrac{1}{\delta_f})e^{-r_d(t-t_c)} + \dfrac{1}{\delta_f}. & t > t_c. \end{cases} \tag{2.3}$$

$c(t)$ is the contract rate which is determined by many factors, such as population density, total population and traffic types. c_0 is the contact rate and δ_0 is the detection rate at the early disease transmission period t_c. c_f is the minimum contact rate under the current control strategies. r_b denotes the contact rate modeled as an exponentially decreasing rate, which assumes that the contact times are decreasing with the implementation of intervention.

$\delta(t)$ is the detection rate of the COVID-19 disease that is mainly resulted by the level of the public health system, the medical resources and the gross domestic product (GDP). δ_f

Table 1: Definitions of the parameters used in the model

Parameter	Definition (Units)	Value	References
$c(t)$	the contact rate at time t		estimated
c_0	the initial contact rate		estimated
c_f	the minimum contact rate		estimated
r_b	the exponential decreasing rate of the contact rate		estimated
t_c	the time period before control	14	assumed
p	the probability of transmission per contact		estimated
$\delta(t)$	the detection rate at time t		estimated
δ_0	the initial detection rate		estimated
δ_f	the maximum detection rate		estimated
r_d	the exponential increasing rate of the detection rate		estimated
σ	the transition rate from E to I	1/5	Tang et al (2020)
γ_I	the recovery rate of I		estimated
γ_c	the recovery rate of C		estimated
α_c	the death rate of C		estimated

is the maximum detection rate under the current control strategies, and each country has its own maximum detection rate value. r_d denotes the exponentially decreasing rate of the testing period. Considering that the contact rate and detection rate will gradually decrease or increase with the gradual strengthening of control measures, and finally reach the minimum contact rate or maximum detection rate, we use the above function form as shown in the literature (Tang et al., 2020).

Parameter p is the transmission rate of COVID-19, which depends on the SARS-CoV-2 virus. σ is the transition rate from exposed individuals $E(t)$ to infectious individuals $I(t)$. γ_I and γ_c are the recovery rates of $I(t)$ and $C(t)$, respectively. α_c is the death rate of $C(t)$. During the incubation period of 14 days (Lauer et al., 2020), for some COVID-19 cases, it is difficult to develop symptoms. Therefore, $t_c = 14$ days is set as the key time period in which the prevention and control measurements are not employed in different countries over the world. Parameters except σ and t_c are estimated by fitting the model to data (cumulatively number of confirmed cases, cumulatively number of recovered cases and cumulatively number of deaths), by the nonlinear least square method as previous study (Cui et al., 2020; Hu et al., 2020; Yu et al., 2021). Definitions of the parameters are shown in Table 1.

According to the model (2.1), the controlled reproductive number R^* is determined by the parameters of the contact rate $c(t)$, the transmission rate p, the detection rate $\delta(t)$, and the recovery rate of γ_I with the following form:

$$R^* = \frac{c(t)p}{\delta(t) + \gamma_I}, \tag{2.4}$$

which indicates the average secondary cases infected by one infected individual in the infectious period.

When $c(t) = c_0$ and $\delta(t) = \delta_0$, the controlled reproductive number R^* is the basic reproductive number R_0

$$R_0 = \frac{c_0 p}{\delta_0 + \gamma_I}. \tag{2.5}$$

It should be noted that although the COVID-19 variations between countries may be caused by different factors, such as different climate factors, population densities, and different responses. In this study, we aim to only employ a reasonable and general model addressing the disease variations to avoid large uncertainties induced by these complex factors.

2.2 Climate classification and selecting the 85 countries

The Köppen-Geiger system classifies climate into five main classes and 30 sub-types. The classification is based on threshold values and seasonality of monthly air temperature and precipitation. The five climatic regions include tropical, arid, temperate, cold, and polar. This classification is identical to that presented by Köppen in 1936 with three differences. First, temperate (C) and cold (D) climates are distinguished using a 0°C threshold instead of a 3°C threshold. Second, the arid (B) sub-climates W (desert) and S (steppe) were identified depending on whether 70% of precipitation occurred in summer or winter. Third, the sub-climates s (dry summer) and w (dry winter) within the C and D climates were made mutually exclusive by assigning s when more precipitation falls in winter than in summer and assigning w otherwise. Note that the tropical (A), temperate (C), cold (D), and polar (E) climates are mutually exclusive but may intersect with the arid (B) class. To account for this, climate type B was given precedence over the other classes. The detailed classification can be found in the Table 2 of the Methods section of Beck et al. (2018).

At April 30, 2020, there are 186 countries reported the COVID-19 cases with the values from 1 to more than 1 million. In this study, we only focus on the countries with a number of cumulative confirmed cases larger than 1,000 are considered and are classified based on the Köppen-Geiger climate classification maps (Figure 2A).

Through April 30, 2020, there were 85 countries with confirmed cases of more than 1,000, which were distributed in the Northern Hemisphere (NH), totaling 78 countries, and in the Southern Hemisphere (SH), totaling 7 countries (Figure 2B). In our study, if a country covers more than two climate types, it will be classified in the climate region with the largest area. Then, for different climate regions, there are 17 countries in the tropical region, 27 countries in the arid region, 16 countries in the temperate region, 24 countries in the cold region, and one country in the polar region (Figure 2B and Table S1). For the simulation and sensitivity analyzes in this study, the focus is on the 85 countries distributed over the five climate regions.

2.3 Hypotheses

A new approach is proposed herein to predict the COVID-19 dynamical behaviors and is based on the following hypotheses.

(1) Two seasons are defined, including a warm season (May to October) and a cold season (November to April).

(2) In the same season, the same climate regions across the NH and SH have the same transmission rates of the SARS-CoV-2 virus. For example, in the warm season, NH and SH have the same transmission rate across the same climate regions.

(3) Because the countries in the NH and SH experience opposite seasons during the same

time period (e.g., from November 2019 to April 2020 defined the cold season in the NH and the warm season in the SH), for the same climate region, the COVID-19 transmission of the countries of the NH in the warm season with a fixed infection rate p^* computed by the data in the countries of the SH is predicted without using the infection rate obtained by the COVID-19 dataset from the cold season, and vice versa.

(4) p^* is established by the COVID-19 data using the SEICR model. To remove the uncertainties of the p^* obtained from the countries in the same climate regions across NH, p^* used in the COVID-19 prediction of the countries in the NH is averaged by the transmission rates of different countries in the SH, and vice versa. For example, for each climate region, the transmission rate of p^* used in predicting the future disease variations in the NH have the following form:

$$p^* = \begin{cases} p_1, & \text{cold} \quad \text{season}, \\ p_2, & \text{warm} \quad \text{season}, \end{cases} \tag{2.6}$$

where p_1 is averaged from the transmission rates of the countries in the NH in the cold season by the data (if available) from November 2019 to April 2020, and p_2 is averaged from the transmission rates of the countries in the SH in the warm season by the data from November 2019 to April 2020.

(5) Since there is no obvious difference in the climate between the warm and cold seasons in tropical regions, the infection rate used in prediction is stilled obtained by the historical data of the countries in the NH and SH, respectively.

(6) When predicting future COVID-19 transmission, it is assumed that immunity to SARS-CoV-2 is not permanent for different scenarios with mR from the recovered individuals to the susceptible individuals again, and $\frac{1}{m}$ is the immune period (in days). The model is as follows:

$$\begin{cases} S' = -\dfrac{c(t)pSI}{N} + mR, \\ E' = \dfrac{c(t)pSI}{N} - \sigma E, \\ I' = \sigma E - (\delta(t) + \gamma_I)I, \\ C' = \delta(t)I - (\alpha_c + \gamma_c)C, \\ R' = \gamma_I I + \gamma_c C - mR, \end{cases} \tag{2.7}$$

In the simulation process, t_c is assumed to be 14 d. The length of the time series for each country is defined as t_*. For the contact rate c_0 and c_f, they are certainly and majorly determined by the population number, population density, culture and travel habits which are difficult to obtain the empirical values. Therefore, they are estimated by fitting model to data. To investigate the impact of immunity and contact parameters on the future transmission period of the COVID-19 pandemic ($t > t_*$), several assumptions were made regarding the immune loss rate m and contact rate c. Immune loss rates are $m = 0$, $\frac{1}{365}$, and $\frac{2}{365}$, which indicate permanent immunity, one year immunity, and half-year immunity, respectively. The corresponding contact rates are $c = c_f, 1.2c_f$, and c_0.

Then, there are nine scenarios for the above immune loss rates and contact rates:

Scenario 1 (S1): $m = 0$, $c = c_f$;.

Scenario 2 (S2): $m = \frac{1}{365}$, $c = c_f$;.

Scenario 3 (S3): $m = \frac{2}{365}$, $c = c_f$;.

Scenario 4 (S4): $m = 0$, $c = 1.2c_f$;.

Scenario 5 (S5): $m = \frac{1}{365}$, $c = 1.2c_f$;.

Scenario 6 (S6): $m = \frac{2}{365}$, $c = 1.2c_f$;.

Scenario 7 (S7): $m = 0$, $c = c_0$;.

Scenario 8 (S8): $m = \frac{1}{365}$, $c = c_0$;.

Scenario 9 (S9): $m = \frac{2}{365}$, $c = c_0$..

2.4 Estimating the parameters and fitting the model

The parameters of model (2.1) and model (2.6) are estimated by the nonlinear least square method by fitting model to the number of cumulative confirmed cases($Y_c(t)$), number of recovered cases($Y_r(t)$), and number of death cases($Y_d(t)$). The objective function for our model (2.1) is

$$L(\theta) = \Sigma_{i=1}^{T}[(C_c(t) - Y_c(t))^2 + (C_d(t) - Y_d(t))^2 + (C_d(t) - Y_r(t))^2]$$

where $dC_c(t)/dt = \delta(t)I, dC_d(t)/dt = \alpha_c C$ and $dC_r(t)/dt = \gamma_c C$. T is the length of the data and $\theta = (E_0, I_0, c_0, \delta_0, \alpha_c, \gamma_I, \gamma_c, c_f, r_b, \delta_f, r_d, p)$.

After obtained the estimated parameters, the simulated COVID-19 data and the predicted COVID-19 data will be computed by the model (2.1) and model (2.7) using the estimated parameters. The model performance (or the simulation accuracy) is quantitatively measured by the correlation coefficient (CC), the relative bias (RB) and the distance between indices of simulation and observation (DISO) as previous studies (Cui et al., 2020; Hu et al., 2020).

The values of the estimated parameters, CC, RB and DISO of the 85 countries are provided in the Table S2 of the supplementary files.

2.5 Framework of this study

From the above analysis, three issues should be emphasised and clarified again. The first issue is that the role of the climate factors on the COVID-19 variations are excluded in this study. The second issue is that a general disease model is established for all the 85 countries across the five different climate regions, and the COVID-19 variations will be analyzed and discussed according to the general model and the COVID-19 data objectively. The last issue is that the general model can not include all the factors (e.g. GDP per capita and population density) impacting the COVID-19 variations. In fact, the detection capacity is mainly determined by the level of the public health system which is largely impacted by the GDP per capita. The contact rate directly reflects the population density. In our model, the detection rate and contact rate are all included. With these issues in mind, the framework of this study is provided in Figure 3 which can help us have a well understanding of the design and structure of this study.

3 Data availability

In this study, the global COVID-19 pandemic data of 85 countries from the date of the first cases of every country to April 30, 2020 is derived from an R package with real-time data(https://github. com/GuangchuangYu/nCov2019). The COVID-19 pandemic data include the number of cumulative confirmed cases, number of recovered cases, and number of death cases. The reason why we chose the data up to April 30, 2020 is that the dataset of the early stage of the COVID-19 transmission has the inherent and the initial characteristics and can avoid many other factors controlled by human activities. The corresponding parameters of the SEICR model established by that period can reflect the initial characteristics.

For each country, the population number is from the 2018 World Health Organization (WHO) data and is considered to be the total population in the simulation and prediction processes. The global shape data were downloaded from https://gadm.org. Global climate is classified into five regions: tropical, arid, temperate, cold, and polar, which is based on the latest Köppen-Geiger climate classification maps at 1-km resolution (Beck, 2018).

4 Results

In this section, the simulation results of the COVID-19 variations and the estimated parameters in Table 1 are firstly provided. Then, we predict the future changes of the COVID-19 pandemic in the 85 countries over different climate regions at nine scenarios with the changes of contact rates and immunity rates.

4.1 Dynamical variations of the present COVID-19 pandemic

COVID-19 was assessed as a pandemic on March 11, 2020 by the WHO with 120,957 cases and 4,390 deaths, and the number of the global cumulative confirmed cases increased to more than 1 million in only 23 days by April 3, 2020. With such rapid transmission, the number of the global cumulative confirmed cases reached more than 2, 4, 6, 8, and 10 million in 24, 12, 21, 16, and 13 d, respectively, which were first reported on April 27, May 9, May 30, June 15, and June 28, 2020, respectively (Figure S1). For the spatial distributions, the United States of America (America), Brazil, India, and Russia contributed to large parts of the global COVID-19 cases (Figures S1C-S1F). The details of the spatial transmission are obtained in supplementary text. The climate classification results and the selected 85 countries are displayed in Figure 1, which are identified by the Köppen-Geiger climate classification maps and the number of the cumulative confirmed cases.

For the simulation, the model (2.1) in this work captured the COVID-19 variations of the cumulative confirmed cases, cumulative recovered cases, and cumulative deaths for the 85 countries distributed over different climate regions (Supplementary Figures S2-S6). The CC values between the observed total cumulative confirmed cases and the simulated total cumulative confirmed cases are nearly to 1. The RB values are smaller than 0.1. And the corresponding comprehensive performances of the model (2.1) are well evaluated with the DISO values nearly to 1 (Table S2).

For tropical regions, the COVID-19 variations of the typical countries of Bolivia, Brazil, Colombia, India, Peru, Philippines, and Singapore are simulated by model (2.1). The cumulative confirmed cases, cumulative recovered cases, and cumulative deaths of Colombia, India, and The Philippines are captured with high accuracy (Figure S2). The variations of cumulative confirmed cases and cumulative deaths of Bolivia and Peru in the SH are well captured.

For typical countries in arid regions, the simulated time series are consistent with the variations of the cumulative confirmed cases, cumulative recovered cases, and cumulative deaths (Figure S3), especially for Chile and Egypt. Moreover, the model has high simulation ability for the countries with confirmed cases larger than 100,000, such as Spain, Turkey, and America. For Mexico and South Africa, the recovered cases are not well captured, which is mainly caused by the quality of the recovered data. The COVID-19 pandemic variations are well simulated in temperate, cold, and polar regions (Figures S4-S6), such as France, Germany, Italy, and Japan in temperate regions (Figures S4) and Canada, Russia, and South Korea in cold regions (Figure S5). The COVID-19 pandemic variations of the other countries over the five climate regions are also well simulated (see Figures S2-S6). For most countries, the CC values are larger than 0.9, and the RB values are smaller than 10%.

The spatial distributions of the corresponding key parameters of the 85 countries are displayed in Figures 4, S7, and S8. Among the 85 countries, six countries have the transmission rates p larger than 0.15, such as Cameroon, Algeria, and Pakistan, followed by 15 countries with an infection rate between 0.1 and 0.15 (i.e., Brazil, Peru, China, and America in Figure 4A). For the basic reproductive number R_0^*, Spain, Germany, South Korea, Spain, and America have the values larger than 10 (Figure 5B), which explains the large number of confirmed cases in these countries (Figures 1A and 1B). Under the current control strategies, the controlled basic reproductive number R_f^* decreased to below the disease transmission threshold value $R_0^* = 1$ in approximately 71% of the countries (Figure 5C). The spatial distributions of the contact rates c_0 at early transmission period and the minimum contact rates c_f in Figures S7 and S8 illustrate the spatial distributions of R_0^* and R_f^*, respectively (Figures 4B and 4C, respectively).

In addition, the averaged parameter values of the 85 countries over the five climate regions using the COVID-19 data before May 1, 2020 were explored (Table 1). The table shows that the contact rate at the early transmission period, c_0, and the minimum contact rate c_f increased from a polar climate to tropical climate with the values ranging from 7.46 to 13.62 and from 0.37 to 8.43, respectively. The transmission rates p in cold and temperate climate regions with the respective values of 0.08 and 0.086 are larger than those in the polar, arid, and tropical climate regions, i.e., 0.055, 0.069, and 0.071, respectively. This result indicates that the COVID-19 pandemic caused by the SARS-CoV-2 virus poses a higher risk for transmission in cold and temperate climate regions than in other climate regions. The basic reproductive number R_0^* of temperate climate regions are the largest compared to those of the other regions at the early transmission period. After some intervention strategies, such as community quarantine, safe social distancing, closing schools and workplaces, limiting the sizes of gathering, and wearing masks, the controlled reproductive number R_f^* values of the five climate regions are 0.03, 0.67, 0.60, 0.81, and 0.94 for polar, cold, temperate, arid, and tropical climate regions, respectively.

Table 2: Parameter values obtained from the simulation, including contact rate at early transmission period, c_0, minimum contact rate c_f, transmission rate p, basic reproductive number R_0^*, and controlled reproductive number R_f^*, which are averaged from the parameter values of COVID-19 data from the 85 countries studied.

Climate regions	c_0	c_f	p	R_0^*	R_f^*
Tropical	13.62	8.43	0.071	4.35	0.94
Arid	11.92	6.99	0.069	4.44	0.81
Temperate	10.62	5.08	0.086	5.99	0.60
Cold	9.62	5.18	0.080	4.17	0.67
Polar	7.46	0.37	0.055	3.93	0.03

According to the above analysis, the cumulative confirmed cases of the countries over the different climate regions have the best simulated accuracy compared with the cumulative recovered cases and deaths due to differences in data quality. Therefore, to investigate COVID-19 pandemic transmission, the focus was on daily new confirmed cases computed from the difference of the cumulative confirmed cases.

4.2 Future risks of the COVID-19 pandemic in different scenarios

In this section, the future changes of the COVID-19 pandemic are explored under nine different scenarios with three contact rates, i.e., $c = c_f, 1.2c_f, and c_0$, indicating the increased contact value, and three immune loss rates, i.e., $m = 0, \frac{1}{365}, and \frac{2}{365}$, indicating permanent immunity, one year immunity, and half-year immunity, respectively. Second outbreak and periodic variations of the COVID-19 pandemic are detected over the five climate regions. The results are displayed in Figures 5-8 and S9-S12.

In tropical climate regions, some obvious periodic variations are obtained in Brazil, Colombia, India, Peru, and Singapore under the conditions of most of Scenarios 4-9 (Figures 5B-5E and 5G). The number of daily new confirmed cases in Bolivia and The Philippines reach their peak values, and then decrease to zero under the nine scenarios, which indicates that the COVID-19 disease will be controlled in the two countries in the future (Figures 5A, 5F). Cameroon, Dominican Republic, Ecuador, Nigeria, Panama, and Puerto Rico exhibit periodic variations of the number of new daily confirmed cases with increased contact rates (Figures S9A, S9C, S9D, and S9G-S9I). Cuba, Ghana, Malaysia, and Thailand will control the disease according to the small number of daily new confirmed cases (Figures S8B, S8E, S9F, and S9J). Moreover, the number of daily new confirmed cases in Bolivia, The Philippines, Cuba, Malaysia, and Thailand will become zero in approximately 200 d (i.e., by the end of 2020). However, more than 1,000 days will be needed to control COVID-19 in Ghana under large contact rates of $c = 1, 2c_f$, and c_0 (Figure S9E).

For the countries in arid climate regions, Chile, Egypt, Mexico, Pakistan, South Africa, Spain, Turkey, and America exhibit multiple periodic variations (Figure 6). Among the aforementioned countries, the periods of Egypt, Mexico, Pakistan, South Africa, Spain, Turkey and America are larger than 1 year. Except for the peak values of the different scenarios for Spain at the same time points (Figure 6I), the other countries have peak values under the different scenarios with different time points. The proposed model successfully predicted the variations of the number of daily new confirmed cases in China (Figure 6B). The number of daily new cases in Iran and Saudi Arabia will become nearly zero in approximately 200 d (Figures 6D and 6G). The number of daily new cases in Afghanistan, Algeria, Bahrain, Iraq, Israel, Kazakhstan, and Kuwait have regular circulations with multiple periods, which indicates that COVID-19 will exist in a long-term period due to the large contact rates mainly caused by the economic recovery (Figure S10).

Except for the number of daily new confirmed cases in Ireland reaching nearly zero in approximately 240 d, the other countries in temperate climate regions have periodic circulations of COVID-19 pandemic transmissions (Figures 7 and S11). Bangladesh, France, Germany, Italy, Japan, New Zealand, Austria, Belgium, Austria, Belgium, Greece, Guinea, Indonesia, and The Netherlands show that the COVID-19 pandemic will reach regular circulation within the period of more than 1 year.

In cold climate regions, several countries exhibit periodic variations of the number of daily new confirmed cases, such as Russia, Sweden, and Armenia (Figures 8B, 8D, and S12A). The number of daily new confirmed cases reaches the peak value in a short time period, and then becomes nearly zero under the different scenarios in countries such as Bulgaria and Solvakia (Figures S12D and S12Q). For Iceland in the polar climate region, the COVID-19 pandemic is controlled under the nine scenarios for future changes (Figure omitted).

5 Discussion

The ongoing COVID-19 pandemic has rapidly spread in more than 200 countries and has caused 157,289,118 cases leading to 3,277,272 deaths according to the data last updated: 2021/5/9, 4:43pm CEST OF WHO COVID-19 Dashboard, and poses a severe threat to public health worldwide. The projection of the transmission dynamics of COVID-19 into the future plays a significant role in devising and implementing prevention and control strategies. In this study, a SEICR model is proposed to investigate the future variations of the COVID-19 pandemic from nine scenarios based on different immune loss rates and contact rates over five different worldwide climate regions.

In the development and constructer of the general SEICR model, the contact rate and the detection rate are considered. In fact, the detection capacity is mainly determined by the level of the public health system which is largely impacted by the GDP per capita. The contact rate directly reflects the population density. It is a huge challenge for a general model to capture the COVID-19 variations for all the 85 countries. Moreover, it is well known that more parameters will caused more uncertainties for a model. Three statistic metrics: CC, RB and DISO are employed to quantify the model performance which suggest that our model can capture the

COVID-19 variations of the 85 countries.

The results obtained from our model are objectively obtained according to the COVID-19 data from the 85 countries. The relationships between the climate factors and the COVID-19 variations or the roles of the climate changes on the COVID-19 are not discussed in this study. We only explore whether there exist COVID-19 transmission differences between the different climate regions. The impacts of the climate factors on the COVID-19 disease will be investigated in our future work with more datasets and new approaches.

Our results show that temperate and cold climate regions have a larger infection rate than arid and tropical climate regions, which illustrates that cold and dry conditions may increase the transmission rate of the SARS-CoV-2 virus. However, it does not mean that a COVID-19 outbreak will not occur in tropical and arid climate regions, because more factors in a complex system contribute to rapid transmission, such as contact rate, medical level, and the quality of the public health system (Hufnagel et al., 2004; Baker et al., 2020; Paraskevis et al., 2021). It should also be considered that our results support the limited role of climate on the transmission of COVID-19 (Baker et al., 2020), rather than cold and dry climates increasing the transmission of the virus, due to the limited data on the current epidemic.

Some recent works try to explore the relationships between climate factors and COVID-19 pandemic which mainly focus on temperature and humidity (Liu et al., 2020; Ma et al., 2020; Meo, et al., 2020; Peter, et al., 2020; Prata et al., 2020). For example, low temperature, mild diurnal temperature range and low humidity likely favor the transmission of COVID-19 (Liu et al., 2020). A positive association is found between daily death counts of COVID-19 and diurnal temperature range (DTR). Absolute humidity is negatively associated with daily death counts of COVID-19 (Ma et al., 2020). A significant decrease in incidence of daily cases and deaths in countries with high temperatures and low humidity (warmest countries), compared to those countries with low temperatures and high humidity (coldest countries) (Meo, et al., 2020). But these results have large uncertainties because the COVID-19 data and climate factor data are insufficient and all the studies only focus on the regional COVID-19 pandemic (Gupta et al., 2020; Liu et al., 2020; Prata et al., 2020). WHO also pointed that there is currently no conclusive evidence that either weather (short term variations in meteorological conditions) or climate (long-term averages) have a strong influence on transmission (https://www.who.int/emergencies/diseases/novel-coronavirus-2019/). Therefore, it must employ more dataset to investigate the effects of climate factors on the COVID-19 transmission. Climatic factors affecting COVID-19 transmission should be cautiously reexamined when the data are sufficient.

Although it may require several months or years to search for effective pharmaceutical treatments and vaccines (Kissler et al., 2020), in this study the following was assumed: permanent immunity with $m = 0$ and duration of immunities with $m = \frac{1}{365}$ and $m = \frac{2}{365}$ (i.e., one year immunity and half-year immunity, respectively) in model (4.1) to explore the COVID-19 variations. Our results suggest that contact rate plays a key role in controlling the disease, while immunity plays a temporary role. In particular, under the same contact rates, the longer immunity period will be beneficial to disease control, but it cannot control disease extinction. When the immunity to SARS-CoV-2 is not permanent, the COVID-19 pandemic exhibits periodic variabilities in some countries of the five climate regions (e.g., Brazil and India in Figures 5B and 5D, respectively), which indicates that the disease will enter into regular circulation as the most recent conclusion (Kissler et al., 2020). If the immunity to SARS-CoV-2 is permanent, the disease could disappear after causing a major outbreak for more than 60 d, such as in Saudi Arabia in Figure 6G.

With the strict disease control measures employed, a small contact rate plays an important role in controlling the COVID-19 pandemic. However, large contact rates (i.e., $c = 1.2c_f$ and $c = c_0$) will result in COVID-19 fluctuations, including some obvious multiple periods, such as in Egypt (Figure 6C), Mexico (Figure 6E), and Germany (Figure 7C). This result suggests that decreasing the contact rate based on the non-pharmaceutical interventions is the most effective means to reduce worldwide transmission of SARS-CoV-2, e.g., by maintaining safe physical distancing, closing schools and workplaces, limiting the sizes of gatherings, wearing face coverings and eye protection, and instituting community quarantines (Chu et al., 2020; Hu et al., 2020; Li et al., 2020).

Since the first COVID-19 case was reported, all the countries and regions of the world have been affected, and peoples' way of life has changed. Comprehensive strategies have been developed to fight against the COVID-19 pandemic by each country based on their specific epidemiological situations, capacities, and the capabilities of their public health systems, especially for low- and middle-income countries. Our findings suggest that this pandemic will spread over all five climate regions in the future which are proved by the present COVID-19 pandemic variations in the world.

The effective strategy to date has been to decrease contact with COVID-19 sufferers, and the reduction of contact rate can help prevent the COVID-19 pandemic from taxing the capacity of public health systems across the globe. Non-pharmaceutical interventions are always the effective strategy in control and prevention the COVID-19 which will may eliminate the COVID-19 pandemic completely together with the roles of the vaccines.

6 Acknowledgements

This study was supported by National Natural Science Foundation of P.R. China [11771373], General Research Fund (Grant Number 15205119) of the Research Grants Council (RGC) of Hong Kong, China and Alibaba (China) Co., Ltd. Collaborative Research project (P0031768), and the Fundamental Research Funds for the Central Universities (GK202007039, GK202003005). All the projects support the data collection, analysis, interpretation and the others processes to the study.

The COVID-19 data are resourced from WHO. The Köppen-Geiger climate classification data is from Beck et al (2018).

7 Data availability statement

The COVID-19 data are sourced from WHO. The Köppen-Geiger climate classification data is from Beck et al (2018).

8 Author contributions

Z. Hu, D. He and Z. Teng developed the structure of this study. Z. Hu, W. Xia, G. Yin, Q. Cui and X. Feng prepared the datasets. Z. Hu, W. Xia, D. He, Q. Cui and X. Feng made the numerical simulations. Z. Hu, G. Yin and Q. Hu designed the spatial analysis. All authors discussed the results and improved the writing of this manuscript.

9 Competing interests

The authors declare no competing interests.

References

[1] Aboubakr, H., Sharafeldin, T. and Goyal, S., Stability of SARS-CoV-2 and other coronaviruses in the environment and on common touch surfaces and the influence of climatic conditions: A review, Transboundary and Emerging Diseases, doi: 10.1111/tbed.13707.

[2] Ali, S., Wanag, L. and Xu, X., 2020, Serial interval of SARS-CoV-2 was shortened over time by nonpharmaceutical interventions, Science, doi:10.1126/science.abc9004.

[3] Araujo MB, Naimi B. Spread of SARS-CoV-2 Coronavirus likely to be constrained by climate. medRxiv 2020; published online March 16. DOI:10.1101/2020.03.12.20034728 (preprint).

[4] Armitage, R., L. B. Nellums, COVID-19 and the consequences of isolating the elderly. Lancet Public Health 5, e256 (2020). doi:10.1016/S2468-2667(20)30061-X Medline.

[5] Baker, R., Yang, W. and Vecchi, G., et al., 2021, Assessing the influence of climate on wintertime SARS-CoV-2 outbreaks, Nature Communications, 12, 846.

[6] Baker, R., Yang, W. and Vecchi, G., 2020, Susceptible supply limits the role of climate in the early SARS-CoV-2-pandemic, Science, 369, 315-319.

[7] Beck, H., Zimmermann, N. and McVicar, T., et al., 2018, Present and future Koppen-Geiger climate classification maps at 1-km resolution, Scientific Data, 5, 180214.

[8] Britton, T., Ball, F. and Trapman, P., et al., Science, A mathematical model reveals the influence of population heterogeneity on herd immunity to SARS-CoV-2, doi: 10.1126/science.abc6810.

[9] Chinazzi, M., J. T. Davis, M. Ajelli, C. Gioannini, M. Litvinova, S. Merler, A. Pastore Y Piontti, K. Mu, L. Rossi, K. Sun, C. Viboud, X. Xiong, H. Yu, M. E. Halloran, I. M. Longini Jr., A. Vespignani, The effect of travel restrictions on the spread of the 2019 novel coronavirus (COVID-19) outbreak. Science 368, 395C400 (2020).

[10] Chu, D., AKl, E. and Duda, S., et al., 2020, Physical distancing, face masks, and eye protection to prevent person-to-person transmission of SARS-CoV-2 and COVID-19: a systematic review and meta-analysis, Lancet, https://doi.org/10.1016/S0140-6736(20)31142-9.

[11] Cohen, M., Corey, L., 2020, Combination prevention for COVID-19, Science, 368, 551.

[12] Cui, Q., Hu, Z. and Han, J., et al., 2020, Dynamic variations of the COVID-19 disease at different quarantine strategies in Wuhan and mainland China, Journal of Infection and Public Health, 13, 849-855, doi.org/10.1016/j.jiph.2020.05.014.

[13] Ferretti, L., Wymant, C. and Kendall, M., et al., 2020, Quantifying SARS-CoV-2 transmission suggests epidemic control with digital contact tracing, Science, 368, eabb6936, DOI: 10.1126/science.abb6936.

[14] Guan, W., Ni, Z. and Hu, Y., 2020, Clinical Characteristics of Coronavirus Disease 2019 in China, The New England Journal of Medicine, 382, 1708-1720.

[15] Gupata, S., Raghuwanshi, G. and Chanda, A., 2020, Effect of weather on COVID-19 spread in the US: A prediction model for India in 2020, Science of the Total Environment, 728, 138860.

[16] Giordano, G., Blanchini, F. and Bruno, R., et al., 2020, Modelling the COVID-19 epidemic and implementation of population-wide interventions in Italy, Nature Medicine, doi: 10.1038/s41591-020-0883-7.

[17] Hao, X., Cheng, S. and Wu, D., et al., Nature, Reconstruction of the full transmission dynamics of COVID-19 in Wuhan, https://doi.org/10.1038/s41586-020-2554-8.

[18] Heesterbeek, H., Anderson, R. and Andreasen, V., et al., 2015, Modeling infectious disease dynamics in the complex landscape of global health, Science 347, aaa4339. DOI: 10.1126/science.aaa4339.

[19] Hsiang, S., Allen, D. and Annan-Phan, S., et al., 2020, The effect of large-scale anti-contagion policies on the covid-19 pandemic, Nature, doi.org/10.1038/s41586-020-2404-8.

[20] Hu, Z., Cui, Q. and Han, J., et al., 2020, Evaluation and prediction of the COVID-19 variations at different input population and quarantine strategies, a case study in Guangdong province, China, International Journal of infectious disease, 95, 231-240.

[21] Hufnagel, L., Brockmann, D. ang Geisel, T., 2004, Forecast and control of epidemics in a globalized world, Proceedings of the National Academy of Sciences of the United States of America, 101, 15124-15129.

[22] Kraemer, M., Yang, C. and Gutierrez, B., 2020, The effects of human mobility and control measures on the COVID-19 epidemic in China, Science ebb4218, doi: 10.1126/science.abb4218.

[23] Lai, S., Ruktanonchai, N., Zhou, L., et al., 2020, Effect of non-pharmaceutical interventions to contain COVID-19 in China. Nature, 585, 410-413.

[24] Lauer, S., Grantz, K. and Bi, Q., et al., 2020, The Incubation Period of Coronavirus Disease 2019 (COVID-19) From Publicly Reported Confirmed Cases: Estimation and Application, Annals of Internal Medicine, 172, 577-582.

[25] Li, Z., Chen, Q. and Feng, et al., 2020, Active case finding with case management: the key to tackling the COVID-19 pandemic, Lancet, 396, 63-70.

[26] Liu, J., Zhou, J. and Yao, J., et al., 2020, Impact of meteorological factors on the COVID-19 transmission: A multicity study in China, Science of the Total Environment, 726, 138513.

[27] Liu, W., Dai, Q. and Bao, J., et al., Influenza activity prediction using meteorological factors in a warm temperate to subtropical transitional zone, Eastern China, Epidemiology and Infection, 147, e325.

[28] Ma, Y., Zhao, Y. and Liu, J., et al., 2020, Effects of temperature variation and humidity on the death of COVID-19 in Wuhan, China, Science of the Total Environment, 724, 138226.

[29] Matteo, C., Jessica, T. and Marco, A., et al., 2020, The effect of travel restrictions on the spread of the 2019 novel coronavirus (COVID-19) outbreak, Science, 368, 395-400.

[30] Meo, S., Abukhalaf, A. and Alomar, A., et al., 2020, Climate and COVID-19 pandemic: effect of heat and humidity on the incidence and mortality in worlds top ten hottest and top ten coldest countries, European Review for Medical and Pharmacological Sciences, 24, 8232-8238.

[31] OReilly, K., Auzenbergs, M. and Jafari, Y., et al., 2020, Effective transmission across the globe: the role of climate in COVID-19 mitigation strategies, Lancet Planetary Health, 5, E172-E172.

[32] Paraskevis, D., Kostaki, E. and Alygizakis, N., et al., 2021, A review of the impact of weather and climate variables to COVID-19: In the absence of public health measures high temperatures cannot probably mitigate outbreaks, Science of the Total Environment, 768, 144578.

[33] Parmet, W. and Sinha, M., Covid-19-The law and limits of quarantine. New England Journal of Medicine (2020), 382, DOI: 10.1056/NEJMp2004211.

[34] Peter, J., Martina, R. and Pavlos, B., et al., 2020, Impact of climate and public health interventions on the COVID-19 pandemic: a prospective cohort study, Canadian Medical Association Journal, 192, E566-E573.

[35] Prata, D., Rodrigues, W. and Bermejo, 2020, Temperature significantly changes COVID-19 transmission in (sub) tropical cities of Brazil, Science of the Total Environment, 729, 138862.

[36] Prem, K., Y. Liu, T. W. Russell, A. J. Kucharski, R. M. Eggo, N. Davies, M. Jit, P. Klepac, S. Flasche, S. Clifford, C. A. B. Pearson, J. D. Munday, S. Abbott, H. Gibbs, A. Rosello, B. J. Quilty, T. Jombart, F. Sun, C. Diamond, A. Gimma, K. van Zandvoort, S. Funk, C. I. Jarvis, W. J. Edmunds, N. I. Bosse, J. Hellewell; Centre for the Mathematical Modelling of Infectious Diseases COVID-19 Working Group, The effect of control strategies to reduce social mixing on outcomes of the COVID-19 epidemic in Wuhan, China: A modelling study. Lancet Public Health 5, e261Ce270 (2020).

[37] Ruktanonchai, N., Floyd, J. and Lai, S., et al., 2020, Assessing the impact of coordinated COVID-19 exit strategies across Europe, Science, 10.1126/science.abc5096 (2020).

[38] Sajadi MM, Habibzadeh P, Vintzileos A, Shokouhi S, Miralles-Wilhelm F, Amoroso A. Temperature, humidity and latitude analysis to predict potential spread and seasonality for COVID-19. SSRN 2020; published online March 5. https://ssrn.com/abstract=3550308(preprint).

[39] Shaman, J., Pitzer, V. and Viboud C, et al., 2010, Absolute humidity and the seasonal onset of influenza in the continental United States. PLoS Biol 8:e1000316.

[40] Sjodin, H., Wilder-Smith, A. and Osman, S., et al., 2020, Only strict quarantine measures can curb the coronavirus disease (COVID-19) outbreak in Italy, 2020, Eurosurveillance, 25, 7-12.

[41] Sundell, N., Andersson, L., Brittain-Long, R., et al.,2016, A four year seasonal survey of the relationship between outdoor climate and epidemiology of viral respiratory tract infections in a temperate climate. Journal of Clinical Virology, 84, 59-63.

[42] Tamerius, J., Shaman, J. and Alonso, W., et al., 2013, Environmental Predictors of Seasonal Influenza Epidemics across Temperate and Tropical Climates, Plos Pathogens, 9, e1003194.

[43] Tang, B., Fang, X. and Tang, S., et al., 2020, The effectiveness of quarantine and isolation determine the trend of the COVID-19 epidemics in the final phase of the current outbreak in China, International Journal of Infectious Diseases, 95, 288-293.

[44] Thorp, H., 2020, Time to pull together, Science, 367, 1282.

[45] Tian, H., Liu, Y. and Li, Y., et al., 2020, An investigation of transmission control measures during the first 50 days of the COVID-19 epidemic in China, Science, doi:10.1126/science.abb6105.

[46] Wang, C., Horby, P. and Hayden, F., et al., 2020, A novel coronavirus outbreak of global health concern. Lancet, 395, 470-473.

[47] Wang J, Tang K, Feng K, Lv W. High temperature and high humidity reduce the transmission of COVID-19. SSRN 2020; published online March 9. https://ssrn.com/ abstract=3551767 (preprint).

[48] World Health Organization, Coronavirus Disease 2019 (COVID-19) Situation Report-121 (WHO, 2020); https://www.who.int/emergencies/diseases/novel-coronavirus-2019/situation-reports.

[49] Wu, Z., McGoogan, J., 2020, Characteristics of and Important Lessons From the Coronavirus Disease 2019 (COVID-19) Outbreak in China Summary of a Report of 72 314 Cases From the Chinese Center for Disease Control and Prevention, Journal of American Medical Association, 323, 1239-1242.

[50] Yang, W., Marr, L. C., 2011, Dynamics of airborne influenza A viruses indoors and dependence on humidity. PLoS One, 6(6).

[51] Yu, D., Zhu, G., Wang, X., et al., 2021, Assessing effects of reopening policies on COVID-19 pandemic in Texas with a data driven transmission model, Infectious Disease Modelling, doi: https://doi.org/10.1016/j.idm.2021.02.001.

[52] Zerhouni, W., Nabel, G., and Zerhouni, E., 2020, Patents, economics, and pandemics, Science, 368, 1035.

[53] Zhang, J., Litvinova, M. and Liang, Y., et al., 2020, Changes in contact patterns shape the dynamics of the COVID-19 outbreak in China, Science, doi:10.1126/science.abb8001 (2020).

[54] Zhou, F., Yu, T. and Du, R., et al., 2020, Clinical course and risk factors for mortality of adult inpatients with COVID-19 in Wuhan, China: a retrospective cohort study, Lancet, 395, 1054-1062.

Future risk evaluation of the global COVID-19 pandemic

Xia Wang[1]*, Gang Yin[2*], Zengyun Hu[3,4*†], Daihai He[5†], Qianqian Cui[6], Xiaomei Feng[7], Zhidong Teng[8]†, Qi Hu[9], Jiansen Li[10]

[1]School of Mathematics and Information Science, Shaanxi Normal University, Xian 710119, China

[2]College of Resource and Environment Science, Xinjiang University, Urumqi, Xinjiang 830046, China

[3]State Key Laboratory of desert and Oasis Ecology, Xinjiang Institute of Ecology and Geography, Chinese Academy of Sciences, Urumqi, Xinjiang 830011, China

[4]Research Center for Ecology and Environment of Central Asia, Chinese Academy of Sciences, Urumqi, Xinjiang 830011, China

[5]Department of Applied Mathematics, Hong Kong Polytechnic University, Hong Kong SAR China

[6]School of Mathematics and Statistics, Ningxia University, Yinchuan, Ningxia 750021, China

[7]School of Mathematics and Informational Technology, Yuncheng University, Yuncheng 044000, China

[8]College of Mathematics and System Sciences, Xinjiang University, Urumqi, Xinjiang 830046, China

[9]School of Natural Resources and Department of Earth and Atmospheric Sciences, University of Nebraska Lincoln, Lincoln, Nebraska

[10]Guangdong Provincial Center for Disease Control and Prevention, Guangzhou 511430, China

---

*These authors contributed equally to this work.

†Corresponding author. Zengyun Hu, email: huzengyun@ms.xjb.ac.cn; Daihai He, email: daihai.he@polyu.edu.hk; Zhidong Teng, emial: zhidong@xju.edu.cn

Figure Captions

Figure 1: Flowchart of COVID-19 SEICR epidemic model.

Figure 2: (A) Climate classification result based on the Köppen-Geiger climate classification maps, where represents the tropical, arid, temperate, cold and polar climate, respectively; (B) 85 countries in the five climate regions.

Figure 3: Framework of this study.

Figure 4: (A) Distributions of the transmission rate p (A); (B) the basic reproductive number R_0^*, and (C) the controlled reproductive number R_f^* of the 85 countries.

Figure 5: Sensitivity analysis of the daily new confirmed cases of Bolivia, Brazil, Colombia, India, Peru, Philippines, and Singapore in tropical region.

Figure 6: Sensitivity analysis of the daily new confirmed cases of Chile, China, Egypt, Iran, Mexico, Pakistan, Saudi Arabia, South Africa, Spain, Turkey, United States in arid region.

Figure 7: Sensitivity analysis of the daily new confirmed cases of Bangladesh, France, Germany, Italy, Japan, New Zealand, and United Kingdom in temperate region.

Figure 8: Sensitivity analysis of the daily new confirmed cases of Canada, Russia, South Korea and Sweden in cold region.

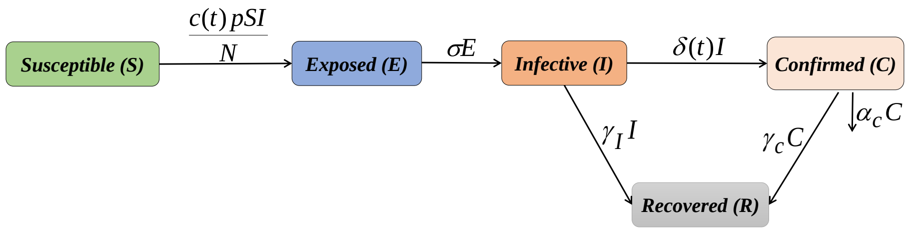

Figure 1: Flowchart of COVID-19 SEICR epidemic model.

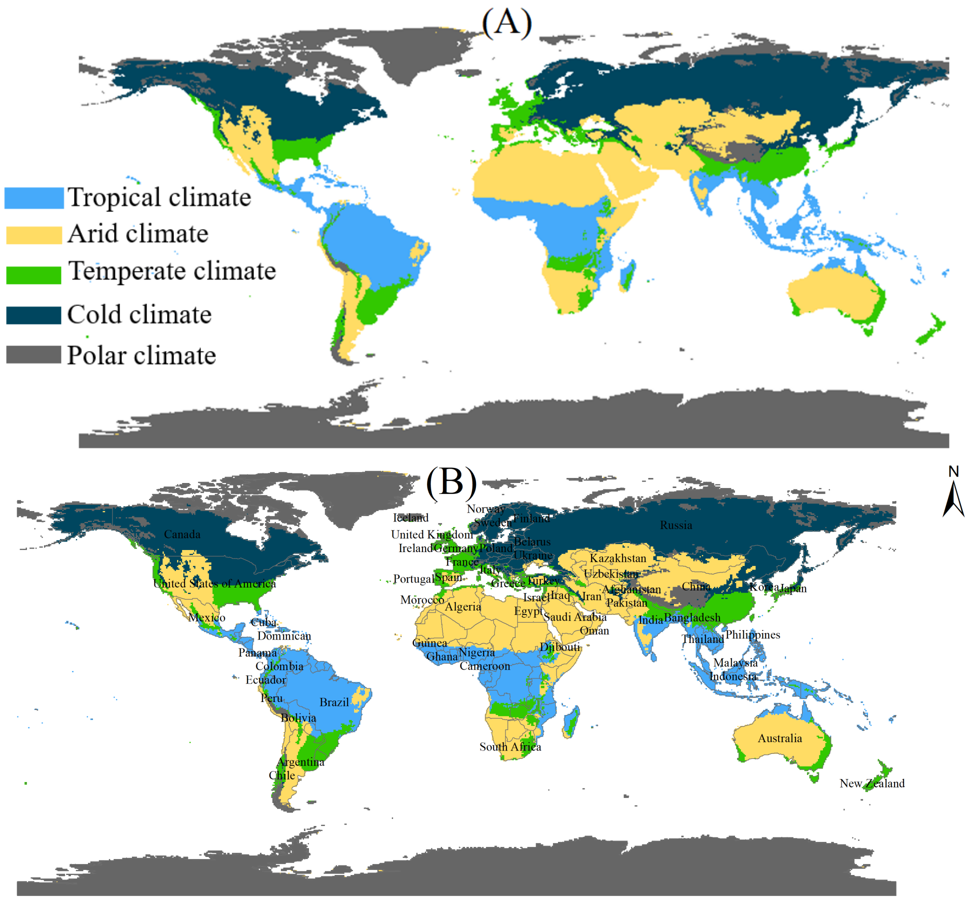

Figure 2: (A) Climate classification result based on the Köppen-Geiger climate classification maps, where represents the tropical, arid, temperate, cold and polar climate, respectively; (B) 85 countries in the five climate regions.

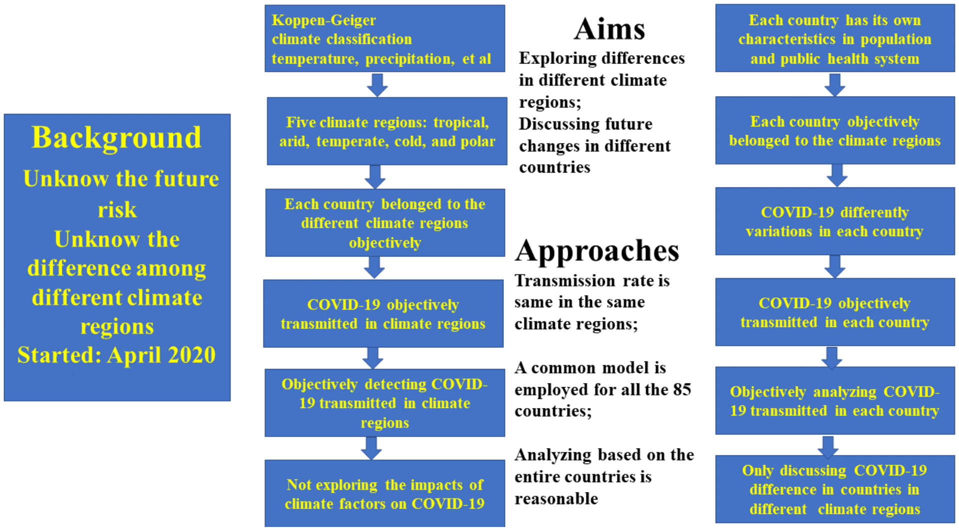

Figure 3: Framework of this study.

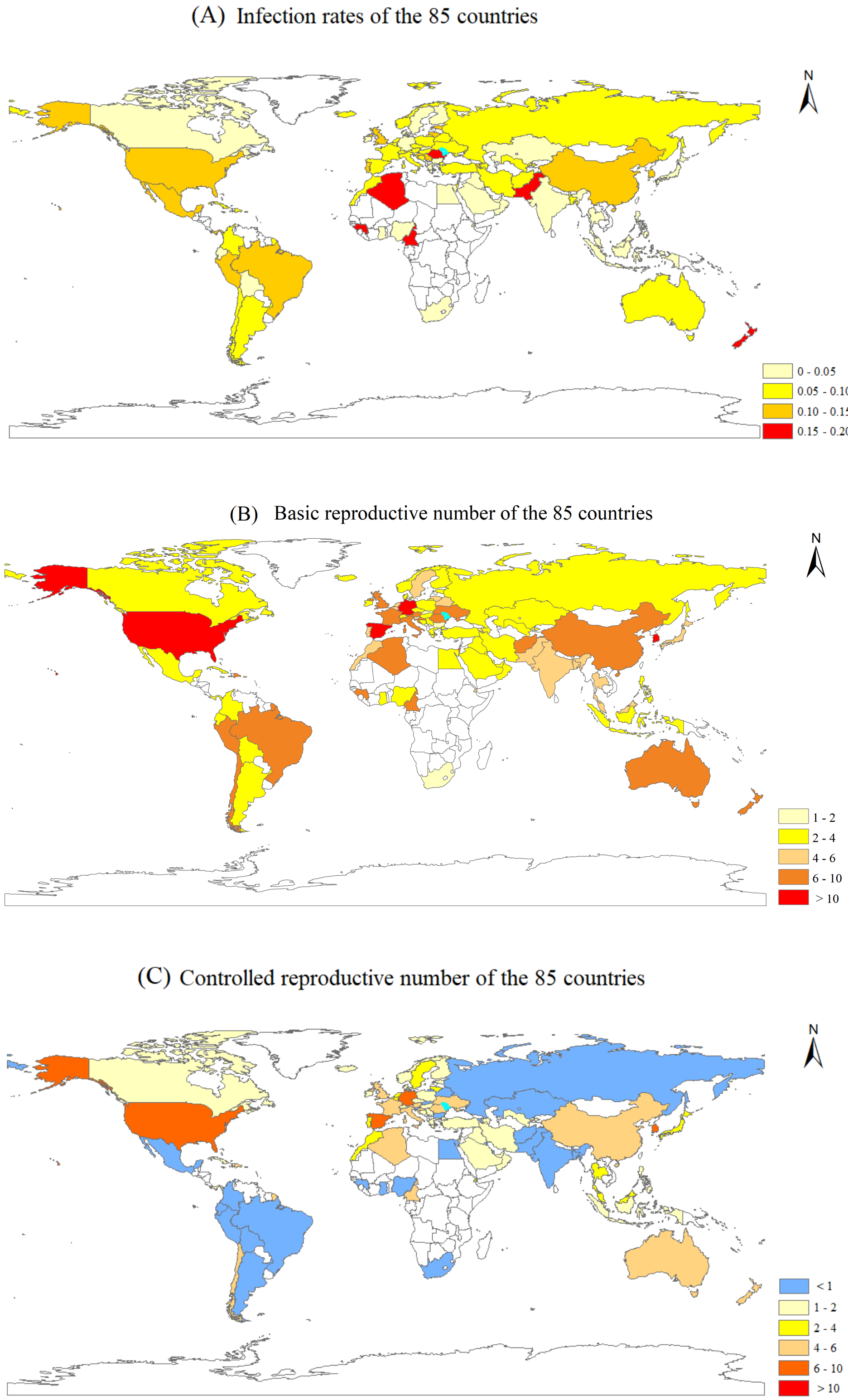

Figure 4: (A) Distributions of the transmission rate p, (B) the basic reproductive number R_0^*, and (C) the controlled reproductive number R_f^* of the 85 countries.

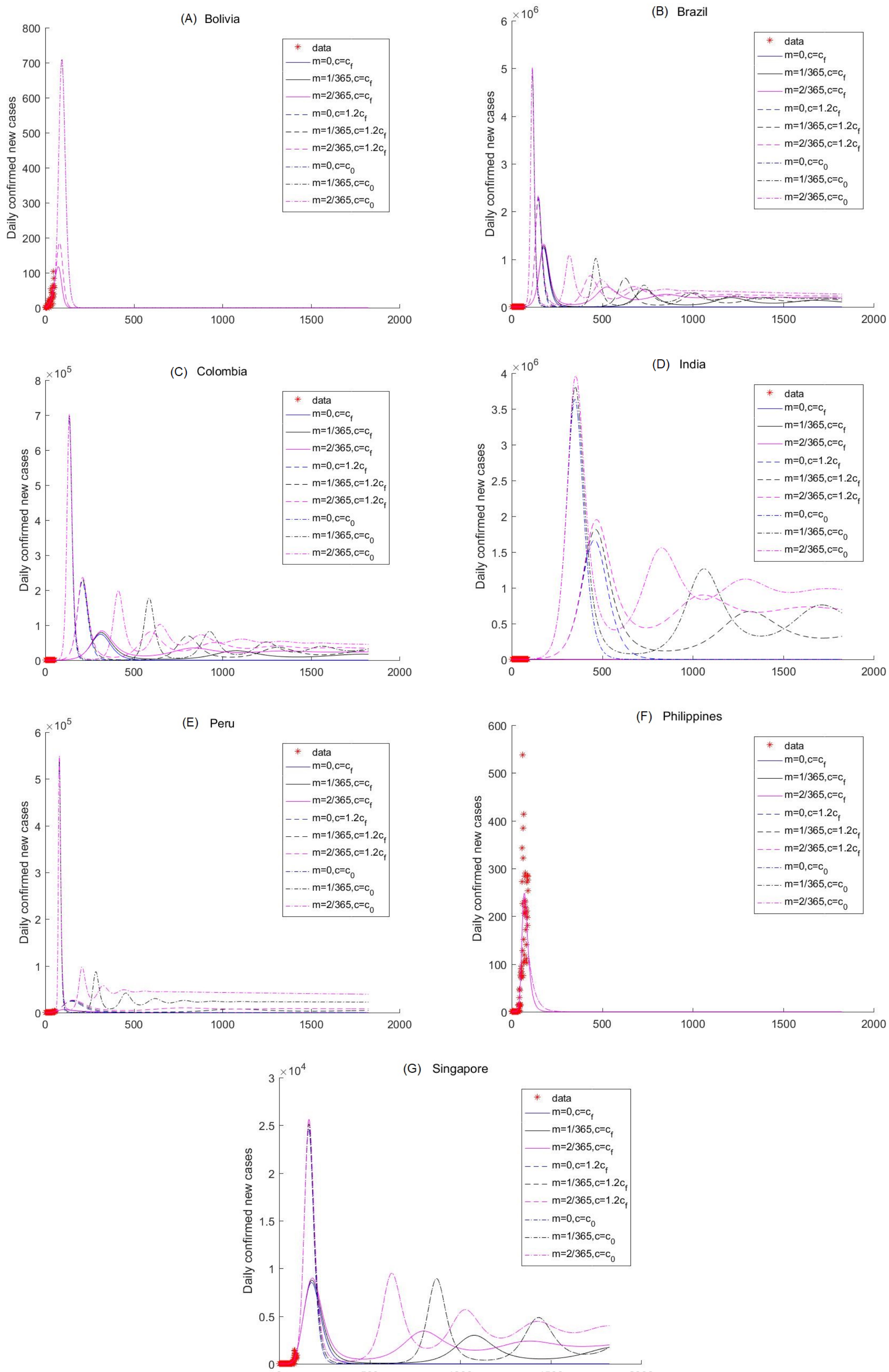

Figure 5: Sensitivity analysis of the daily new confirmed cases of Bolivia, Brazil, Colombia, India, Peru, Philippines, and Singapore in tropical region.

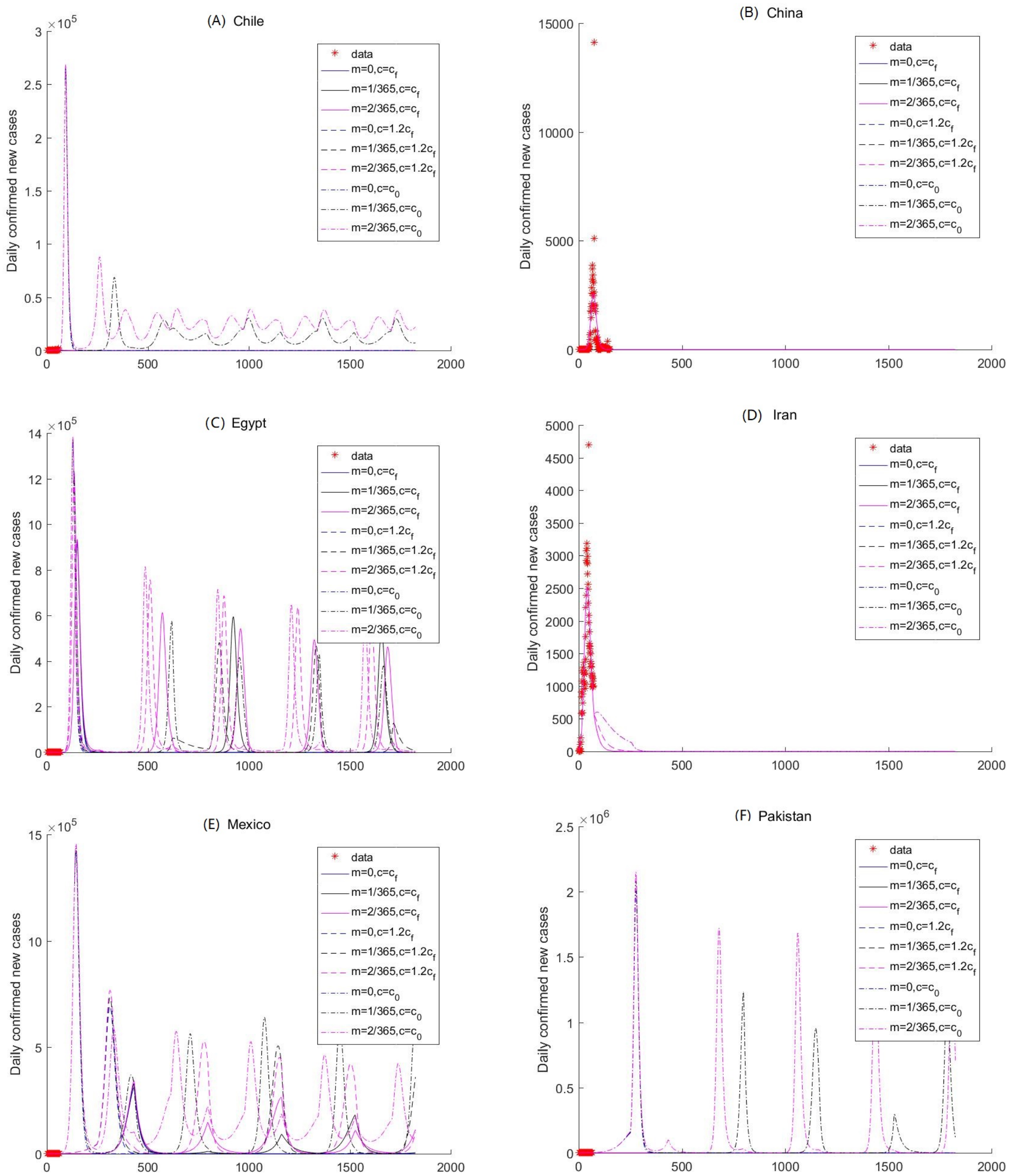
(A) Chile
Daily confirmed new cases
×10^5
data
m=0,c=c_f
m=1/365,c=c_f
m=2/365,c=c_f
m=0,c=1.2c_f
m=1/365,c=1.2c_f
m=2/365,c=1.2c_f
m=0,c=c_0
m=1/365,c=c_0
m=2/365,c=c_0
(B) China
Daily confirmed new cases
data
m=0,c=c_f
m=1/365,c=c_f
m=2/365,c=c_f
m=0,c=1.2c_f
m=1/365,c=1.2c_f
m=2/365,c=1.2c_f
m=0,c=c_0
m=1/365,c=c_0
m=2/365,c=c_0
(C) Egypt
Daily confirmed new cases
×10^5
data
m=0,c=c_f
m=1/365,c=c_f
m=2/365,c=c_f
m=0,c=1.2c_f
m=1/365,c=1.2c_f
m=2/365,c=1.2c_f
m=0,c=c_0
m=1/365,c=c_0
m=2/365,c=c_0
(D) Iran
Daily confirmed new cases
data
m=0,c=c_f
m=1/365,c=c_f
m=2/365,c=c_f
m=0,c=1.2c_f
m=1/365,c=1.2c_f
m=2/365,c=1.2c_f
m=0,c=c_0
m=1/365,c=c_0
m=2/365,c=c_0
(E) Mexico
Daily confirmed new cases
×10^5
data
m=0,c=c_f
m=1/365,c=c_f
m=2/365,c=c_f
m=0,c=1.2c_f
m=1/365,c=1.2c_f
m=2/365,c=1.2c_f
m=0,c=c_0
m=1/365,c=c_0
m=2/365,c=c_0
(F) Pakistan
Daily confirmed new cases
×10^6
data
m=0,c=c_f
m=1/365,c=c_f
m=2/365,c=c_f
m=0,c=1.2c_f
m=1/365,c=1.2c_f
m=2/365,c=1.2c_f
m=0,c=c_0
m=1/365,c=c_0
m=2/365,c=c_0

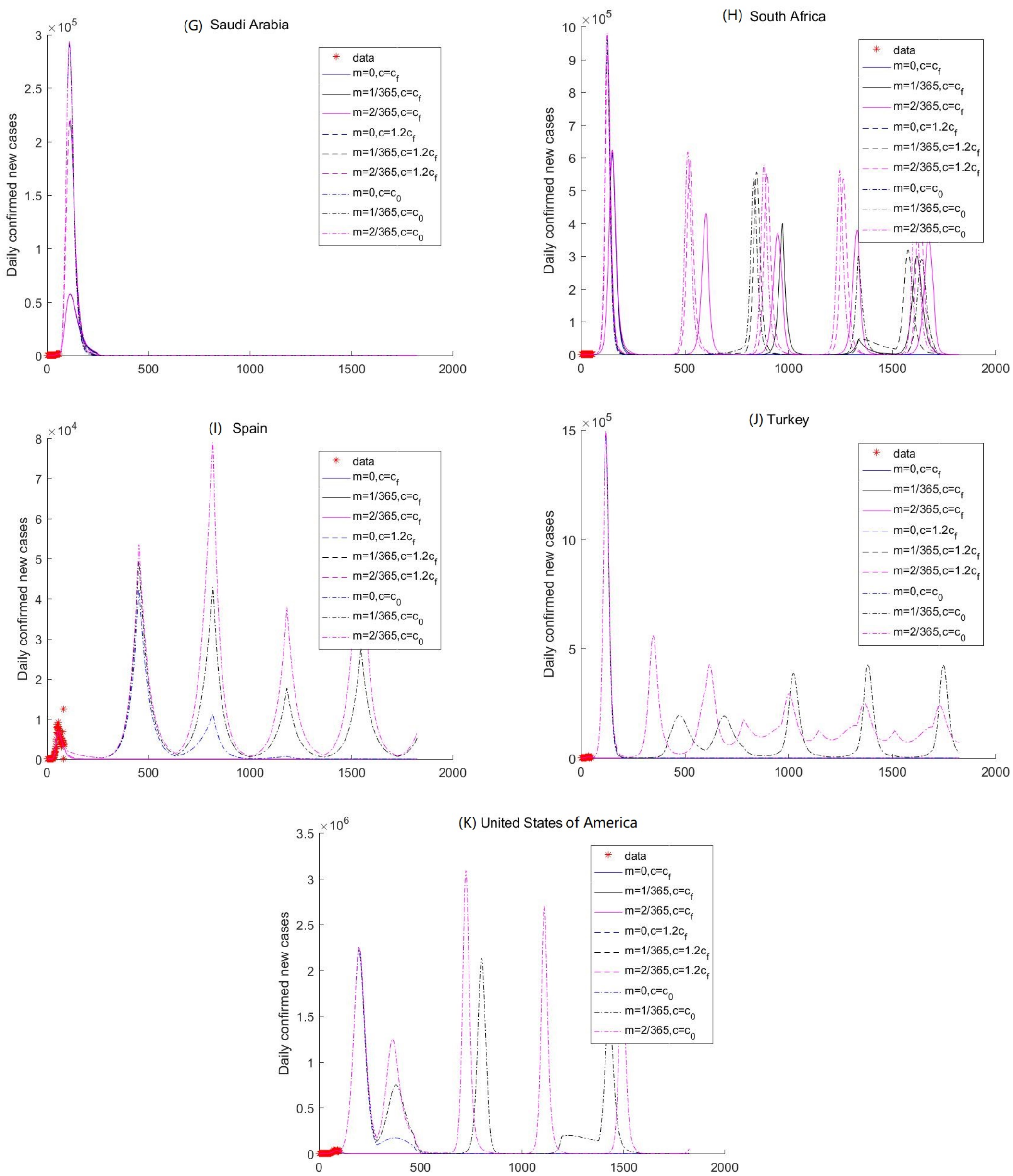

Figure 6: Sensitivity analysis of the daily new confirmed cases of Chile, China, Egypt, Iran, Mexico, Pakistan, Saudi Arabia, South Africa, Spain, Turkey, United States in arid region.

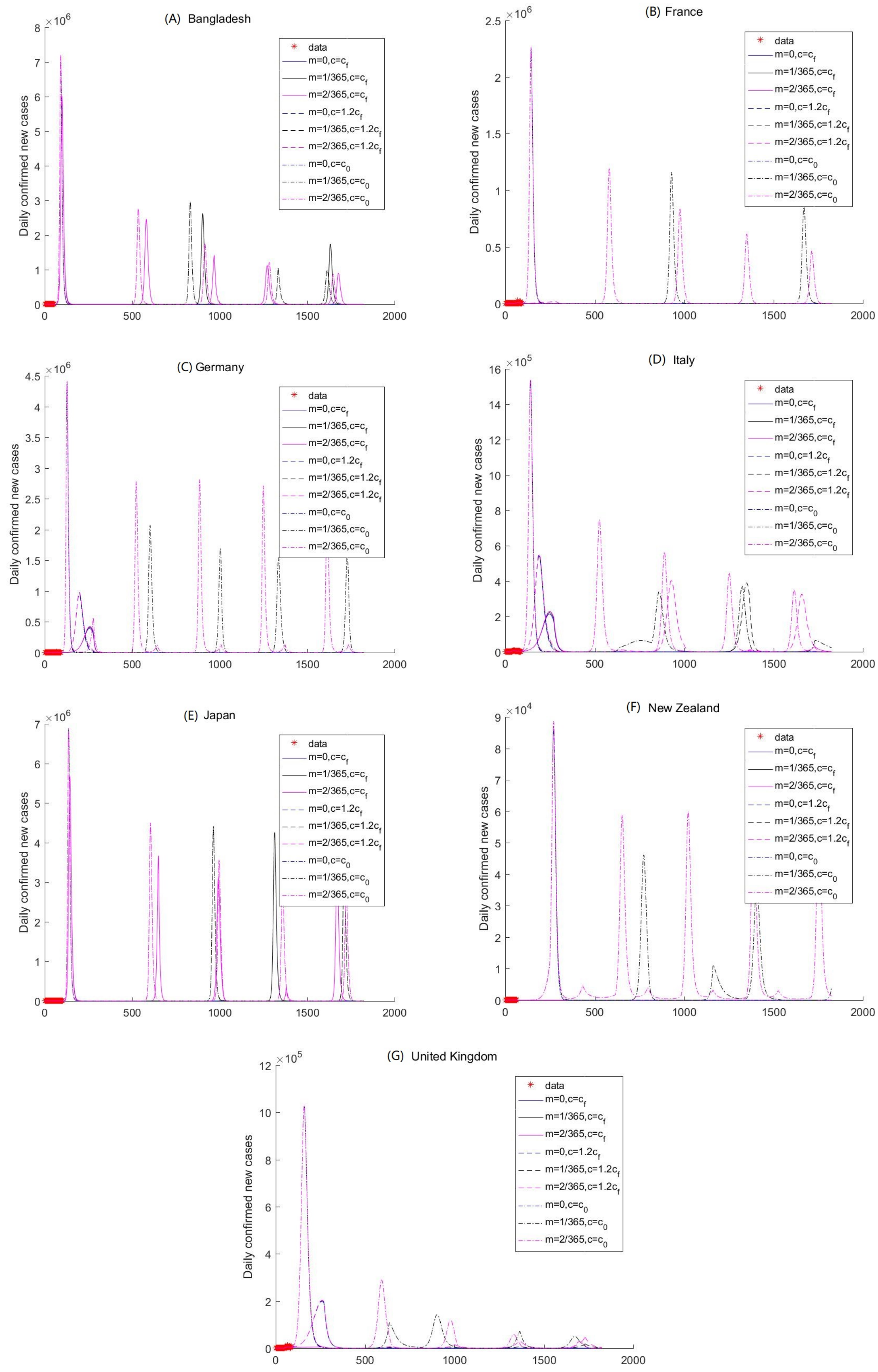

Figure 7: Sensitivity analysis of the daily new confirmed cases of Bangladesh, France, Germany, Italy, Japan, New Zealand, and United Kingdom in temperate region.

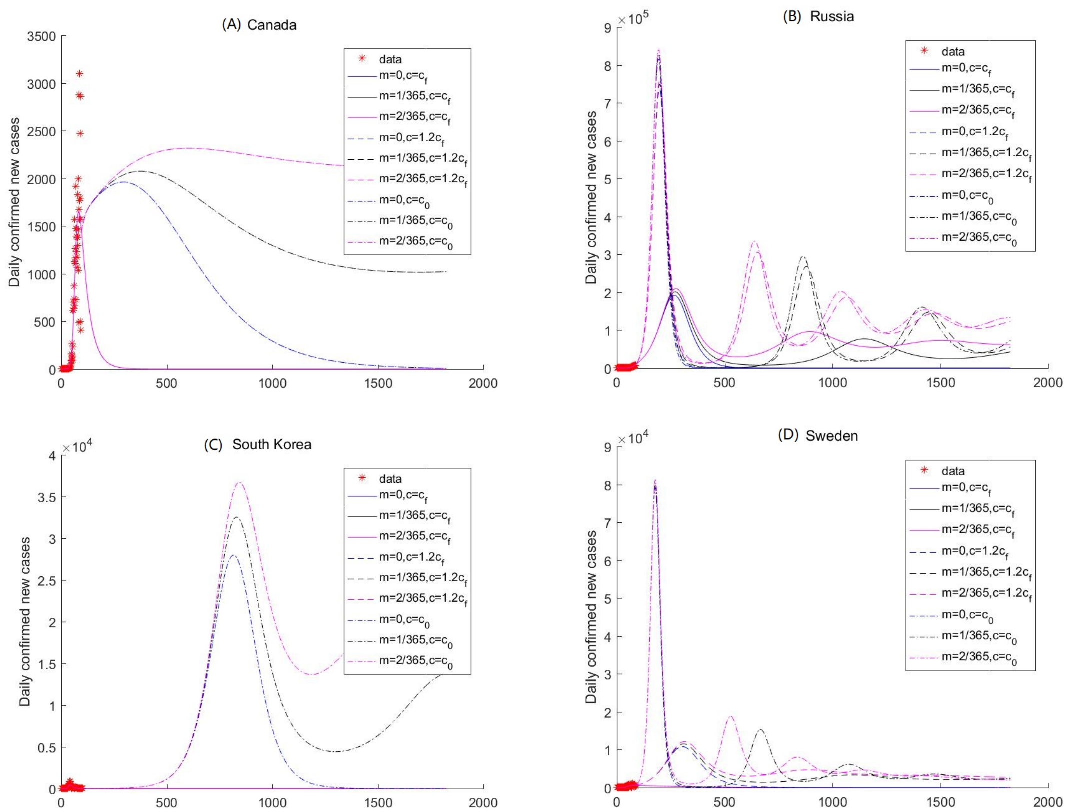

Figure 8: Sensitivity analysis of the daily new confirmed cases of Canada, Russia, South Korea and Sweden in cold region.

Supplementary materials for
Future risk evaluation of the global COVID-19 pandemic

Xia Wang[1*], Gang Yin[2*], Zengyun Hu[3,4*†], Daihai He[5†], Qianqian Cui[6], Xiaomei Feng[7], Zhidong Teng[8†], Qi Hu[9], Jiansen Li[10]

[1]School of Mathematics and Information Science, Shaanxi Normal University, Xian 710119, China

[2]College of Resource and Environment Science, Xinjiang University, Urumqi, Xinjiang 830046, China

[3]State Key Laboratory of desert and Oasis Ecology, Xinjiang Institute of Ecology and Geography, Chinese Academy of Sciences, Urumqi, Xinjiang 830011, China

[4]Research Center for Ecology and Environment of Central Asia, Chinese Academy of Sciences, Urumqi, Xinjiang 830011, China

[5]Department of Applied Mathematics, Hong Kong Polytechnic University, Hong Kong SAR China

[6]School of Mathematics and Statistics, Ningxia University, Yinchuan, Ningxia 750021, China

[7]School of Mathematics and Informational Technology, Yuncheng University, Yuncheng 044000, China

[8]College of Mathematics and System Sciences, Xinjiang University, Urumqi, Xinjiang 830046, China

[9]School of Natural Resources and Department of Earth and Atmospheric Sciences, University of Nebraska Lincoln, Lincoln, Nebraska

[10]Guangdong Provincial Center for Disease Control and Prevention, Guangzhou 511430, China

---

*These authors contributed equally to this work.

†Corresponding author. Zengyun Hu, email: huzengyun@ms.xjb.ac.cn; Daihai He, email: daihai.he@polyu.edu.hk; Zhidong Teng, emial: zhidong@xju.edu.cn

Text S Background of the COVID-19 pandemic

For the spatial diffusions of the COVID-19 pandemic, different countries have significant differences that mainly result from economic restart and increased testing capability (Figure S1). On April 3, 2020, the confirmed cases were mainly distributed over the NH, while the tropical regions of the NH and the SH had a small proportion of confirmed cases. In particular, the United States of America (America), Spain, and Italy had confirmed COVID-19 cases numbering greater than 100,000, i.e., 254,556, 117,710, and 115,242 cases, respectively. The countries with confirmed cases numbering between 80,000 and 100,000 were China (82,875) and Germany (85,122). The countries within Central Asia, Mongolia, and the countries in Africa (except south Africa) had confirmed cases numbering fewer than 1,000 (Figure S1A).

Except for America, Spain, and Italy, the new countries with numbers of confirmed cases greater than 100,000 on April 27, 2020 were Germany (increased from 85,122 to 159,103) and France (increased from 59,929 to 162,220), and the total number of confirmed cases worldwide (2,026,027) was larger than 2 million by the same date (Figure S1B). In fact, America (increased from 254,556 to 987,916), Germany, and France contributed to more than 90% of the increase in confirmed cases. There was no significant increase in South America and Africa at this time.

It only took 12 d for the number of worldwide confirmed cases to increase from 2 million to 4 million by May 9, 2020. The new countries with numbers of confirmed cases larger than 100,000 at this point were Russia (198,676), Turkey (135,569), Iran (106,220), and Brazil (147,003) (Figure S1C). America had the largest number of confirmed cases, i.e., 1,324,352 at this point.

Peru and India were the newest countries with confirmed cases numbering more than 100,000 on May 30, 2020, at which time the total number of confirmed cases worldwide was 6,069,385 (Figure S1D). On June 15 and 28, 2020, the total number of worldwide confirmed cases reached 8,035,398 and 10,138,506, respectively (Figures S1E and S1F, respectively). More than 15 countries had confirmed cases numbering greater than 100,000 at this point, including Brazil, Peru, and South Africa in the Southern Hemisphere (SH) (Figure S1F). America had the largest number of confirmed cases at this point, i.e., 2,597,742, followed by Brazil with 1,319,385 confirmed cases.

Table Captions

Table S1 85 countries in the five climate regions: tropical climate, arid climate, temperate climate, cold climate and polar climate base on the Koppen-Geiger climate classification criteria.

Table S2 12 estimated parameters and 3 statistical metrics (CC: correlation coefficient, AE: absolute error, DISO: distance between indices of simulation and observation) of the 85 countries. Where N, S represent the northern hemisphere and southern hemisphere; A, B, C, D, E represent the tropical climate, arid climate, temperate climate, cold climate and polar climate.

Table S1 85 countries in the five climate regions: tropical climate, arid climate, temperate climate, cold climate and polar climate base on the Koppen-Geiger climate classification criteria.

Climate regions	Countries					
Tropical climate	Bolivia	Brazil	Cameroon	Colombia	Cuba	Dominican Republic
	Ecuador	Ghana	India	Malaysia	Peru	Nigeria
	Panama	Philippines	Puerto Rico	Singapore	Thailand	
Arid climate	Afghanistan	Algeria	Argentina	Australia	Azerbaijan	Bahrain
	Chile	China	Djibouti	Egypt	Iran	Iraq
	Israel	Mexico	Kazakhstan	Kuwait	Morocco	Oman
	Qatar	Saudi Arabia	South Africa	Spain	Turkey	United Arab Emirates
	Uzbekistan					
Temperate climate	Austria	Bangladesh	Belgium	France	Germany	Greece
	Guinea	Indonesia	Ireland	Italy	Japan	Luxembourg
	Netherlands	New Zealand	Portugal	United Kingdom	Netherlands	New Zealand
Cold climate	Armenia	Belarus	Bosnia and Herzegovina	Bulgaria	Canada	Croatia
	Czech Republic	Denmark	Estonia	Finland	Hungary	Lithuania
	Moldova	Norway	Poland	Romania	Russia	Serbia
	Slovakia	Slovenia	South Korea	Sweden	Switzerland	Ukraine
Polar climate	Iceland					

Table S2 12 estimated parameters and 3 statistical metrics (CC: correlation coefficient, AE: absolute error, DISO: distance between indices of simulation and observation) of the 85 countries. Where N, S represent the northern hemisphere and southern hemisphere; A, B, C, D, E represent the tropical climate, arid climate, temperate climate, cold climate and polar climate.

	NA			NB	
	Cuba	India	Philippines	Afghanistan	Algeria
c0	6.473391	17.99993	17.99987	19.18607	11.83355
delta0	0.023963	0.01	0.01	0.01	0.01
alphaC	0.003706	0.003571	0.004335	0.002948	0.014827
gammaI	0.105591	0.177656	0.199994	0.199996	0.199997
gammaC	0.032575	0.024361	0.006633	0.011508	0.045085
cf	1.74794	14.99993	14.99983	4.803405	1.230857
rb	0.39233	0.399998	0.39996	0.268468	0.18541
deltaf	0.668788	0.71	0.670747	0.110002	0.110001
rd	0.081773	0.062332	0.09073	0.05	0.05
p	0.069742	0.036635	0.03927	0.066569	0.151795
R0	3.484791	3.514036	3.366098	6.081999	8.553778
Rf	0.318895	0.889606	0.710822	1.209116	0.714235
relative bias	0.122338	0.119231	0.692627	0.10073	-0.15757
Correlation coefficent	0.999822	0.99982	0.998544	0.998266	0.998802
DISO	0.999997	1.000434	1.001528	1.001473	1.000313

	NB				
	Azerbaijan	Bahrain	China	Djibouti	Egypt
c0	8.006466	17.99999	5.268128	9.368391	12.4351
delta0	0.010031	0.033129	0.01	0.01	0.021189
alphaC	0.001441	0.000373	0.002398	0.000261	0.006995
gammaI	0.188126	0.2	0.071429	0.071429	0.19998
gammaC	0.065094	0.049522	0.046451	0.049952	0.024218
cf	4.980231	14.99999	1.74408	0.100001	9.434349
rb	0.396904	0.399999	0.05	0.093453	0.399866
deltaf	0.546805	0.133129	0.71	0.71	0.121205
rd	0.200461	0.05	0.067832	0.249745	0.075996
p	0.096008	0.022816	0.139062	0.040303	0.038897
R0	3.879173	1.761656	8.996824	4.636904	2.186956
Rf	0.651998	1.104982	0.312708	0.035328	1.172342
relative bias	-0.27053	-0.11486	2.678121	-0.0136	1.361281
Correlation coefficent	0.999377	0.99596	0.993808	0.997008	0.999815
DISO	1.000388	1.000551	0.998805	1.001186	1.000124

	NB				
	Iran	Iraq	Israel	Kazakhstan	Kuwait
c0	11.48556	10.25557	9.496015	18.72308	14.99292
delta0	0.167351	0.010042	0.011043	0.199857	0.060944
alphaC	0.006966	0.005787	0.000891	0.000909	0.000633
gammaI	0.071432	0.148548	0.072022	0.19259	0.199982
gammaC	0.074694	0.069057	0.025218	0.024088	0.034893
cf	8.437349	7.245433	6.441313	13.63191	11.99284
rb	0.399979	0.398494	0.125846	0.399953	0.399958
deltaf	0.867345	0.18063	0.429571	0.305528	0.160945
rd	0.05714	0.159471	0.215372	0.050011	0.07029
p	0.05573	0.032269	0.053925	0.04376	0.042885
R0	2.680642	2.086739	6.164758	2.08774	2.464216
Rf	0.574508	0.711464	0.693061	1.262733	1.449582
relative bias	0.197539	-0.11186	-0.17356	0.060506	-0.24035
Correlation coefficent	0.999093	0.998241	0.999837	0.999291	0.998857
DISO	0.999977	1.000209	1.000029	1.00006	1.001363

	NB				
	Mexico	Morocco	Oman	Pakistan	Qatar
c0	9.952451	5.36876	14.56819	4.971046	16.45529
delta0	0.101969	0.01	0.010008	0.01	0.012526
alphaC	0.017626	0.003791	0.000467	0.002016	0.000105
gammaI	0.177966	0.071429	0.072039	0.199999	0.07151
gammaC	0.092334	0.013672	0.017411	0.02176	0.009826
cf	4.864495	1.591385	11.5562	1.573758	13.45325
rb	0.050027	0.4	0.396649	0.399993	0.399343
deltaf	0.210527	0.71	0.709219	0.110001	0.710101
rd	0.398634	0.083547	0.078516	0.05	0.050006
p	0.106124	0.069903	0.018064	0.185912	0.014681
R0	3.773003	4.608804	3.207461	4.400865	2.874792
Rf	1.448607	0.325895	0.524922	1.117705	1.045745
relative bias	-0.03705	0.472568	-0.09072	0.461512	0.239072
Correlation coefficent	0.999702	0.999244	0.999438	0.999115	0.999178
DISO	1.000374	1.000225	1.000483	1.000489	1.000853

	NB				
	Saudi Arabia	Spain	Turkey	United Arab Emirates	United States
c0	14.47283	9.463395	11.3827	17.99957	9.709275
delta0	0.016991	0.01	0.199988	0.01	0.01
alphaC	0.000881	0.008833	0.002233	0.000698	0.003983
gammaI	0.192148	0.071429	0.103888	0.19875	0.080743
gammaC	0.014987	0.036849	0.021394	0.018224	0.00822

cf	11.45962	6.005123	0.100141	14.99954	6.70927
rb	0.399847	0.072505	0.055116	0.399981	0.05
deltaf	0.716722	0.71	0.299996	0.709996	0.704733
rd	0.059099	0.14808	0.399976	0.062419	0.073671
p	0.031719	0.099154	0.094762	0.036069	0.074129
R0	2.194983	11.52337	3.549625	3.110051	7.931598
Rf	0.964744	0.765848	0.367956	0.831996	0.71783
relative bias	0.322516	0.191984	2.091825	-0.05728	1.155269
Correlation coefficent	0.999093	0.999589	0.999823	0.99909	0.999556
DISO	1.000792	1.000182	1.000008	1.001999	1.000787
	NB	NC			
	Uzbekistan	Austria	Bangladesh	Belgium	Brazil
c0	8.184808	7.340245	18.00005	10.06183	8.761158
delta0	0.043367	0.028074	0.01	0.01	0.010046
alphaC	0.000401	0.002567	0.003281	0.011714	0.01082
gammaI	0.153218	0.072188	0.199957	0.19918	0.137728
gammaC	0.035533	0.053602	0.002955	0.018327	0.072269
cf	5.18463	3.723683	14.99997	7.061719	4.789163
rb	0.061691	0.396964	0.099771	0.050001	0.311581
deltaf	0.743336	0.663903	0.533082	0.677825	0.262098
rd	0.179193	0.219949	0.185108	0.121085	0.301128
p	0.050319	0.082193	0.052614	0.093473	0.126294
R0	2.095041	6.017343	4.510695	4.496172	7.487622
Rf	0.324213	0.415882	1.105406	0.769077	1.512767
relative bias	-0.0399	0.113345	-0.34945	0.611867	-0.2205
Correlation coefficent	0.998905	0.999824	0.999791	0.999844	0.999518
DISO	1.000014	0.999969	1.000353	1.000111	1.000522
	NC				
	Cameroon	Colombia	Dominican Republic	Ecuador	France
c0	9.492254	9.942427	10.69862	17.99999	12.79555
delta0	0.01	0.092983	0.011912	0.2	0.01
alphaC	0.003343	0.003883	0.003811	0.003461	0.009272
gammaI	0.199996	0.130853	0.113308	0.2	0.071429
gammaC	0.04133	0.016915	0.01037	0.006984	0.018066
cf	0.9562	5.575623	1.477094	14.99999	4.673993
rb	0.399995	0.382788	0.393681	0.399999	0.05
deltaf	0.110023	0.197742	0.700477	0.3	0.71
rd	0.05	0.308576	0.071754	0.05	0.072445
p	0.199986	0.072646	0.094498	0.04898	0.06096
R0	9.039745	3.226837	8.073767	2.204122	9.57908
Rf	0.766594	1.232673	0.414111	1.510668	0.436846

relative bias	-0.12169	0.250526	0.57464	1.478985	0.780343
Correlation coefficent	0.991382	0.999287	0.999611	0.979518	0.996487
DISO	1.001216	1.00005	1.000108	1.016614	1.003933

	NC				
	Germany	Ghana	Greece	Guinea	Indonesia
c0	18.81672	17.99728	7.138195	8.770922	6.777624
delta0	0.01	0.015226	0.022894	0.010071	0.042376
alphaC	0.003444	0.000841	0.002706	0.000745	0.006817
gammaI	0.071429	0.071615	0.080468	0.198052	0.071481
gammaC	0.072925	0.009586	0.010581	0.026067	0.010164
cf	6.750704	14.99473	3.41983	1.540469	3.753583
rb	0.05	0.050044	0.386614	0.398491	0.053214
deltaf	0.71	0.11537	0.174496	0.607388	0.356422
rd	0.088863	0.050079	0.142307	0.05013	0.05001
p	0.044817	0.010122	0.035573	0.182876	0.044078
R0	10.35633	2.097721	2.456706	7.706946	2.623829
Rf	0.425942	1.251073	0.478668	1.117939	0.641197
relative bias	0.205364	0.198528	0.206366	0.005824	0.751881
Correlation coefficent	0.999738	0.996198	0.999207	0.998703	0.999776
DISO	1.000168	1.000903	0.999736	1.000927	1.000049

	NC				
	Ireland	Italy	Japan	Luxembourg	Malaysia
c0	6.128225	8.036487	18.00078	11.20151	12.5507
delta0	0.017721	0.01	0.01	0.055575	0.01
alphaC	0.00534	0.008387	0.002033	0.001339	0.001384
gammaI	0.071554	0.074965	0.071431	0.173354	0.094522
gammaC	0.040518	0.017404	0.013883	0.025799	0.047609
cf	3.109068	4.436377	14.99857	0.835687	9.550633
rb	0.050172	0.399963	0.398578	0.399993	0.050002
deltaf	0.717106	0.453987	0.709996	0.155582	0.709997
rd	0.084532	0.163169	0.057109	0.097667	0.086095
p	0.043469	0.0956	0.022466	0.148512	0.038812
R0	2.983888	9.042397	4.96613	7.266669	4.66044
Rf	0.305475	0.802095	0.624021	0.380534	0.489854
relative bias	0.721503	0.467122	-0.38225	0.24839	-0.10463
Correlation coefficent	0.999149	0.999944	0.998472	0.99965	0.99963
DISO	1.000315	1.000007	1.002438	0.999872	1.000169

	NC				
	Netherlands	Nigeria	Panama	Portugal	Puerto Rico
c0	16.18329	16.86809	7.456741	6.046566	18.71613
delta0	0.078154	0.010001	0.155537	0.126875	0.174435
alphaC	0.006923	0.003747	0.001946	0.002144	0.003704
gammaI	0.199996	0.199944	0.197588	0.088246	0.199994
gammaC	0.001	0.024218	0.003841	0.002673	0.001
cf	4.656963	13.86596	3.325681	3.038055	3.814382
rb	0.330706	0.399541	0.294889	0.074671	0.399988
deltaf	0.778153	0.110047	0.25605	0.528075	0.874398
rd	0.05	0.050001	0.050653	0.242884	0.058711
p	0.072154	0.027737	0.119637	0.143682	0.086611
R0	4.198049	2.228556	2.526297	4.038582	4.329348
Rf	0.525921	1.484907	0.921922	0.73089	0.431355
relative bias	0.016501	0.789146	0.092852	0.290766	0.163482
Correlation coefficent	0.999856	0.996418	0.999579	0.999848	0.998105
DISO	0.999981	1.004192	0.999928	0.99998	0.999686

	NC			ND	
	Singapore	Thailand	United Kingdom	Armenia	Belarus
c0	18	18	7.174881	9.349559	17.99991
delta0	0.01	0.01	0.01	0.192244	0.01
alphaC	0.000107	0.001535	0.01029	0.001331	0.000852
gammaI	0.2	0.071429	0.071429	0.085355	0.199858
gammaC	0.008325	0.065163	0.001	0.034402	0.018949
cf	15	15	4.174201	5.159436	14.99986
rb	0.4	0.4	0.064296	0.398786	0.399936
deltaf	0.229108	0.71	0.556076	0.507335	0.382843
rd	0.05	0.070412	0.097263	0.399464	0.170297
p	0.034208	0.021002	0.104852	0.126457	0.051902
R0	2.932092	4.64246	9.238751	4.259079	4.451748
Rf	1.385719	0.458404	0.736565	1.100821	1.343821
relative bias	-0.42694	-0.0288	-0.1548	0.603834	-0.2567
Correlation coefficent	0.993065	0.994608	0.999762	0.997592	0.999299
DISO	1.019029	1.003338	1.000251	0.999863	1.001087

	ND				
	Bosnia and Herzegovina	Bulgaria	Canada	Croatia	Czech Republic
c0	6.478302	17.99998	18	4.240905	10.50122
delta0	0.028147	0.019695	0.01	0.010016	0.179312
alphaC	0.003179	0.003044	0.004967	0.001845	0.00166
gammaI	0.192389	0.130459	0.2	0.071807	0.098007

gammaC	0.027956	0.010958	0.035085	0.032247	0.015252
cf	3.179862	14.99993	15	0.141038	2.039459
rb	0.389094	0.050002	0.4	0.050038	0.15286
deltaf	0.132607	0.119698	0.577441	0.178246	0.28241
rd	0.296674	0.05	0.084935	0.370415	0.088892
p	0.092303	0.010188	0.043834	0.136164	0.095031
R0	2.711418	1.221362	3.757167	7.057327	3.598522
Rf	0.903123	0.779341	0.888414	0.242291	0.514987
relative bias	0.019559	0.188882	0.221225	-0.19582	0.108214
Correlation coefficent	0.999382	0.995255	0.999497	0.999697	0.99977
DISO	0.999925	0.9985	1.000785	1.000006	0.999929

	ND				
	Denmark	Estonia	Finland	Hungary	Lithuania
c0	6.107866	6.143929	14.34974	4.649406	6.149698
delta0	0.04799	0.052792	0.010004	0.019767	0.017288
alphaC	0.004489	0.001348	0.002745	0.008434	0.001774
gammaI	0.072804	0.186411	0.198675	0.071833	0.17696
gammaC	0.054363	0.005906	0.03648	0.013828	0.016418
cf	3.098829	2.614569	10.83475	0.635325	1.517232
rb	0.052364	0.392527	0.063218	0.077137	0.050052
deltaf	0.213865	0.440529	0.426119	0.120369	0.344554
rd	0.084165	0.101748	0.099829	0.05005	0.399874
p	0.04477	0.108735	0.047487	0.067179	0.135536
R0	2.263758	2.792857	3.265411	3.409875	4.290936
Rf	0.537845	0.467721	0.837468	0.355754	0.497941
relative bias	1.066476	0.850237	0.552484	0.103281	0.103745
Correlation coefficent	0.998746	0.998811	0.999651	0.999339	0.998679
DISO	0.999835	0.99964	1.000235	1.000002	0.999841

	ND				
	Moldova	Norway	Poland	Romania	Russia
c0	12.05996	7.368357	9.682529	11.13287	10.54204
delta0	0.012808	0.178133	0.089174	0.010007	0.01
alphaC	0.00257	0.000977	0.003332	0.004484	0.001099
gammaI	0.073539	0.071429	0.071798	0.199817	0.190059
gammaC	0.02089	0.001	0.013673	0.021416	0.010975
cf	9.013071	1.864943	6.614747	0.955953	7.542038
rb	0.310429	0.145819	0.153558	0.182804	0.05
deltaf	0.117477	0.278133	0.326283	0.110057	0.709999
rd	0.275821	0.088392	0.144269	0.050004	0.061107
p	0.022077	0.090918	0.054082	0.173001	0.075265
R0	3.083456	2.684387	3.25308	9.179138	3.966088
Rf	1.041785	0.488644	0.902577	0.636146	1.023346

relative bias	0.149725	0.185195	0.271386	-0.18828	0.396332
Correlation coefficent	0.999242	0.999406	0.999903	0.999734	0.999544
DISO	1.000153	0.99973	1.000002	1.000069	1.001501

	ND				
	Serbia	Slovakia	Slovenia	South Korea	Sweden
c0	4.086788	10.14991	6.900642	5.793026	10.64219
delta0	0.052178	0.015447	0.08138	0.01	0.010024
alphaC	0.001632	0.000833	0.002568	0.000964	0.007685
gammaI	0.084019	0.071429	0.105732	0.071429	0.103098
gammaC	0.011131	0.017933	0.00684	0.031809	0.002888
cf	1.032082	7.149813	2.591537	2.739499	6.229471
rb	0.060297	0.050001	0.332845	0.086901	0.313593
deltaf	0.490176	0.715444	0.182539	0.709999	0.214989
rd	0.065146	0.085174	0.081802	0.1987	0.097353
p	0.121694	0.01	0.044453	0.14743	0.049685
R0	3.65161	1.168347	1.639397	10.48842	4.67417
Rf	0.386431	0.19421	0.408836	0.517182	0.986335
relative bias	0.246419	0.224956	0.088009	0.147601	2.210679
Correlation coefficent	0.999301	0.997907	0.999488	0.99728	0.999683
DISO	1.000138	0.999494	0.999703	0.999014	1.000216

	ND		NE	SA	
	Switzerland	Ukraine	Iceland	Bolivia	Peru
c0	10.31769	10.22659	7.459023	10.01187	12.59996
delta0	0.081772	0.010206	0.032352	0.01	0.01
alphaC	0.004267	0.002476	0.000402	0.00528	0.003876
gammaI	0.145388	0.073033	0.071598	0.199984	0.199998
gammaC	0.052118	0.009228	0.056206	0.007565	0.045943
cf	1.874143	2.441369	0.368887	6.090962	2.201096
rb	0.050066	0.380431	0.229365	0.399978	0.218712
deltaf	0.44988	0.218734	0.728983	0.709337	0.110001
rd	0.255594	0.099513	0.083182	0.050001	0.05
p	0.086883	0.075355	0.054769	0.042801	0.136258
R0	3.946274	9.258054	3.929978	2.040719	8.175553
Rf	0.364765	0.734191	0.034062	1.006105	1.202916
relative bias	0.01713	0.499648	-0.02387	0.129968	-0.20721
Correlation coefficent	0.999809	0.999879	0.999092	0.999038	0.998669
DISO	0.999969	1.00009	0.999683	1.000201	1.001295

	SB			SC	
	Argentina	Australia	Chile	South Africa	New Zealand
c0	10.11513	6.483388	17.05675	16.59293	7.523986
delta0	0.199939	0.01	0.010001	0.2	0.010097

alphaC	0.003851	0.000828	0.001486	0.0015	0.000765
gammaI	0.071534	0.071429	0.199987	0.2	0.17202
gammaC	0.021153	0.048676	0.051542	0.027286	0.055639
cf	7.111305	3.464129	2.168132	13.4288	0.101654
rb	0.399958	0.05	0.39998	0.399999	0.117325
deltaf	0.540229	0.71	0.11002	0.3	0.251505
rd	0.39999	0.084629	0.050001	0.05	0.217022
p	0.093931	0.080612	0.091104	0.041954	0.153375
R0	3.49989	6.418324	7.400119	1.740335	6.336556
Rf	1.09188	0.386945	0.783284	1.165253	0.045393
relative bias	0.045542	0.196499	-0.16595	1.048383	-0.06725
Correlation coefficent	0.999734	0.993513	0.999147	0.994234	0.999802
DISO	0.999986	1.003262	1.000228	0.999523	0.999976

Figure Captions

Figure S1: Spatial distributions of the cumulative confirmed COVID-19 cases over the world, for the numbers of 1 million cases (A), 2 millions cases (B), 4 millions cases (C), 6 millions cases (D), 8 millions cases (E), and 10 millions cases (F).

Figure S2: Simulation results of the cumulative confirmed cases, cumulative recovered cases, and cumulative deaths of Bolivia, Brazil, Cameroon, Colombia, Cuba, Dominican Republic, Ecuador, Ghana, India, Malaysia, Nigeria, Panama, Peru, Philippines, Puerto Rico, Singapore and Thailand in tropical region.

Figure S3: Simulation results of the cumulative confirmed cases, cumulative recovered cases, and cumulative deaths of Afghanistan, Algeria, Argentina, Australia, Azerbaijan, Bahrain, Chile, China, Djibouti, Egypt, Iran, Iraq, Israel, Kazakhstan, Kuwait, Mexico, Morocco, Oman, Pakistan, Qatar, Saudi Arabia, South Africa, Spain, Turkey, United Arab Emirates, United States and Uzbekistan in arid region.

Figure S4: Simulation results of the cumulative confirmed cases, cumulative recovered cases, and cumulative deaths of Austria, Bangladesh, Belgium, France, Germany, Greece, Guinea, Indonesia, Ireland, Italy, Japan, Luxembourg, Netherlands, New Zealand, Portugal and United Kingdom in temperate region.

Figure S5: Simulation results of the cumulative confirmed cases, cumulative recovered cases, and cumulative deaths of Armenia, Belarus, Bosnia and Herzegovina, Bulgaria, Canada, Croatia, Czech Republic, Denmark, Estonia, Finland, Hungary, Lithuania, Moldova, Norway, Poland, Romania, Russia, Serbia, Slovakia, Slovenia, South Korea, Sweden, Switzerland and Ukraine in cold region.

Figure S6: Simulation results of the cumulative confirmed cases, cumulative recovered cases, and cumulative deaths of Iceland in polar region.

Figure S7: Distribution of the contact rates c_0 at early transmission period of the 85 countries.

Figure S8: Same as Figure S6, but for the minimum contact rates c_f.

Figure S9: Sensitivity analysis of the daily new confirmed cases of Cameroon, Cuba, Dominican Republic, Ecuador, Ghana, Malaysia, Nigeria, Panama, Puerto Rico, and Thailand in tropical region.

Figure S10: Sensitivity analysis of the daily new confirmed cases of Afghanistan, Algeria, Argentina, Austrialia, Azerbaijan, Bahrain, Djibouti, Iraq, Israel, Kazakstan, Kuwait, Morocco, Oman, Qatar, United Arab Emirates and Uzbekistan in arid region.

Figure S11: Sensitivity analysis of the daily new confirmed cases of Austria, Belgium, Greece, Guinea, Indonesia, Ireland, Luxembourg, Netherlands, and Portugal in temperate region.

Figure S12: Sensitivity analysis of the daily new confirmed cases of Armenia, Belarus, Bosnia and Herzegovina, Bulgaria, Croatia, Czech Republic, Denmark, Estonia, Finland, Hungary, Lithuania, Moldova, Norway, Poland, Romania, Servia, Slovakia, Slovenia, Switzerland, and Ukraine in cold region.

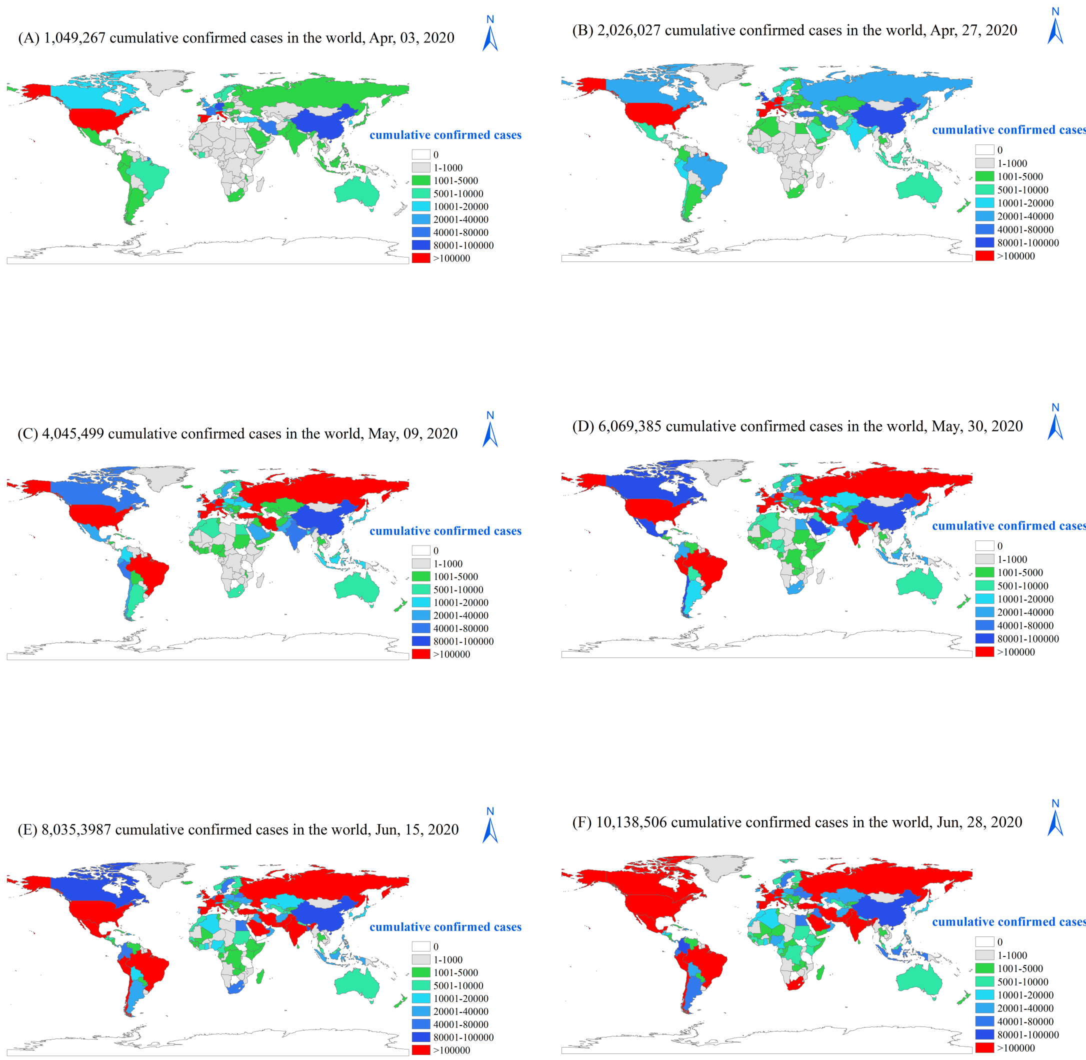

Figure S1: Spatial distributions of the cumulative confirmed COVID-19 cases over the world, for the numbers of 1 million cases (A), 2 millions cases (B), 4 millions cases (C), 6 millions cases (D), 8 millions cases (E), and 10 millions cases (F).

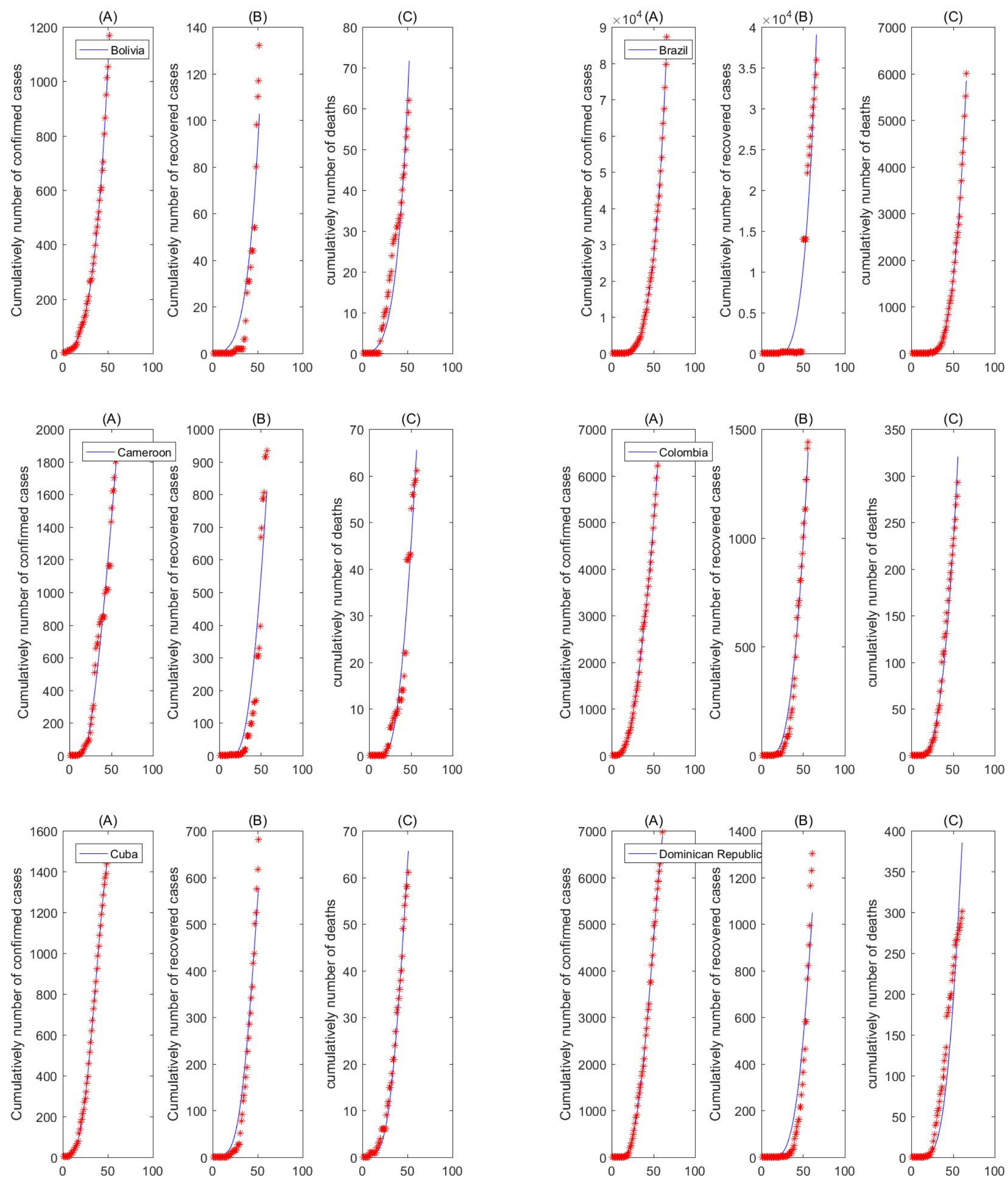

(A)
(B)
(C)
Bolivia
Brazil
Cameroon
Colombia
Cuba
Dominican Republic
Cumulatively number of confirmed cases
Cumulatively number of recovered cases
cumulatively number of deaths
×10^4

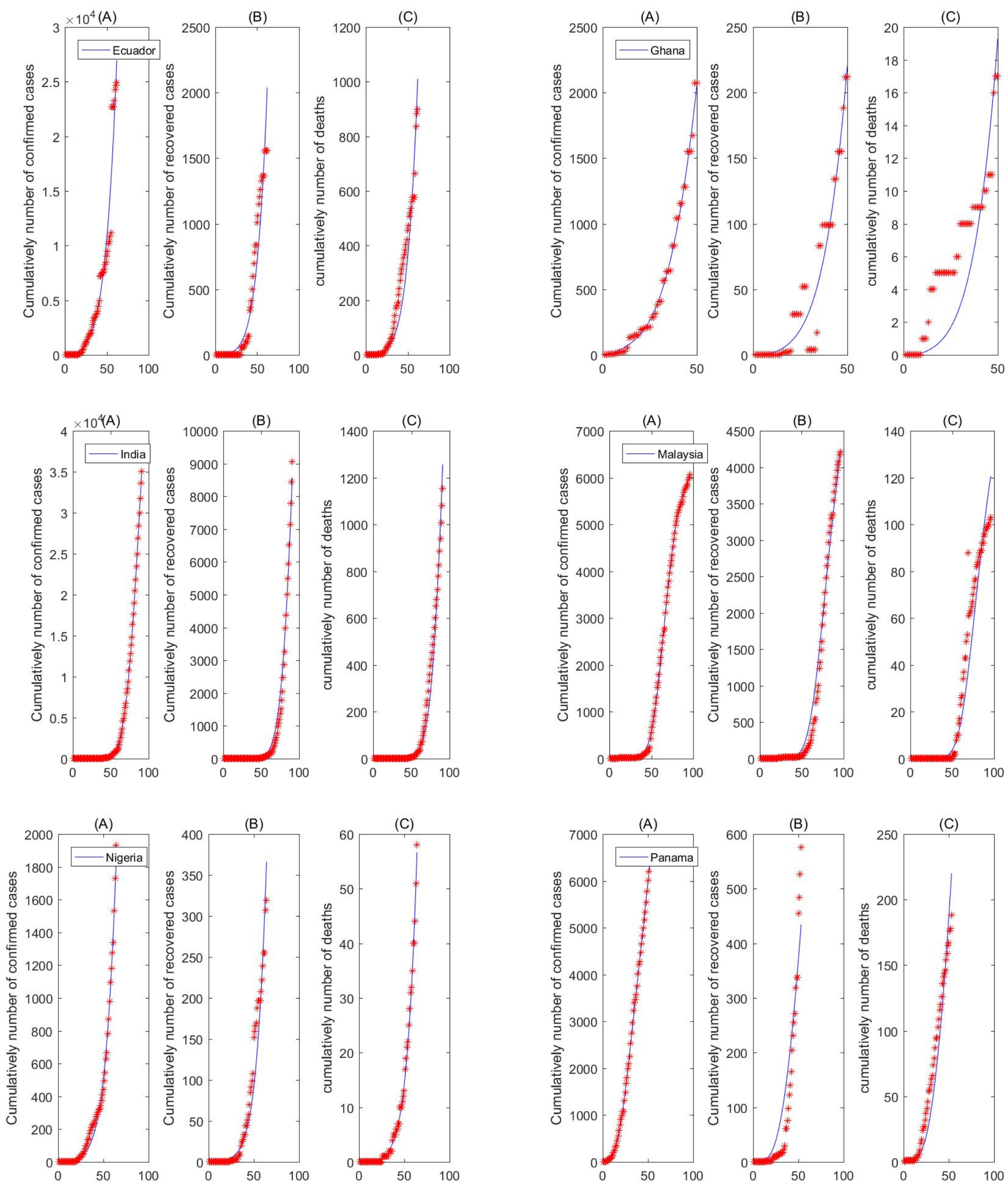
(A)
(B)
(C)
Ecuador
Ghana
India
Malaysia
Nigeria
Panama
$\times 10^4$
Cumulatively number of confirmed cases
Cumulatively number of recovered cases
cumulatively number of deaths

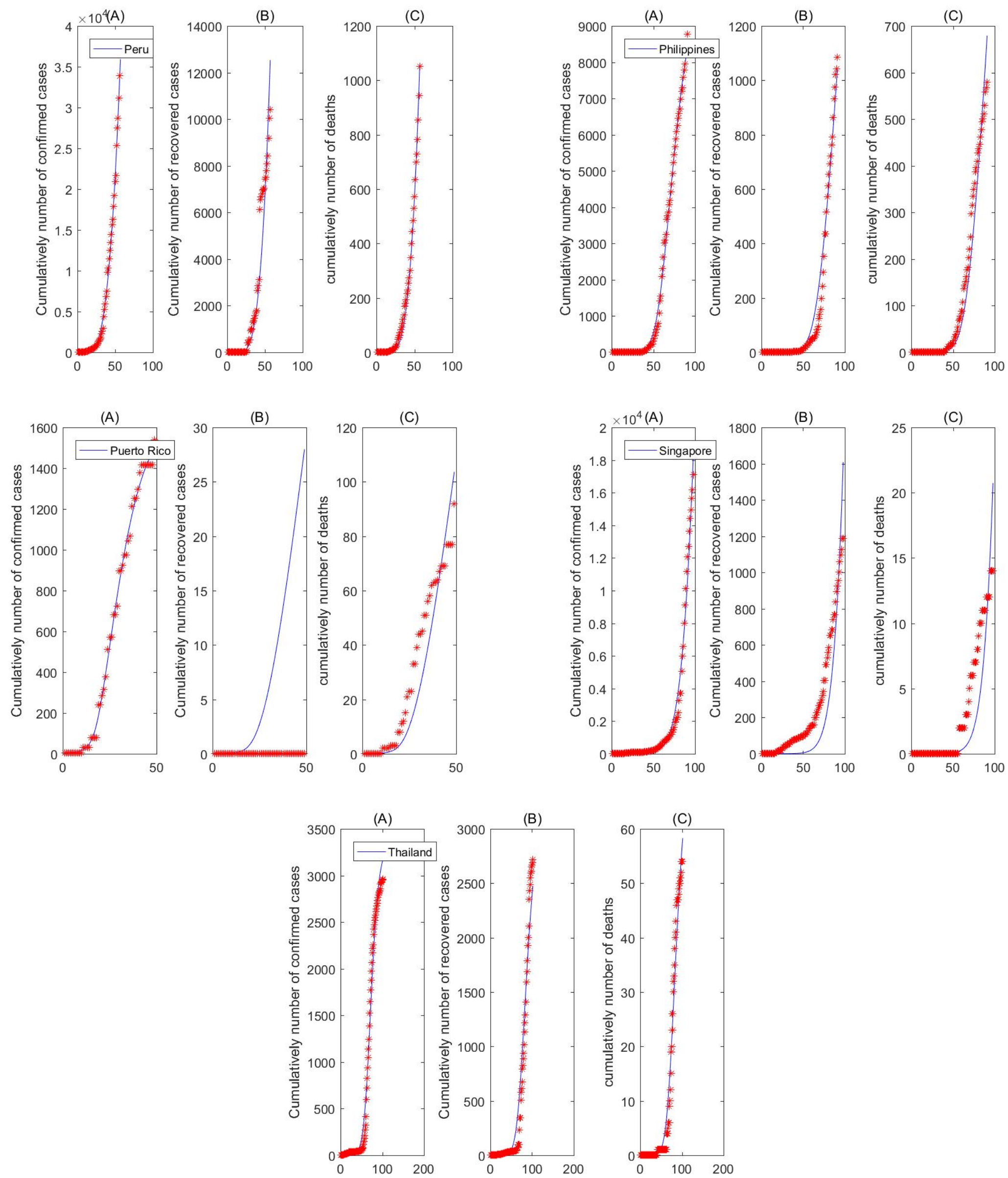

Figure S2: Simulation results of the cumulative confirmed cases, cumulative recovered cases, and cumulative deaths of Bolivia, Brazil, Cameroon, Colombia, Cuba, Dominican Republic, Ecuador, Ghana, India, Malaysia, Nigeria, Panama, Peru, Philippines, Puerto Rico, Singapore and Thailand in tropical region.

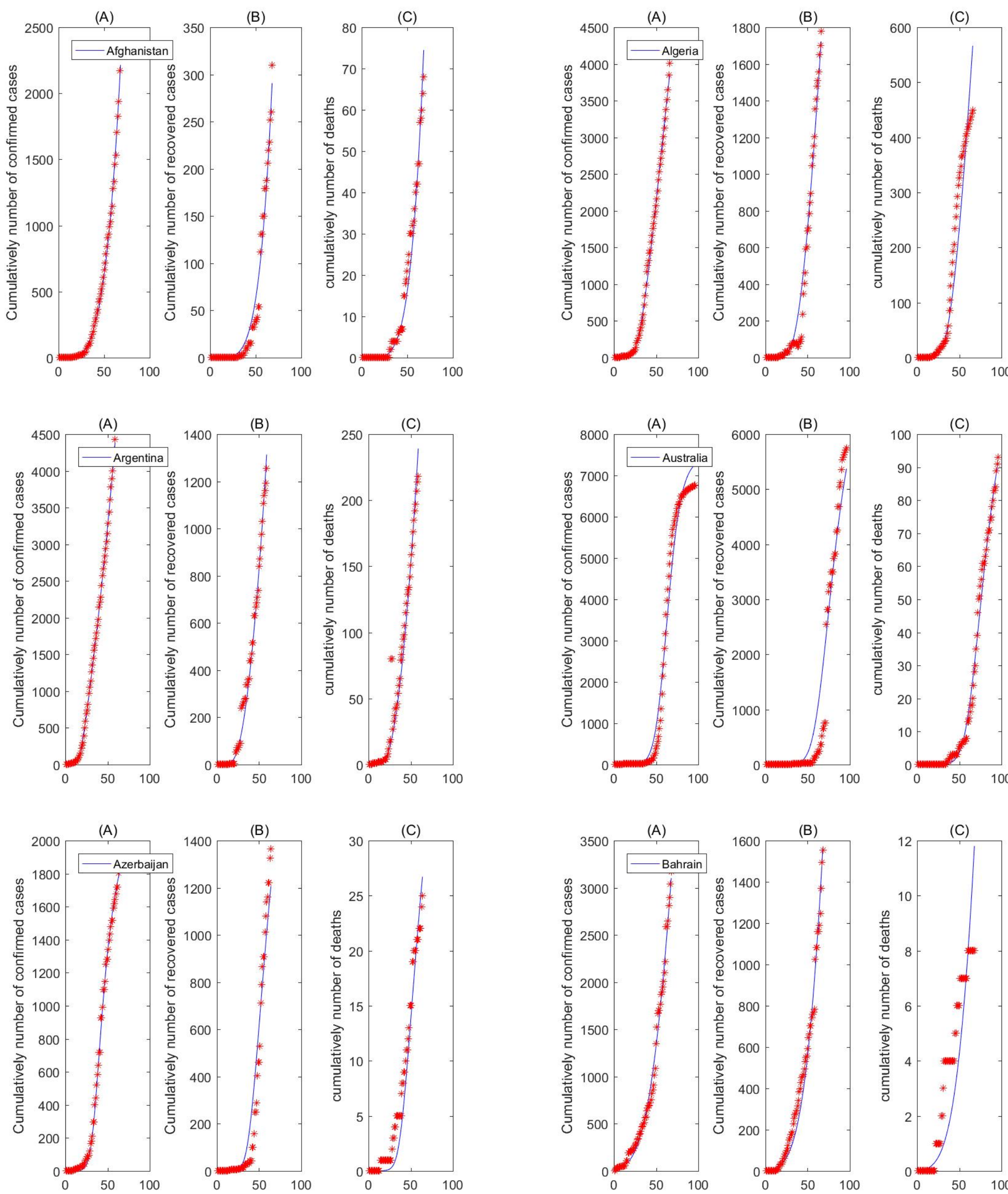
(A)
(B)
(C)
Afghanistan
Algeria
Argentina
Australia
Azerbaijan
Bahrain
Cumulatively number of confirmed cases
Cumulatively number of recovered cases
cumulatively number of deaths

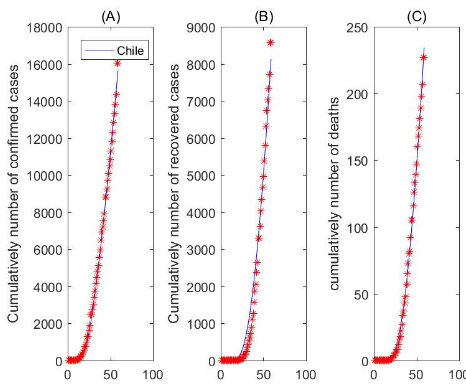
(A)
(B)
(C)
Chile
Cumulatively number of confirmed cases
Cumulatively number of recovered cases
cumulatively number of deaths

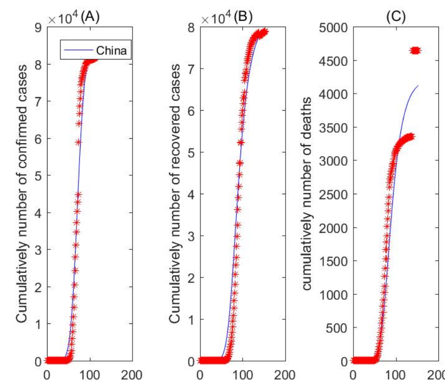
(A)
(B)
(C)
China
Cumulatively number of confirmed cases
Cumulatively number of recovered cases
cumulatively number of deaths

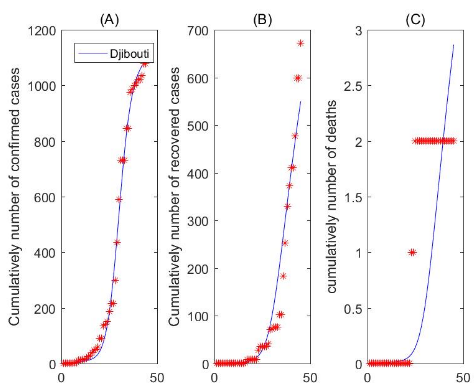
(A)
(B)
(C)
Djibouti
Cumulatively number of confirmed cases
Cumulatively number of recovered cases
cumulatively number of deaths

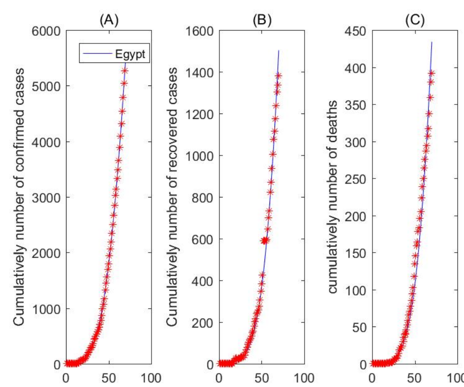
(A)
(B)
(C)
Egypt
Cumulatively number of confirmed cases
Cumulatively number of recovered cases
cumulatively number of deaths

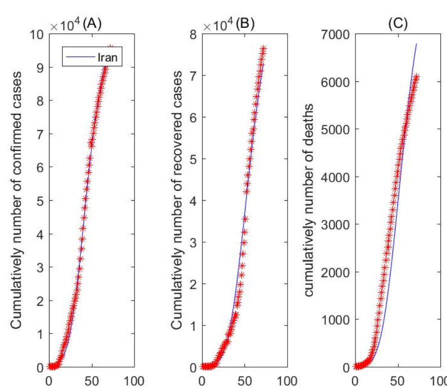
(A)
(B)
(C)
Iran
Cumulatively number of confirmed cases
Cumulatively number of recovered cases
cumulatively number of deaths

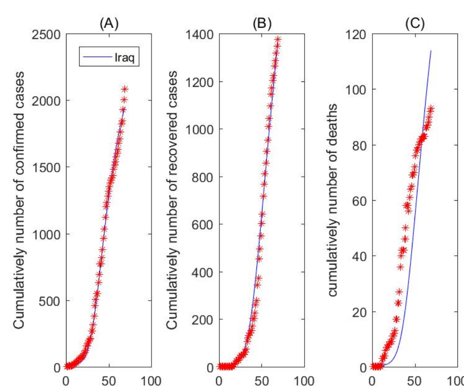
(A)
(B)
(C)
Iraq
Cumulatively number of confirmed cases
Cumulatively number of recovered cases
cumulatively number of deaths

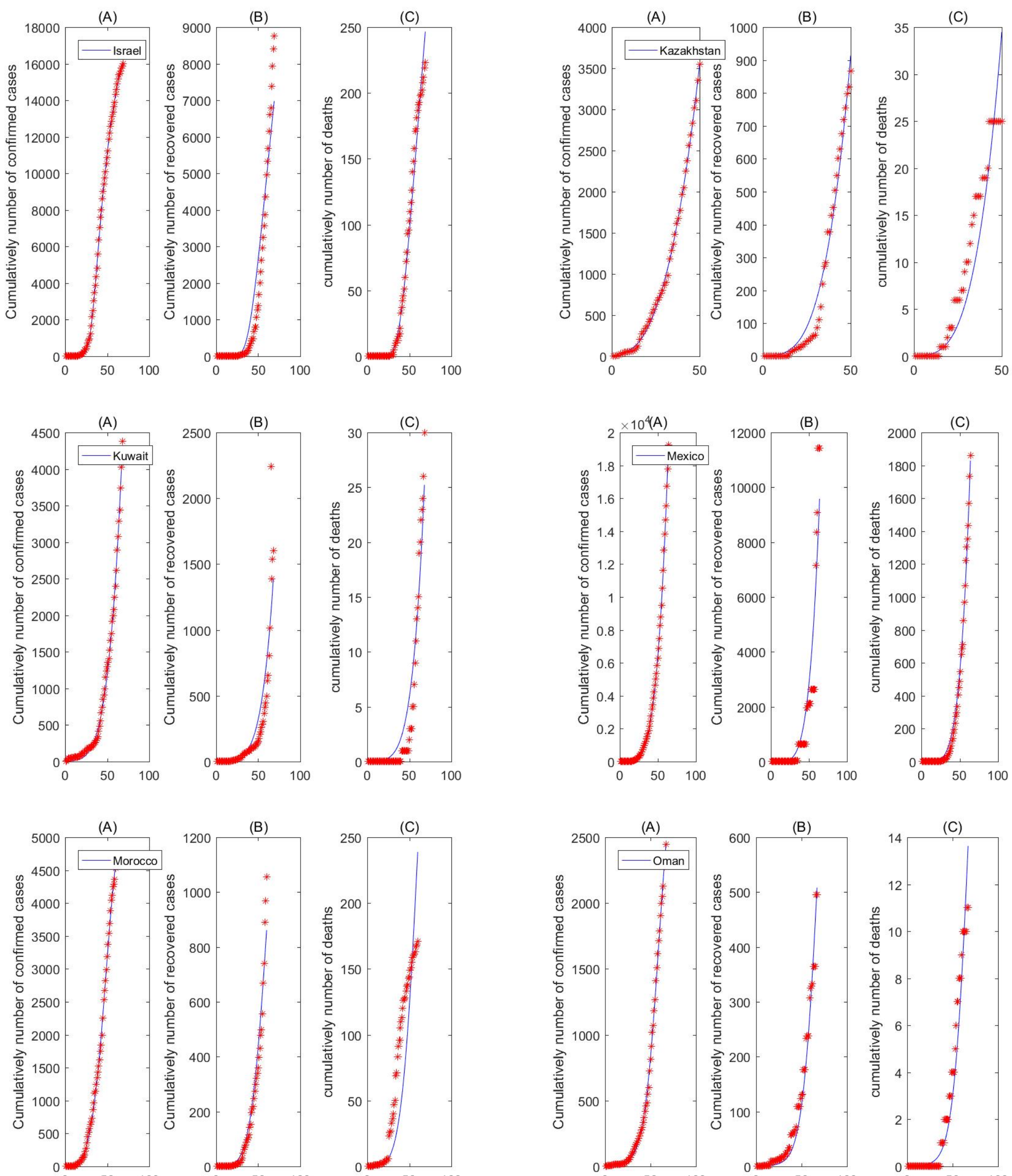
(A)
(B)
(C)
Israel
Kazakhstan
Kuwait
Mexico
Morocco
Oman
Cumulatively number of confirmed cases
Cumulatively number of recovered cases
cumulatively number of deaths
$\times 10^4$

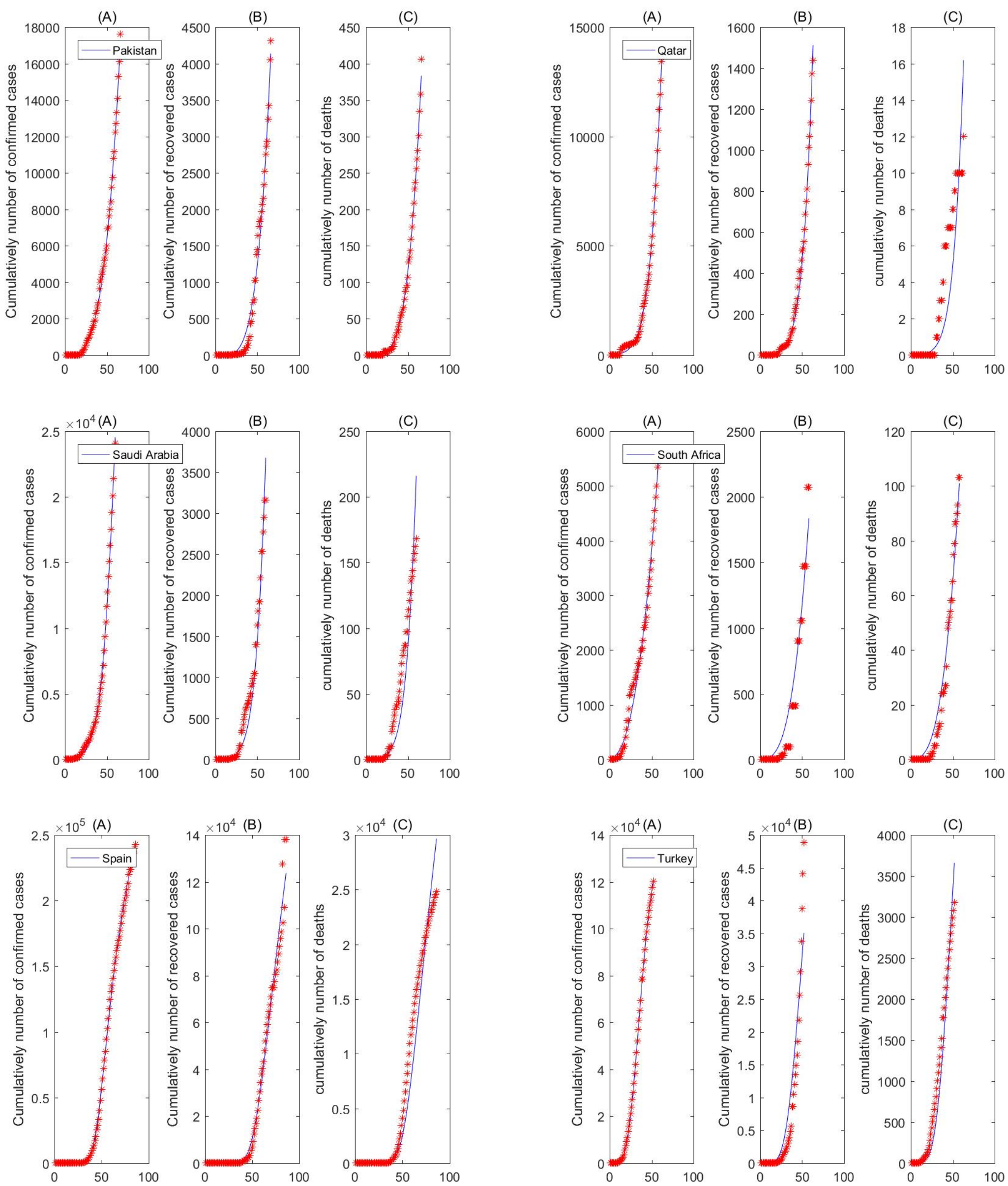
(A)
(B)
(C)
Pakistan
Qatar
Saudi Arabia
South Africa
Spain
Turkey
Cumulatively number of confirmed cases
Cumulatively number of recovered cases
cumulatively number of deaths
$\times10^4$
$\times10^5$

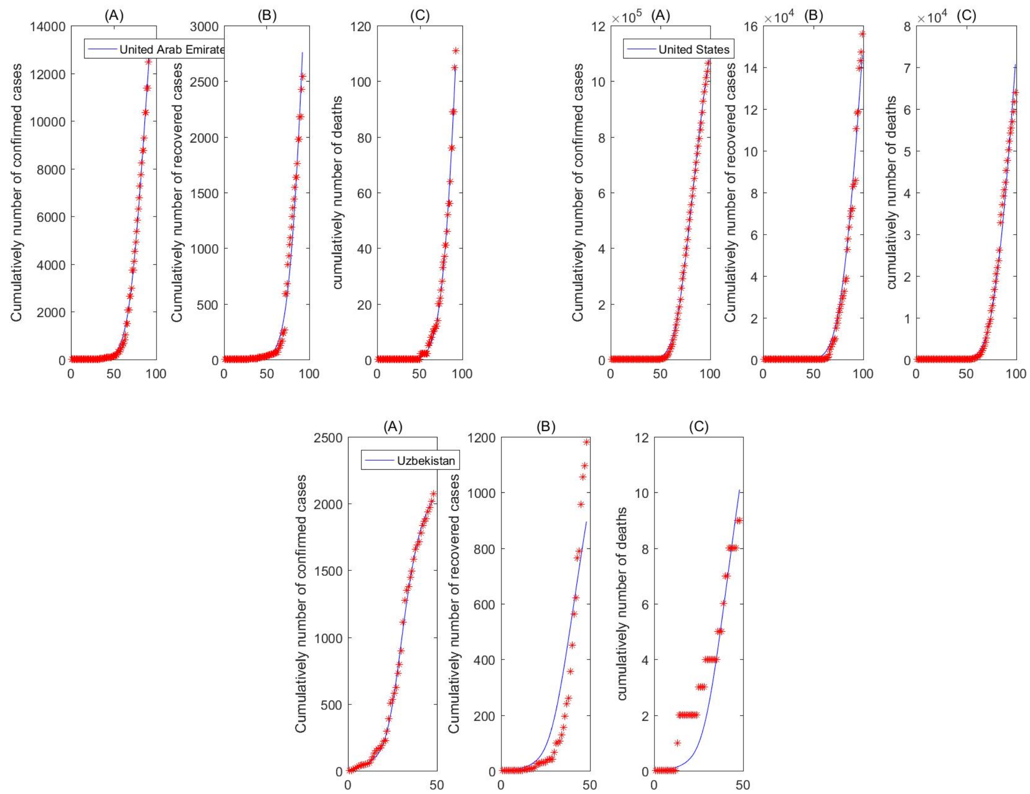

Figure S3: Simulation results of the cumulative confirmed cases, cumulative recovered cases, and cumulative deaths of Afghanistan, Algeria, Argentina, Australia, Azerbaijan, Bahrain, Chile, China, Djibouti, Egypt, Iran, Iraq, Israel, Kazakhstan, Kuwait, Mexico, Morocco, Oman, Pakistan, Qatar, Saudi Arabia, South Africa, Spain, Turkey, United Arab Emirates, United States and Uzbekistan in arid region.

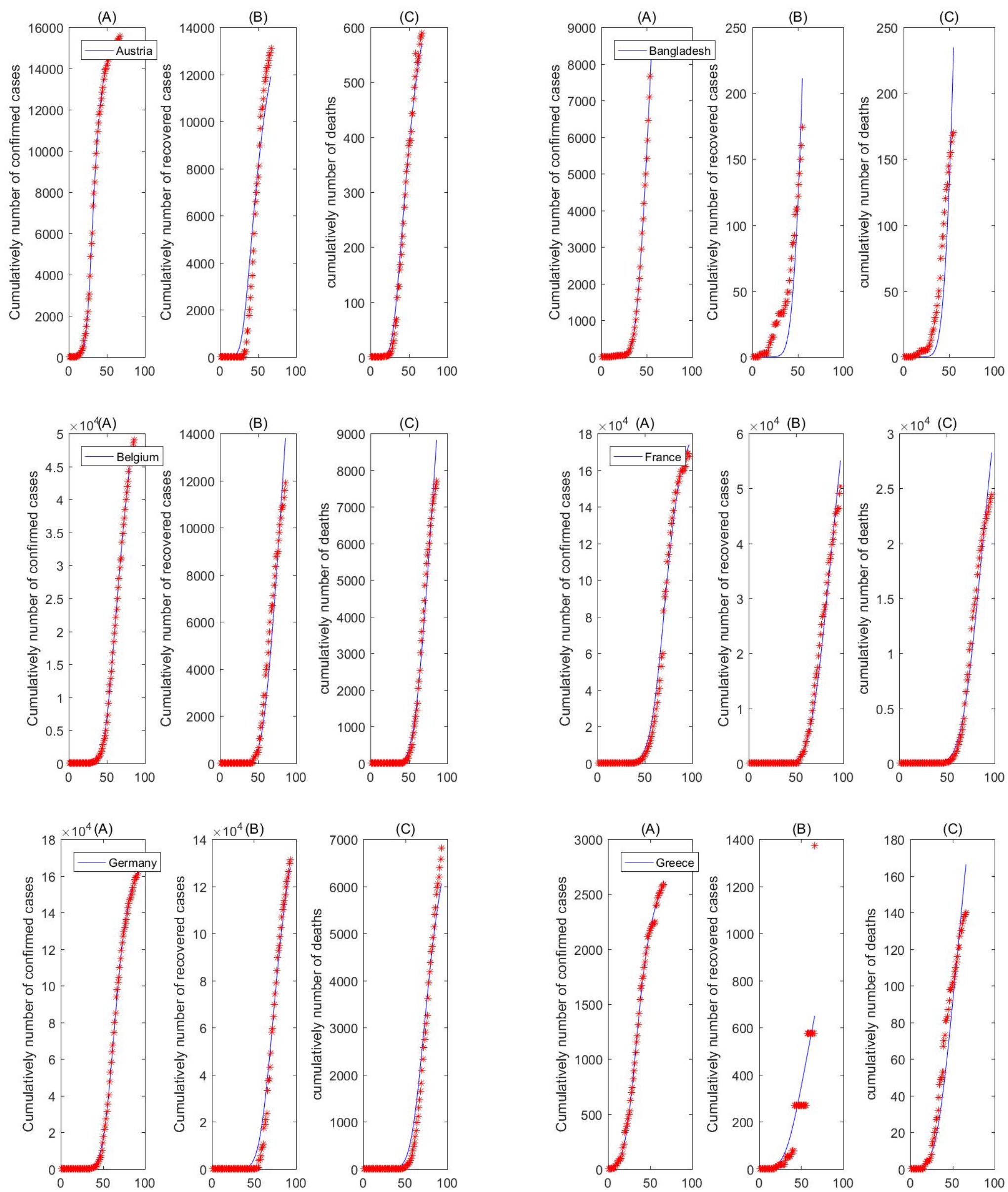
(A)
(B)
(C)
Austria
Bangladesh
Belgium
France
Germany
Greece
Cumulatively number of confirmed cases
Cumulatively number of recovered cases
cumulatively number of deaths
×10^4

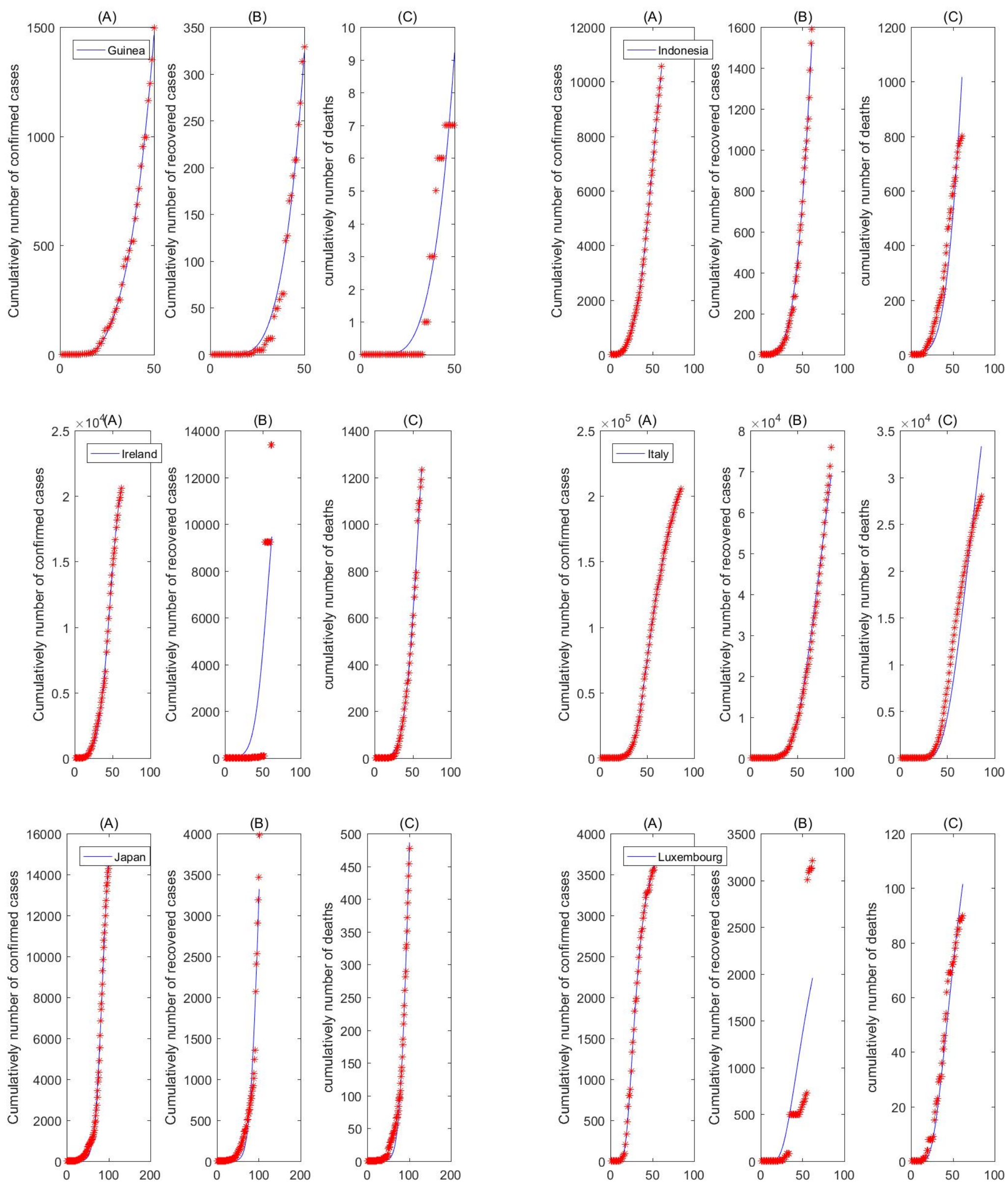
(A)
(B)
(C)
Guinea
Cumulatively number of confirmed cases
Cumulatively number of recovered cases
cumulatively number of deaths
(A)
(B)
(C)
Indonesia
Cumulatively number of confirmed cases
Cumulatively number of recovered cases
cumulatively number of deaths
(A)
(B)
(C)
Ireland
Cumulatively number of confirmed cases
Cumulatively number of recovered cases
cumulatively number of deaths
(A)
(B)
(C)
Italy
Cumulatively number of confirmed cases
Cumulatively number of recovered cases
cumulatively number of deaths
(A)
(B)
(C)
Japan
Cumulatively number of confirmed cases
Cumulatively number of recovered cases
cumulatively number of deaths
(A)
(B)
(C)
Luxembourg
Cumulatively number of confirmed cases
Cumulatively number of recovered cases
cumulatively number of deaths

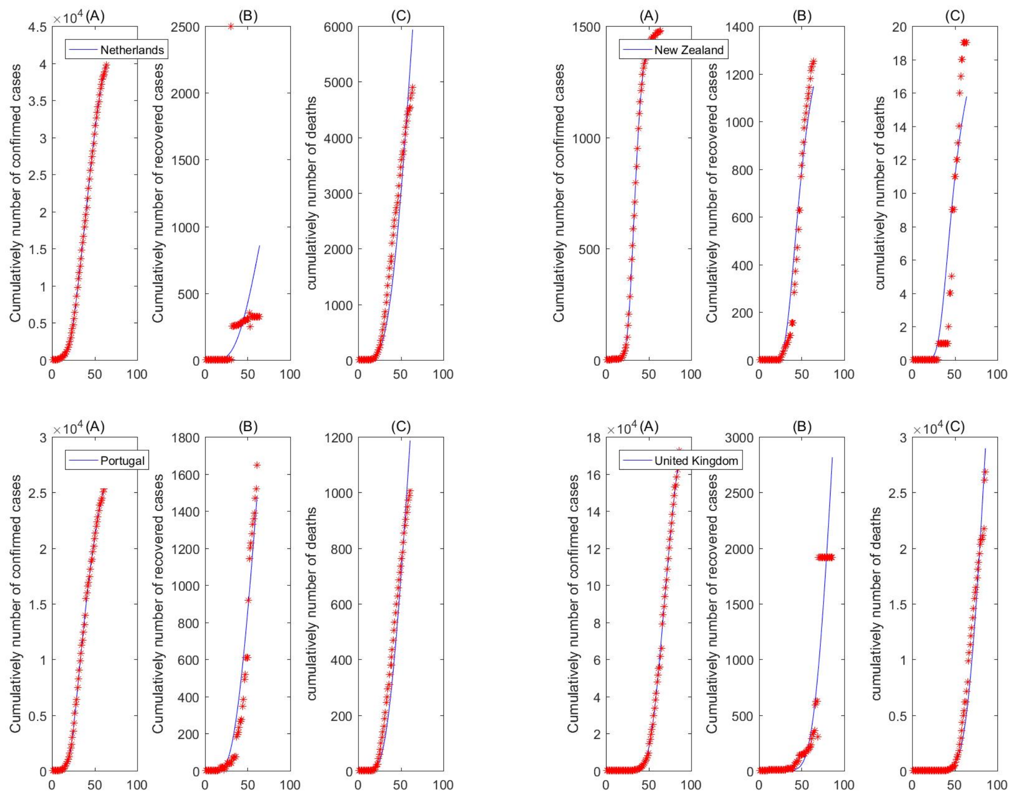

Figure S4: Simulation results of the cumulative confirmed cases, cumulative recovered cases, and cumulative deaths of Austria, Bangladesh, Belgium, France, Germany, Greece, Guinea, Indonesia, Ireland, Italy, Japan, Luxembourg, Netherlands, New Zealand, Portugal and United Kingdom in temperate region.

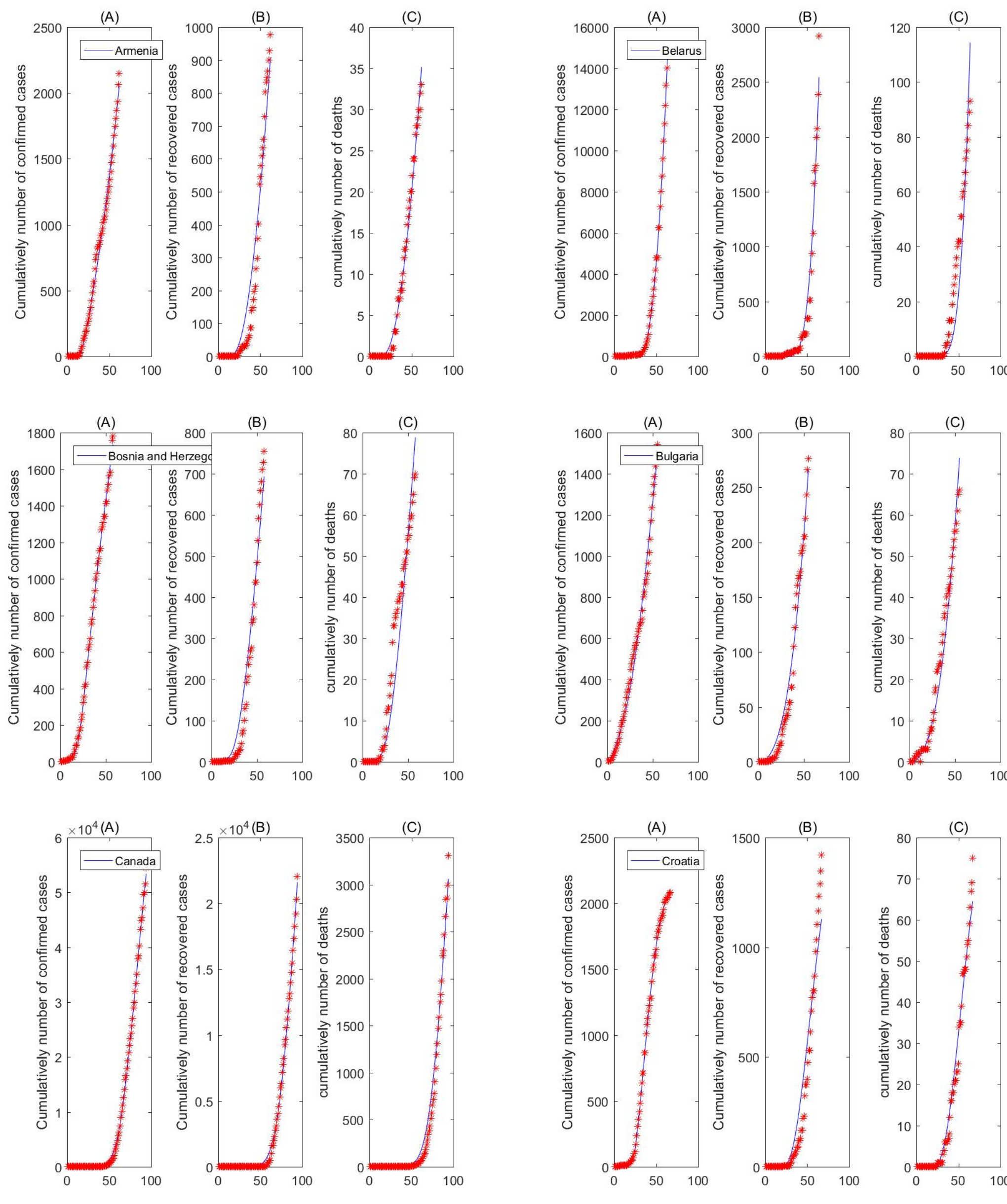
(A)
(B)
(C)
Armenia
Belarus
Bosnia and Herzego
Bulgaria
Canada
Croatia
Cumulatively number of confirmed cases
Cumulatively number of recovered cases
cumulatively number of deaths
×10^4

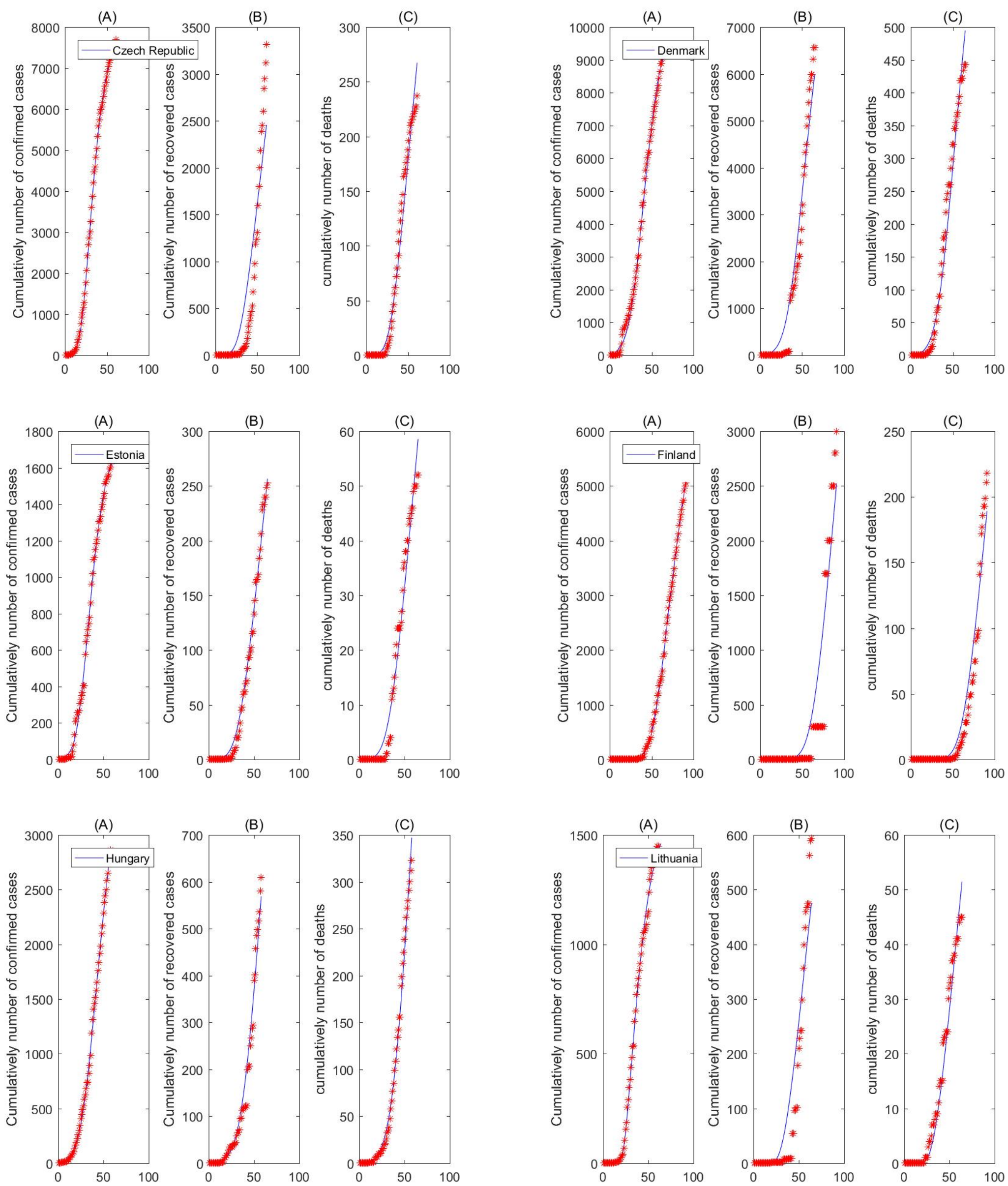
(A)
(B)
(C)
Czech Republic
Denmark
Estonia
Finland
Hungary
Lithuania
Cumulatively number of confirmed cases
Cumulatively number of recovered cases
cumulatively number of deaths

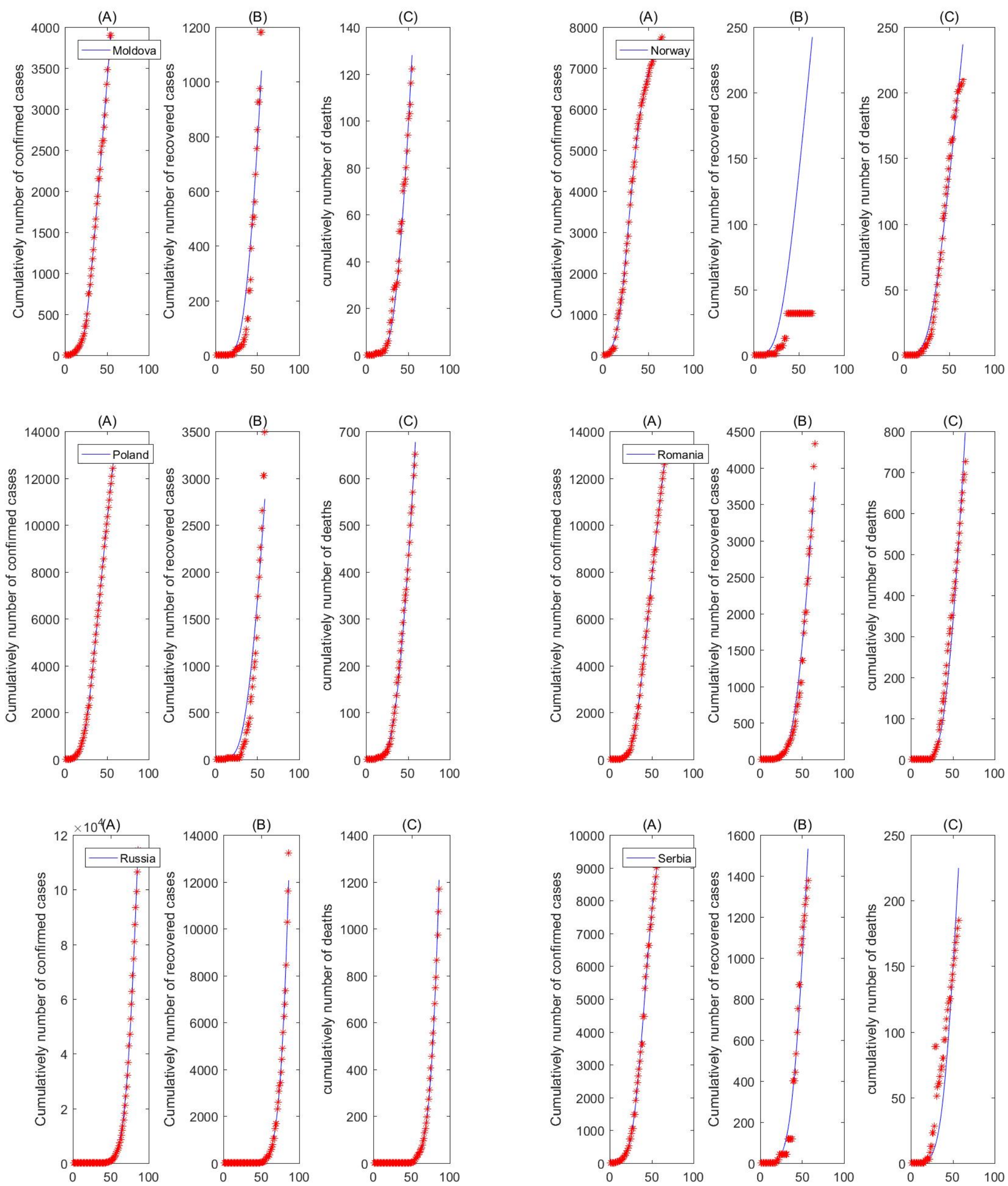
(A)
(B)
(C)
Moldova
Norway
Poland
Romania
Russia
Serbia
Cumulatively number of confirmed cases
Cumulatively number of recovered cases
cumulatively number of deaths
$\times 10^4$

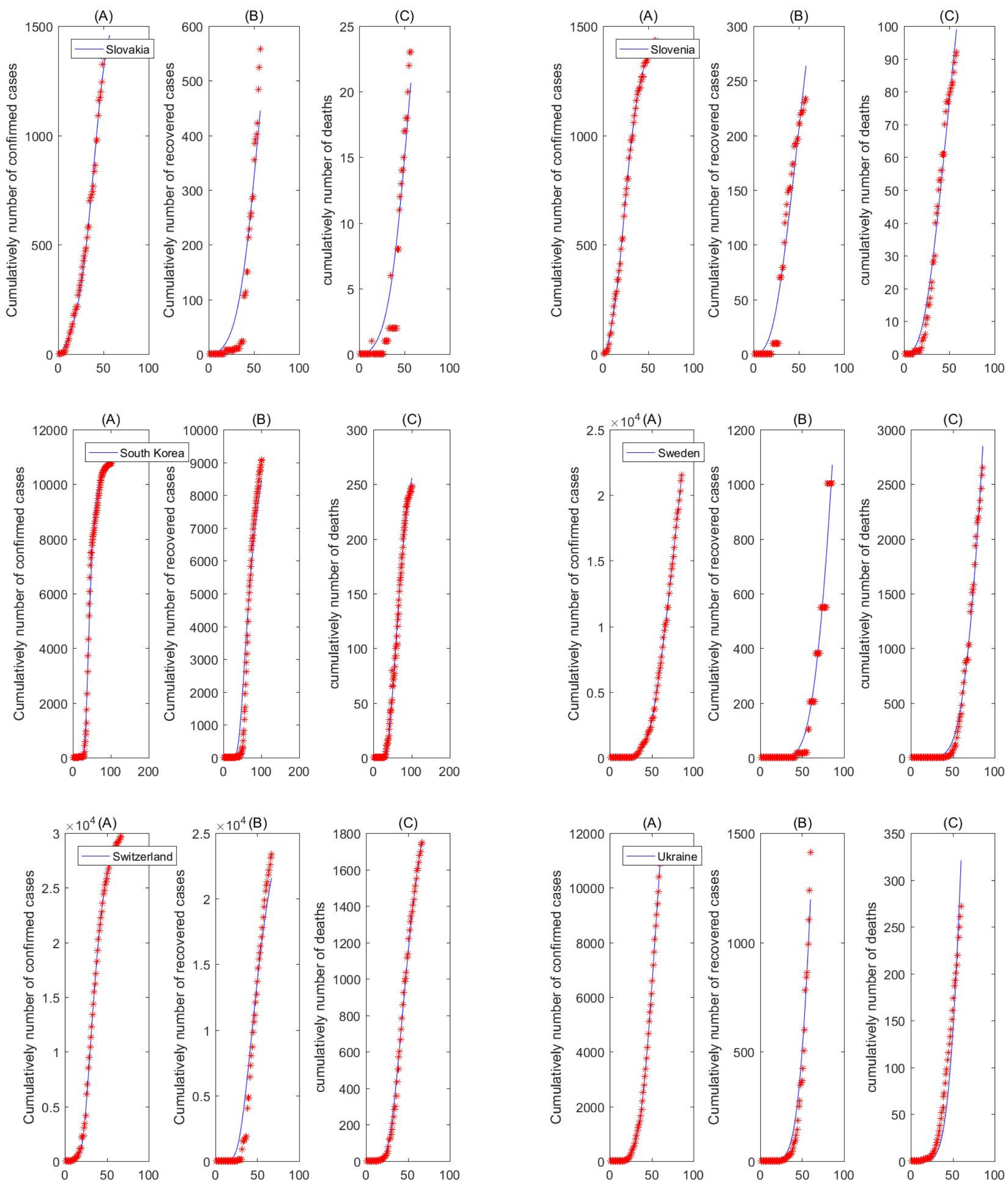

Figure S5: Simulation results of the cumulative confirmed cases, cumulative recovered cases, and cumulative deaths of Armenia, Belarus, Bosnia and Herzegovina, Bulgaria, Canada, Croatia, Czech Republic, Denmark, Estonia, Finland, Hungary, Lithuania, Moldova, Norway, Poland, Romania, Russia, Serbia, Slovakia, Slovenia, South Korea, Sweden, Switzerland and Ukraine in cold region.

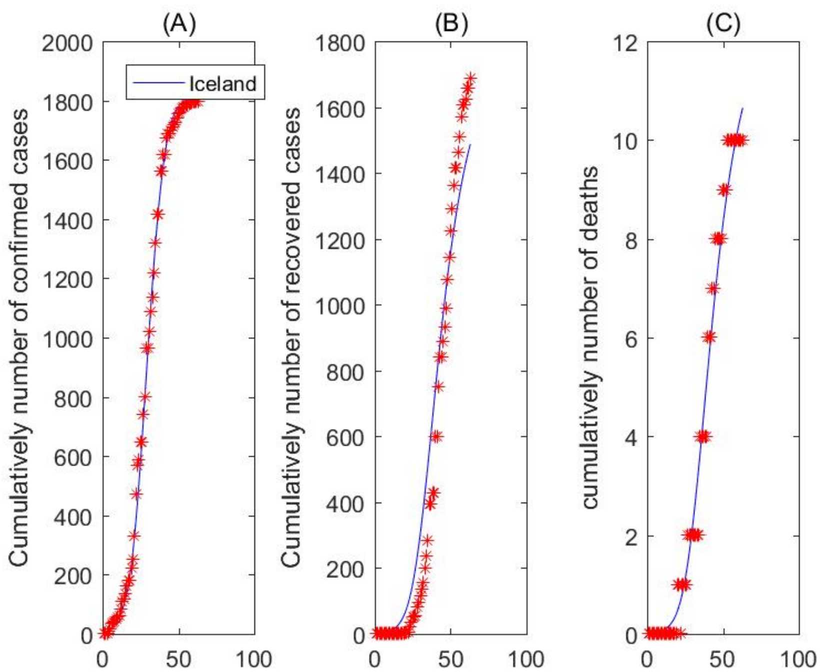

Figure S6: Simulation results of the cumulative confirmed cases, cumulative recovered cases, and cumulative deaths of Iceland in polar region.

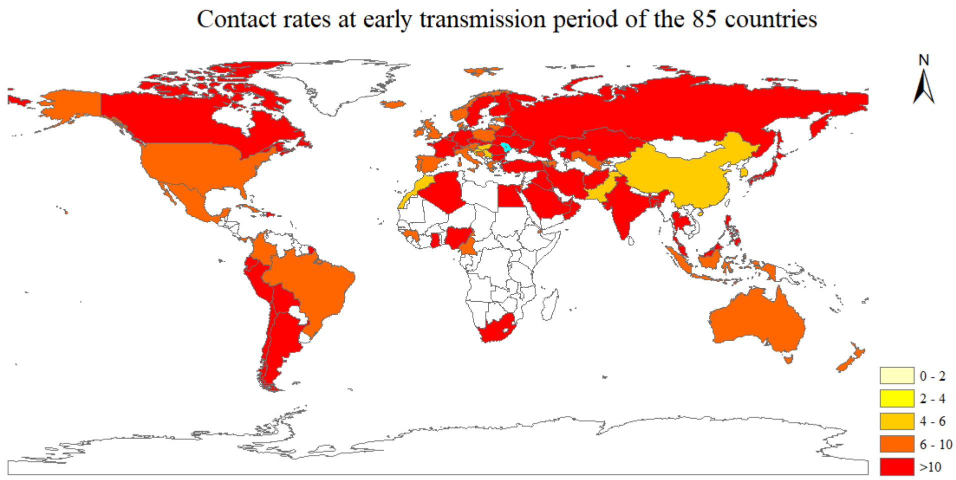

Figure S7: Distribution of the contact rates c_0 at early transmission period of the 85 countries.

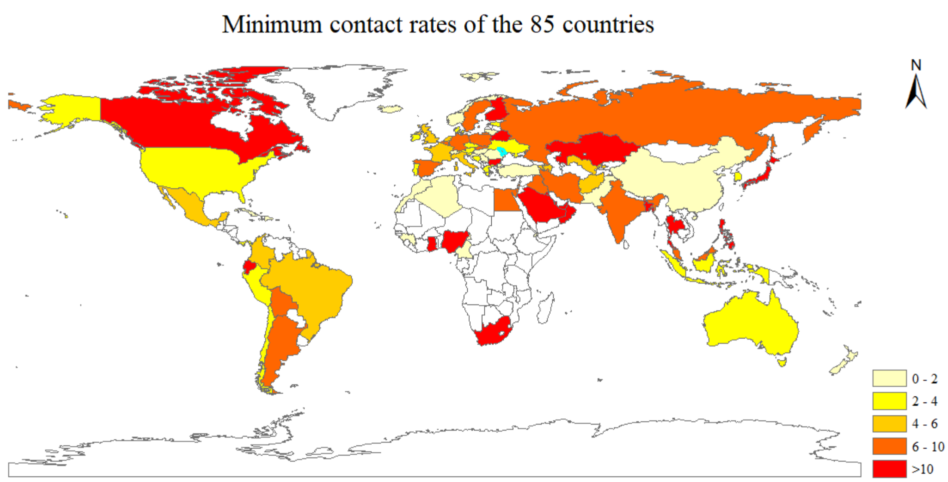

Figure S8: Same as Figure S5, but for the minimum contact rates c_f.

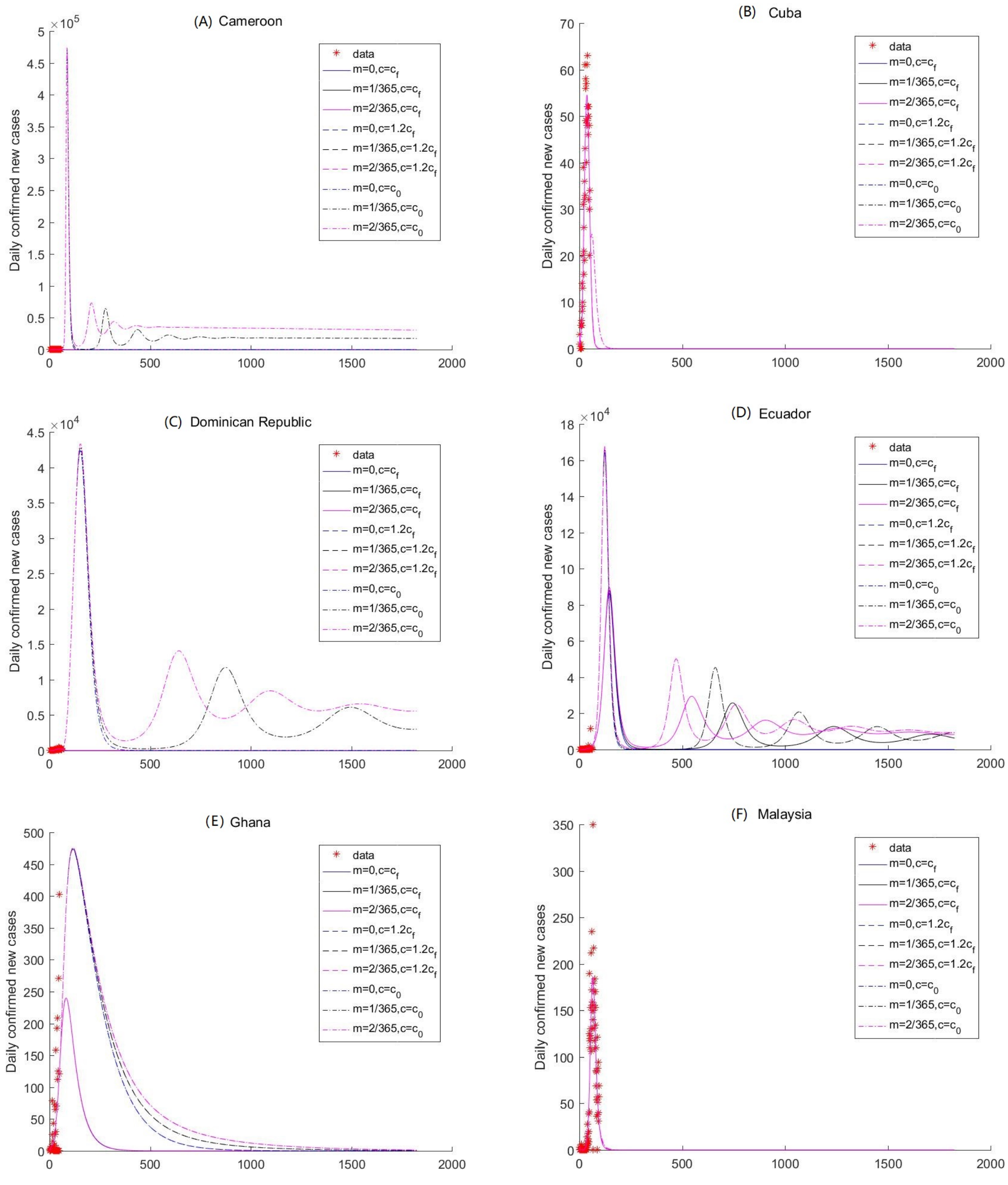
(A) Cameroon
(B) Cuba
(C) Dominican Republic
(D) Ecuador
(E) Ghana
(F) Malaysia
Daily confirmed new cases
data
m=0,c=c_f
m=1/365,c=c_f
m=2/365,c=c_f
m=0,c=1.2c_f
m=1/365,c=1.2c_f
m=2/365,c=1.2c_f
m=0,c=c_0
m=1/365,c=c_0
m=2/365,c=c_0

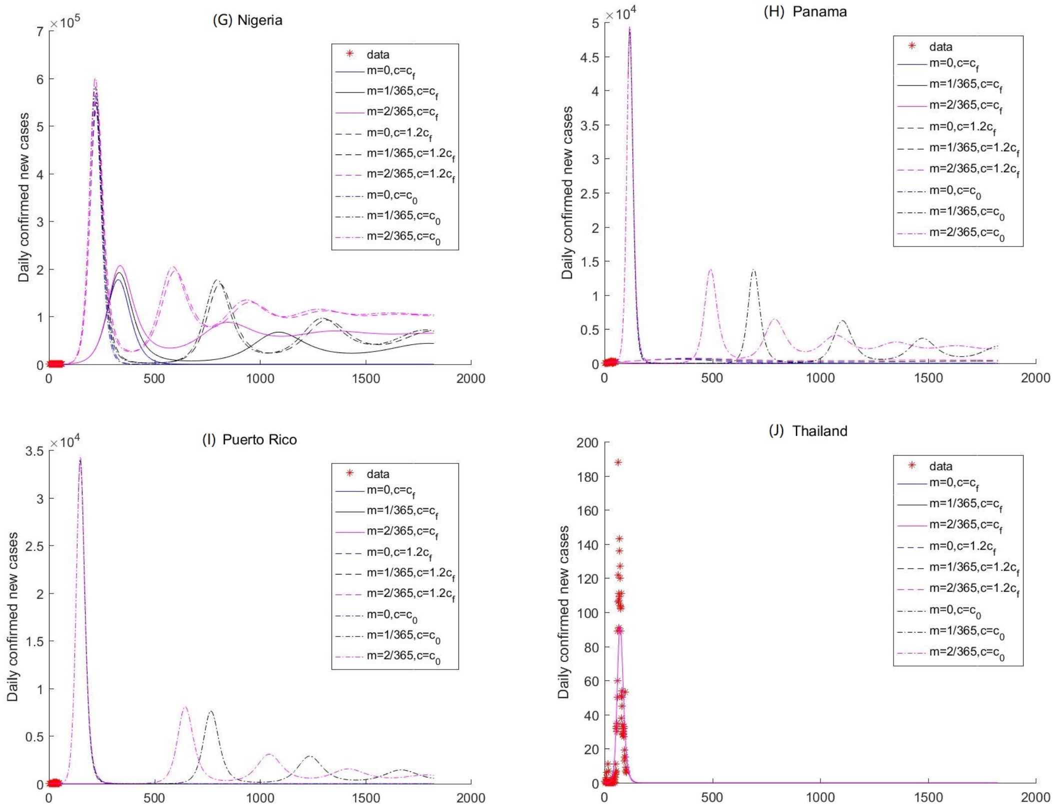

Figure S9: Sensitivity analysis of the daily new confirmed cases of Cameroon, Cuba, Dominican Republic, Ecuador, Ghana, Malaysia, Nigeria, Panama, Puerto Rico, and Thailand in tropical region.

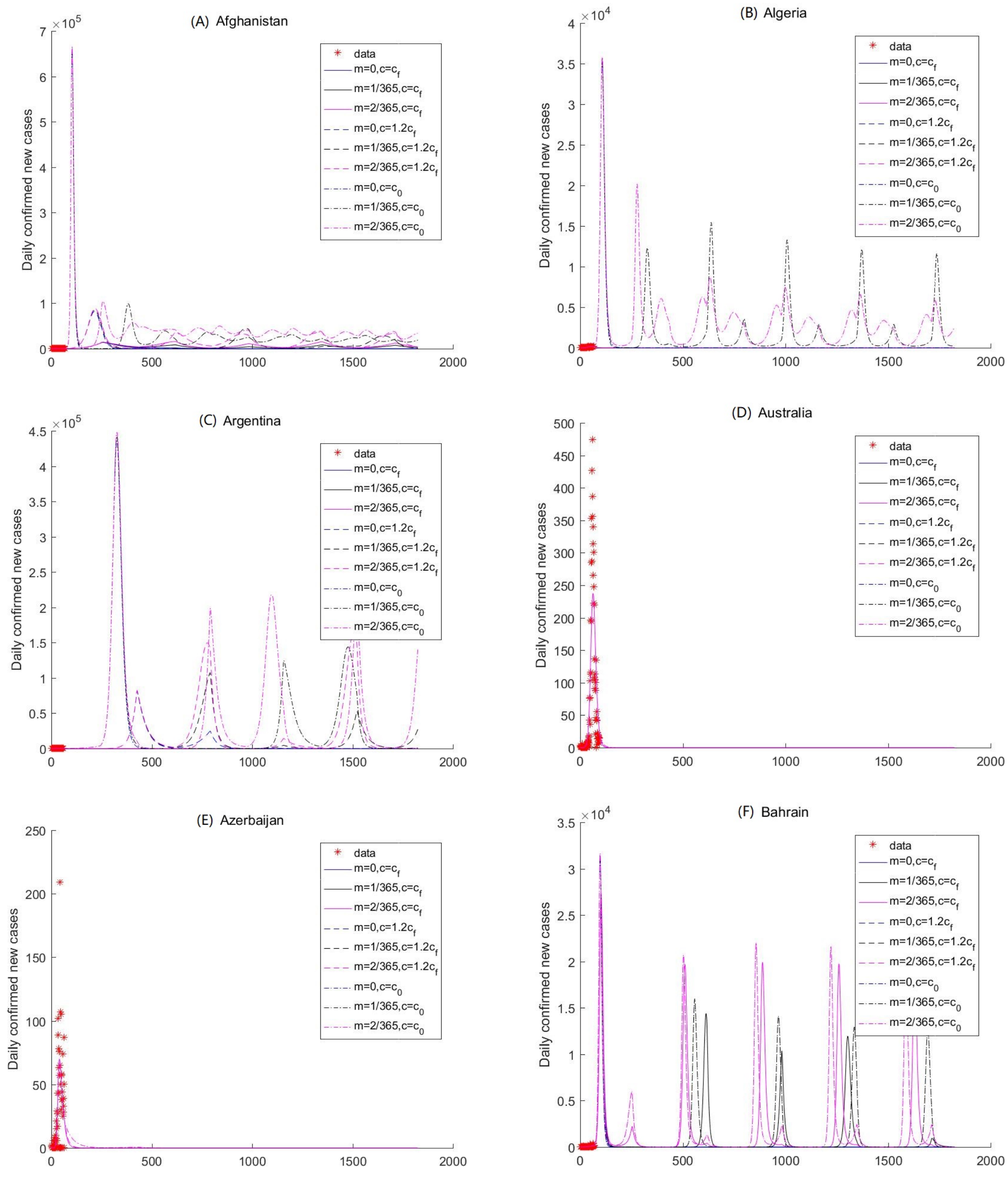
(A) Afghanistan
(B) Algeria
(C) Argentina
(D) Australia
(E) Azerbaijan
(F) Bahrain
Daily confirmed new cases
×10^5
×10^4
data
m=0,c=c_f
m=1/365,c=c_f
m=2/365,c=c_f
m=0,c=1.2c_f
m=1/365,c=1.2c_f
m=2/365,c=1.2c_f
m=0,c=c_0
m=1/365,c=c_0
m=2/365,c=c_0
0
500
1000
1500
2000

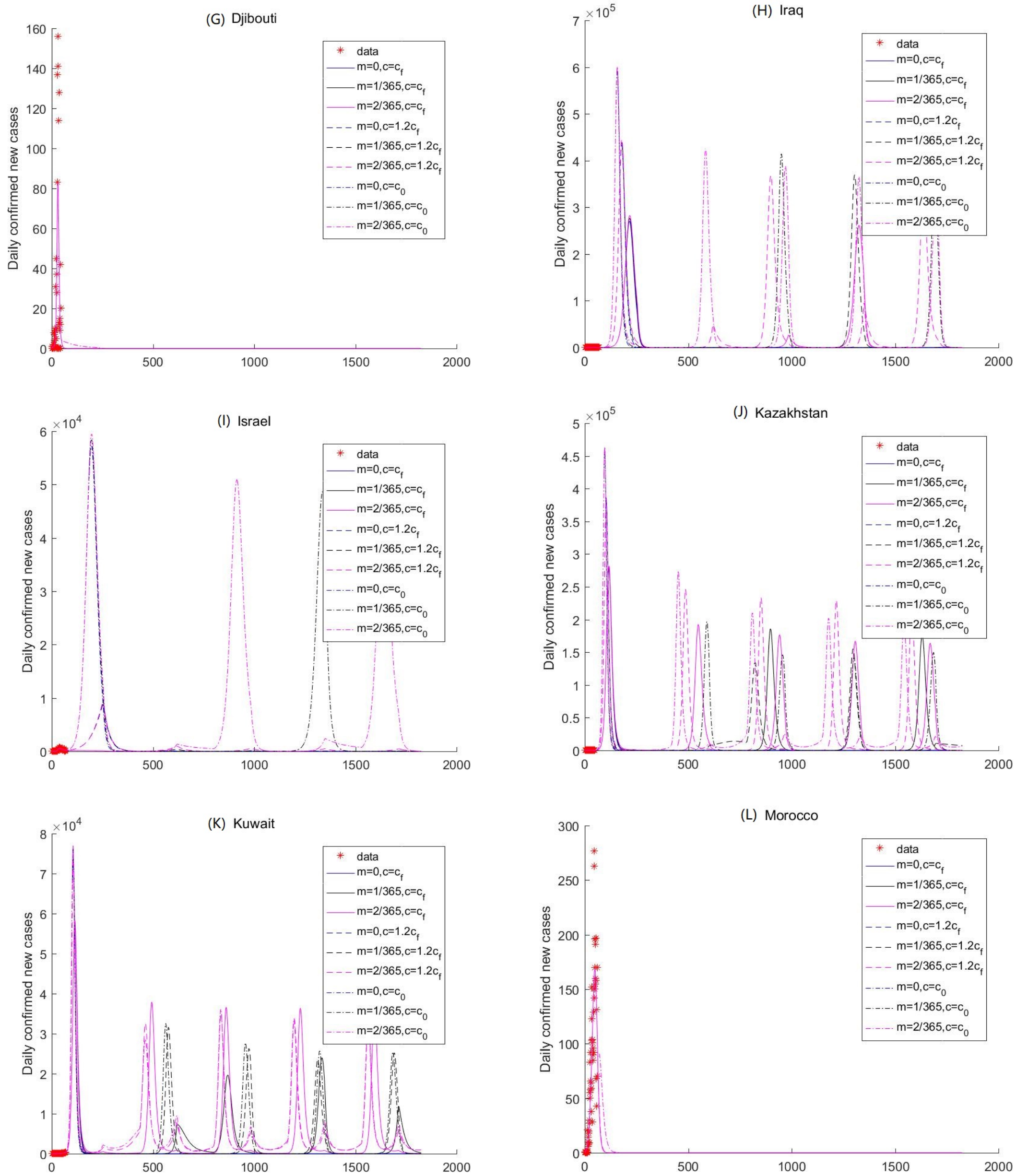
(G) Djibouti
(H) Iraq
(I) Israel
(J) Kazakhstan
(K) Kuwait
(L) Morocco
Daily confirmed new cases
data
m=0,c=c_f
m=1/365,c=c_f
m=2/365,c=c_f
m=0,c=1.2c_f
m=1/365,c=1.2c_f
m=2/365,c=1.2c_f
m=0,c=c_0
m=1/365,c=c_0
m=2/365,c=c_0

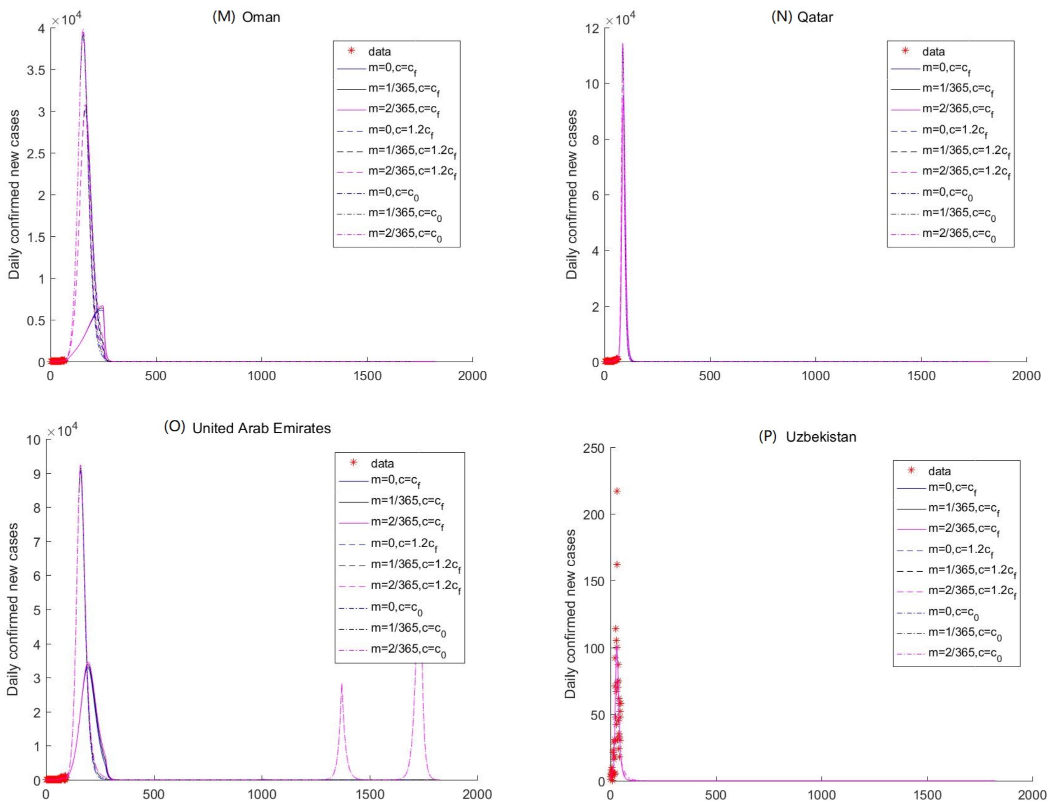

Figure S10: Sensitivity analysis of the daily new confirmed cases of Afghanistan, Algeria, Argentina, Austrialia, Azerbaijan, Bahrain, Djibouti, Iraq, Israel, Kazakstan, Kuwait, Morocco, Oman, Qatar, United Arab Emirates and Uzbekistan in arid region.

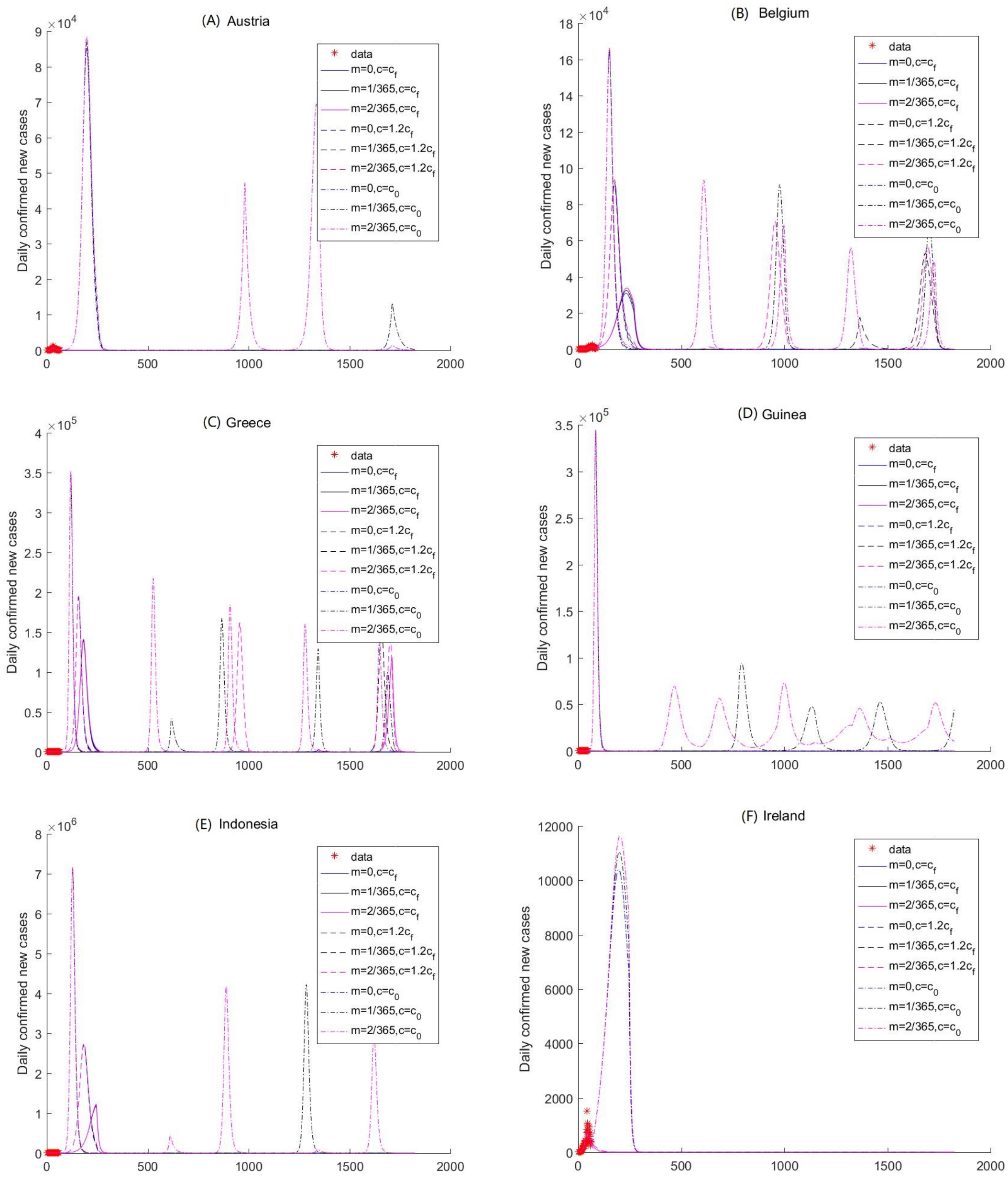
(A) Austria
(B) Belgium
(C) Greece
(D) Guinea
(E) Indonesia
(F) Ireland
Daily confirmed new cases
data
m=0,c=c$_f$
m=1/365,c=c$_f$
m=2/365,c=c$_f$
m=0,c=1.2c$_f$
m=1/365,c=1.2c$_f$
m=2/365,c=1.2c$_f$
m=0,c=c$_0$
m=1/365,c=c$_0$
m=2/365,c=c$_0$

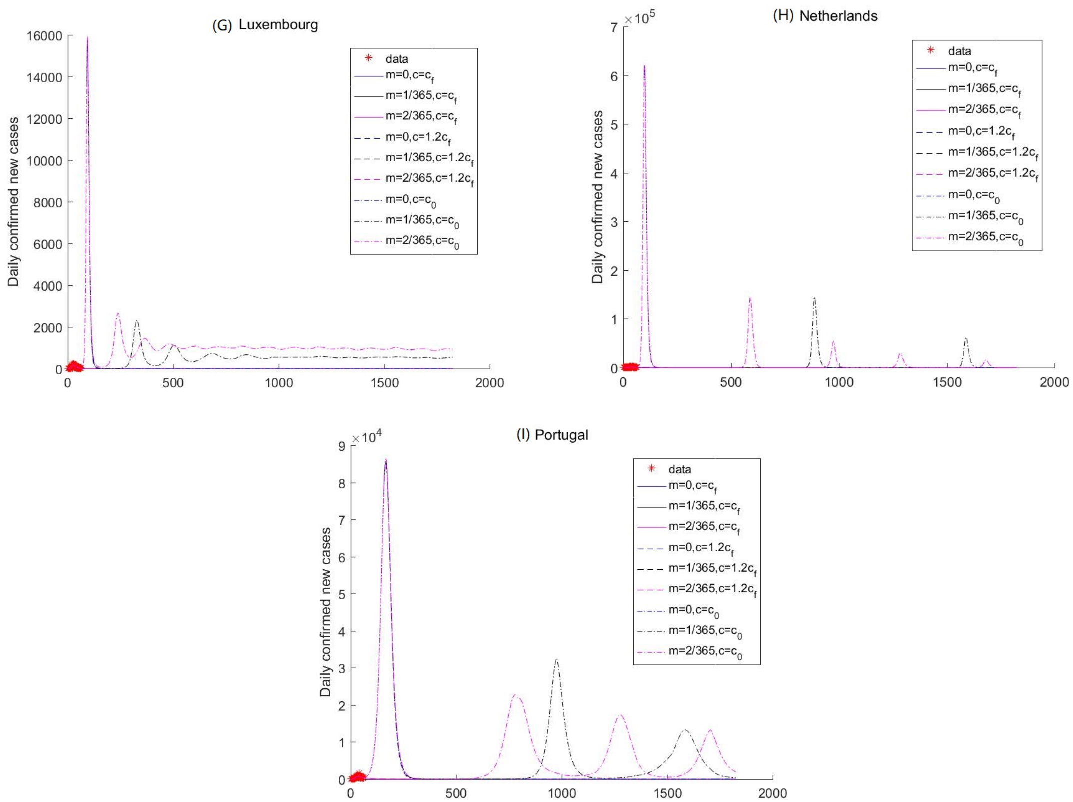

Figure S11: Sensitivity analysis of the daily new confirmed cases of Austria, Belgium, Greece, Guinea, Indonesia, Ireland, Luxembourg, Netherlands, and Portugal in temperate region.

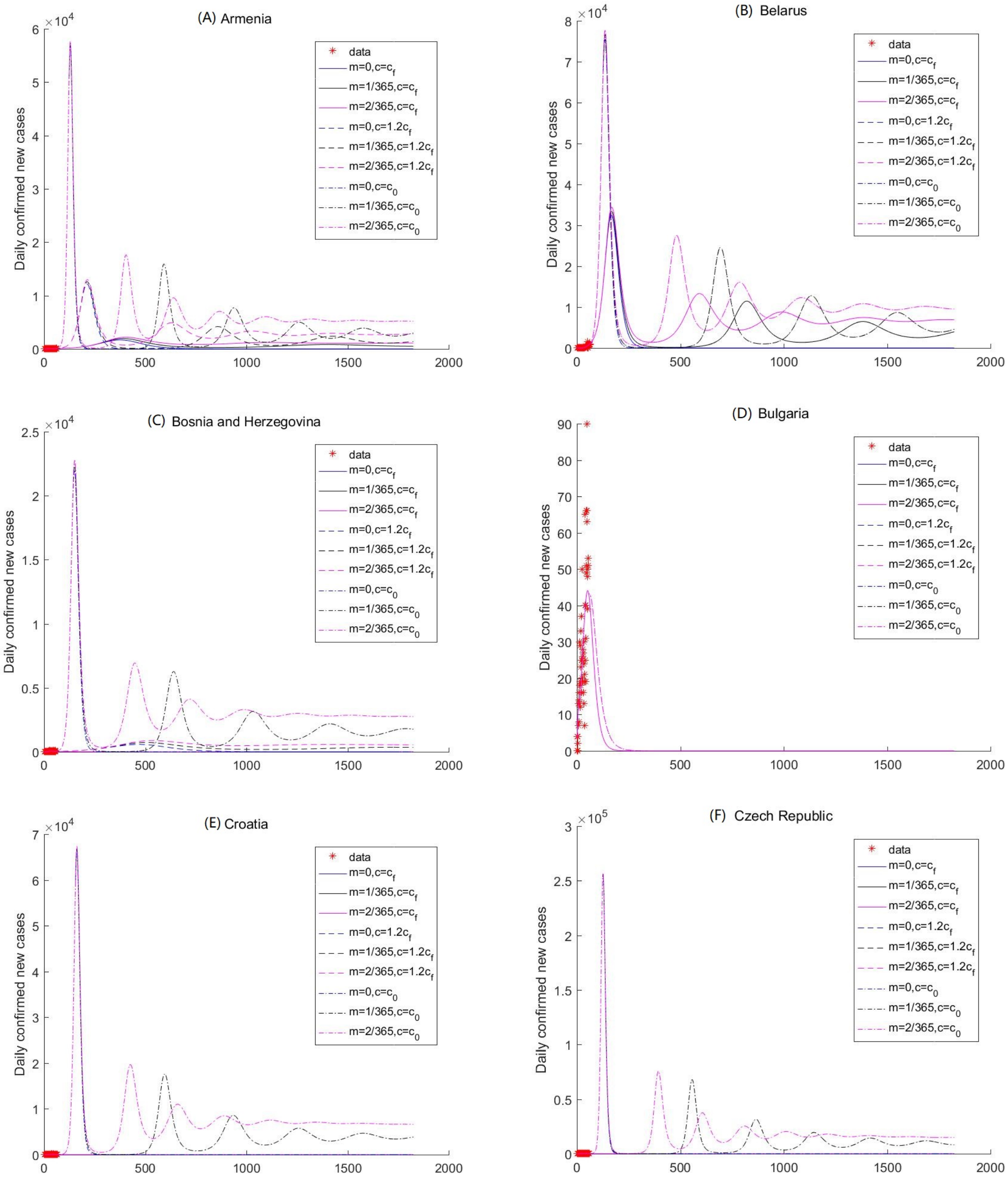
(A) Armenia
(B) Belarus
(C) Bosnia and Herzegovina
(D) Bulgaria
(E) Croatia
(F) Czech Republic
Daily confirmed new cases
data
m=0,c=c$_f$
m=1/365,c=c$_f$
m=2/365,c=c$_f$
m=0,c=1.2c$_f$
m=1/365,c=1.2c$_f$
m=2/365,c=1.2c$_f$
m=0,c=c$_0$
m=1/365,c=c$_0$
m=2/365,c=c$_0$

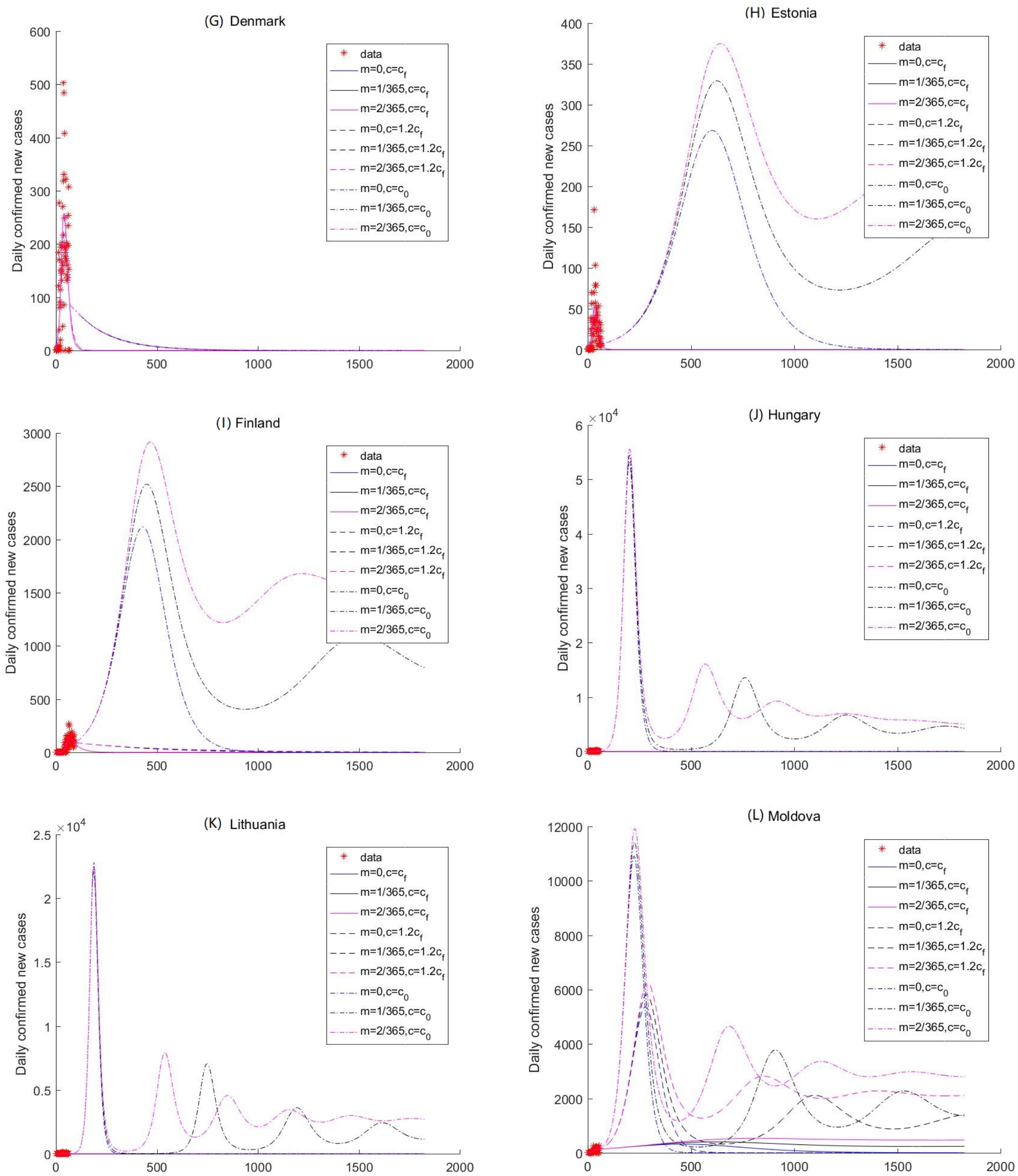
(G) Denmark
(H) Estonia
(I) Finland
(J) Hungary
(K) Lithuania
(L) Moldova
Daily confirmed new cases
data
m=0,c=c_f
m=1/365,c=c_f
m=2/365,c=c_f
m=0,c=1.2c_f
m=1/365,c=1.2c_f
m=2/365,c=1.2c_f
m=0,c=c_0
m=1/365,c=c_0
m=2/365,c=c_0

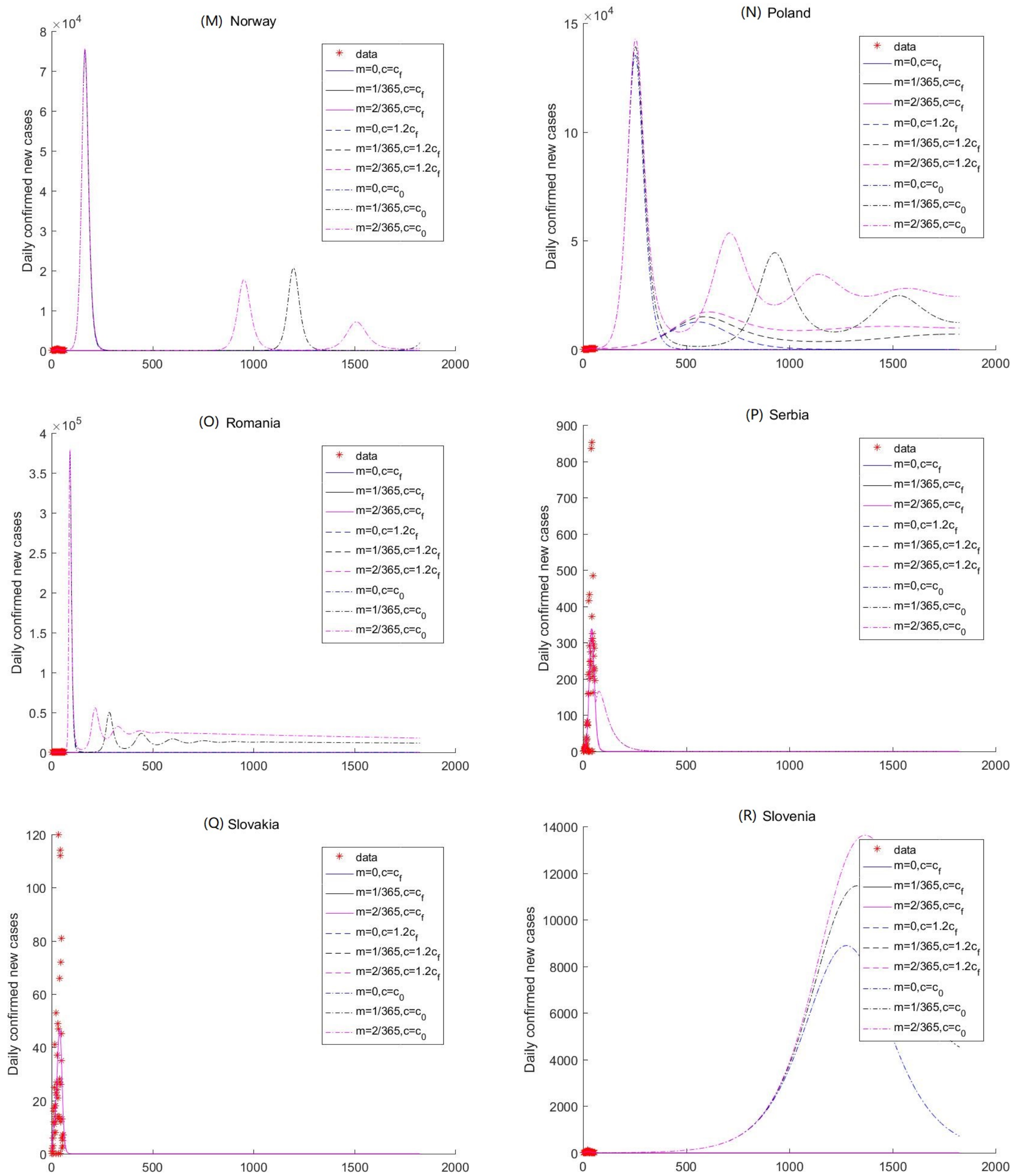
(M) Norway
(N) Poland
(O) Romania
(P) Serbia
(Q) Slovakia
(R) Slovenia
Daily confirmed new cases
data
m=0,c=c$_f$
m=1/365,c=c$_f$
m=2/365,c=c$_f$
m=0,c=1.2c$_f$
m=1/365,c=1.2c$_f$
m=2/365,c=1.2c$_f$
m=0,c=c$_0$
m=1/365,c=c$_0$
m=2/365,c=c$_0$

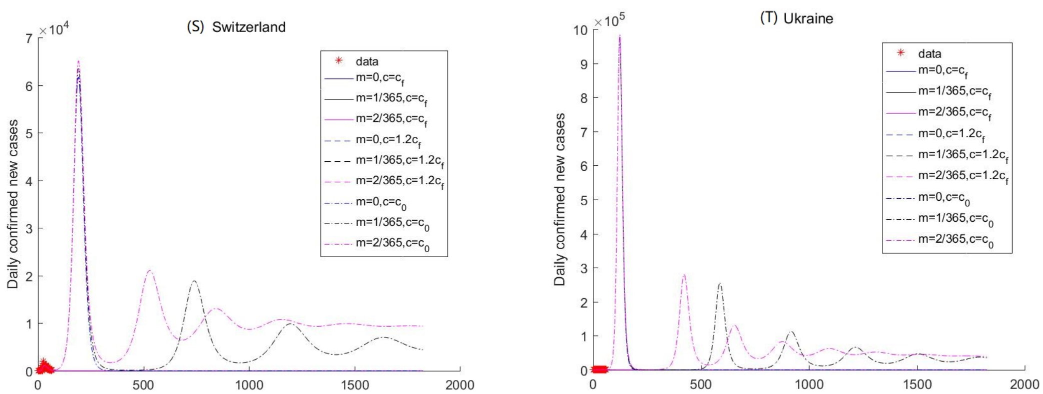

Figure S12: Sensitivity analysis of the daily new confirmed cases of Armenia, Belarus, Bosnia and Herzegovina, Bulgaria, Croatia, Czech Republic, Denmark, Estonia, Finland, Hungary, Lithuania, Moldova, Norway, Poland, Romania, Servia, Slovakia, Slovenia, Switzerland, and Ukraine in cold region.